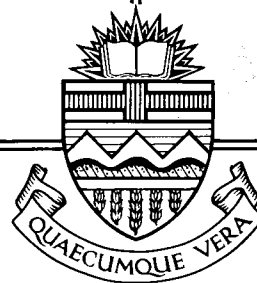


Structural Engineering Report No. 135



FINITE ELEMENT PREDICTION OF BIN LOADS

by

A. H. ASKARI

A. E. ELWI

June, 1986

RECENT STRUCTURAL ENGINEERING REPORTS

Department of Civil Engineering

University of Alberta

104. *Test Methods for Evaluating Mechanical Properties of Waferboard: A Preliminary Study* by M. MacIntosh and J. Longworth, May 1982.
105. *Fatigue Strength of Two Steel Details* by K.A. Baker and G.L. Kulak, October 1982.
106. *Designing Floor Systems for Dynamic Response* by C.M. Matthews, C.J. Montgomery and D.W. Murray, October 1982.
107. *Analysis of Steel Plate Shear Walls* by L. Jane Thorburn, G.L. Kulak, and C.J. Montgomery, May 1983.
108. *Analysis of Shells of Revolution* by N. Hernandez and S.H. Simmonds, August 1983.
109. *Tests of Reinforced Concrete Deep Beams* by D.M. Rogowsky, J.G. MacGregor and S.Y. Ong, September 1983.
110. *Shear Strength of Deep Reinforced Concrete Continuous Beams* by D.M. Rogowsky and J.G. MacGregor, September 1983.
111. *Drilled-In Inserts in Masonry Construction* by M.A. Hatzinikolas, R. Lee, J. Longworth and J. Warwaruk, October 1983.
112. *Ultimate Strength of Timber Beam Columns* by T.M. Olatunji and J. Longworth, November 1983.
113. *Lateral Coal Pressures in a Mass Flow Silo* by A.B.B. Smith and S.H. Simmonds, November 1983.
114. *Experimental Study of Steel Plate Shear Walls* by P.A. Timler and G.L. Kulak, November 1983.
115. *End Connection Effects on the Strength of Concrete Filled HSS Columns* by S.J. Kennedy and J.G. MacGregor, April 1984.
116. *Reinforced Concrete Column Design Program* by C-K. Leung and S.H. Simmonds, April 1984.
117. *Deflections of Two-way Slabs under Construction Loading* by C. Graham and A. Scanlon, August 1984.
118. *Effective Lengths of Laterally Unsupported Steel Beams* by C.D. Schmitke and D.J.L. Kennedy, October 1984.

119. *Flexural and Shear Behaviour of Large Diameter Steel Tubes* by R.W. Bailey and G.L. Kulak, November 1984.
120. *Concrete Masonry Prism Response due to Loads Parallel and Perpendicular to Bed Joints* by R. Lee, J. Longworth and J. Warwaruk.
121. *Standardized Flexible End Plate Connections for Steel Beams* by G.J. Kriviak and D.J.L. Kennedy, December 1984.
122. *The Effects of Restrained Shrinkage on Concrete Slabs* by K.S.S. Tam and A. Scanlon, December 1984.
123. *Prestressed Concrete Beams with Large Rectangular Web Openings* by T. do M.J. Alves and A. Scanlon, December 1984.
124. *Tests on Eccentrically Loaded Fillet Welds* by G.L. Kulak and P.A. Timler, December 1984.
125. *Analysis of Field Measured Deflections Scotia Place Office Tower* by A. Scanlon and E. Ho, December 1984.
126. *Ultimate Behaviour of Continuous Deep Reinforced Concrete Beams* by D.R. Ricketts and J.G. MacGregor, January 1985.
127. *The Interaction of Masonry Veneer and Steel Studs in Curtain Wall Construction* by W.M. McGinley, J. Warwaruk, J. Longworth and M. Hatzinikolas, May 1985.
128. *Evaluation of Existing Bridge Structure by Nondestructive Test Methods* by L. Mikhailovsky and A. Scanlon, May 1985.
129. *Finite Element Modelling of Buried Structures* by D.K. Playdon and S.H. Simmonds, October 1985.
130. *Behaviour and Ultimate Strength of Transversely Loaded Continuous Steel Plates* by K.P. Ratzlaff and D.J.L. Kennedy, November 1985.
131. *Inelastic Lateral Buckling of Steel Beam-Columns* by P.E. Cuk, M.A. Bradford and N.S. Trahair, December 1985.
132. *Design Strengths of Steel Beam-Columns* by N.S. Trahair, December 1985.
133. *Behaviour of Fillet Welds as a Function of the Angle of Loading* by G.S. Miazga and D.J.L. Kennedy, March 1986.
134. *Inelastic Seismic Response of Precast Concrete Large Panel Coupled Shear Wall Systems* by M.R. Kianoush and A. Scanlon, March 1986.
135. *Finite Element Prediction of Bin Loads* by A.H. Askari and A.E. Elwi, June 1986.

FINITE ELEMENT PREDICTION OF BIN LOADS

by

A.H. Askari

A.E. Elwi

Structural Engineering Report #135

Department of Civil Engineering

University of Alberta

Edmonton, Alberta, Canada

June 1986

ABSTRACT

A finite element formulation based on the principle of Virtual Work, for the analysis of material behavior flowing in an axisymmetric silo is presented. The formulation incorporates the Coloumb's friction mechanism through an iterative solution scheme. In the absence of a rate dependent constitutive law for stored material, an elastic perfectly plastic material is proposed as a first approach to the solution of such problems.

A finite element program, FEPILS, based on program FEPARCS5 (Elwi and Murray, 1980) is used as a tool to analyze a finite element model of flowing material in axisymmetric silos.

A series of problems are analyzed using program FEPILS. The results of these analyses are compared with the classical theories. The stress and the displacement/velocity fields are presented. A parametric study is carried out to investigate the effect of the angle of internal friction, the angle of wall friction, the hopper slope, the height to diameter ratio and the Poisson's ratio, on the pressure, the stress and the displacement/velocity fields.

ACKNOWLEDGEMENTS

This study has been funded by the National Sciences and Engineering Research Council of Canada Grant No. A5877 and by the Central Research Fund of the University of Alberta. Thanks are extended to Ms. Nola Shaw for her skill and patience in typing this manuscript and to Mrs. D. Nickel who drew the figures.

TABLE OF CONTENTS

	Page
CHAPTER 1 - INTRODUCTION.....	1
1.1 Silos and History.....	1
1.2 Scope and Objectives of Thesis.....	4
1.3 Organization of Thesis.....	5
CHAPTER 2 - THEORY AND ANALYSES.....	7
2.1 Static Pressure Theories.....	7
2.1.1 Introduction.....	7
2.1.2 Janssen's Theory.....	7
2.1.3 Reimbert's Theory.....	11
2.1.4 Discussion.....	14
2.2 Flow Pressure Theories.....	15
2.2.1 Introduction.....	15
2.2.2 Flow Patterns.....	17
2.2.3 Jenike's Theories.....	20
2.3 Finite Element Analysis.....	37
2.3.1 The Ohio State University Group.....	37
2.3.2 University of Guelph Group.....	39
2.3.3 University of Karlsruhe Group.....	42
2.4 Field Measurements.....	46
2.4.1 Simmonds and Smith (1983).....	46
2.4.2 Technical University of Denmark (1980).....	48

	Page
CHAPTER 3 - THE FINITE ELEMENT FRICTION MODEL.....	51
3.1 Introduction.....	51
3.2 Incremental Virtual Work Formulation.....	52
3.3 The Friction Force Formulation.....	57
3.3.1 Solution Technique.....	61
CHAPTER 4 - MATERIAL MODEL.....	64
4.1 Introduction.....	64
4.2 Plasticity Model.....	65
4.3 Failure Surface.....	72
4.3.1 Willam-Warnke Surface.....	73
4.3.2 Drucker-Prager Surface.....	76
4.3.3 Degeneration of Willam-Warnke Surface to Drucker-Prager Surface.....	79
CHAPTER 5 - ANALYSIS AND COMPARISON.....	80
5.1 Introduction.....	80
5.2 Model Description.....	80
5.2.1 Description of Test Structures.....	80
5.2.2 Material Properties.....	82
5.2.3 Description of Analysis.....	85
5.3 Discussion of Results.....	86
5.3.1 Comparison of Pressure with Classical Theories.....	86
5.3.2 Stress Field.....	89
5.3.3 Displacement/Velocity Field.....	96

5.3.4 Influence of Various Variables on	
Lateral Wall Pressure.....	104
CHAPTER 6 - SUMMARY AND RECOMMENDATIONS.....	112
REFERENCES.....	116
APPENDIX A - PROGRAM STRUCTURE (FEPILS).....	126

LIST OF FIGURES

Figure	Page
2.1 The Free Body Diagram for Janssen's Material Slice.....	9
2.2 Reimbert's Distribution of Material Weight.....	12
2.3 Comparison of Different methods of Pressure Calculation.....	16
2.4 Funnel Flow Below an Effective Transition.....	19
2.5 Mass Flow.....	19
2.6 Yield Locus of Coulomb's Solid.....	22
2.7 Stresses on an Element Flowing through Bin and Hopper.....	22
2.8 Mass Flow Loading.....	25
2.9 Stresses on an Element of Solid.....	27
2.10 Radial Pressure Field in Hopper.....	30
2.11 Pressure in Mass-Flow Bins.....	32
2.12 Section of Fording Coal Silo.....	47
2.13 Section of Test Silo - Technical University of Denmark.....	49
3.1 Forces on Element k.....	59
3.2 Boundary Element and Friction Forces.....	59
3.3 Flow Chart for Solution Scheme of Friction Force.....	63
4.1 Idealized Stress-Strain Curve.....	68
4.2 Yield Surface and Criteria of Loading and Unloading.....	68
4.3 William Warnke Failure Surface.....	74

Figure	Page
4.4 Drucker-Prager Failure Surface.....	77
5.1 Finite Element Idealization of Silos.....	83
5.2 Comparison of Finite Element Results with Classical Theories.....	87
5.3 Stress Field When Outlet is Closed and Silo Charged.....	90
5.4 Stress Field During Flow for $\theta' = 20.56^\circ$	91
5.5 Stress Field During Flow for $\theta' = 24.78^\circ$	92
5.6 Stress Field During Flow for $\theta' = 29.98^\circ$	93
5.7 Stress Field During Flow for $H/D = 2.5$	94
5.8 Stress Field During Flow for $H/D = 3.0$	95
5.9 Yielded Material Zones When θ' is Varied.....	97
5.10 Yielded Material Zones When ϕ is Varied.....	98
5.11 Yielded Material Zones When ϕ' is Varied.....	99
5.12 Yielded Material Zones When v is Varied.....	100
5.13 Displacement/Velocity Field for $\phi' = 25^\circ$	101
5.14 Displacement/Velocity Field for $\phi' = 20^\circ$	102
5.15 Displacement/Velocity Field for $\phi' = 15^\circ$	103
5.16 Pressure Distribution When ϕ is Varied.....	105
5.17 Pressure Distribution When ϕ' is Varied.....	106
5.18 Pressure Distribution When θ' is Varied.....	108
5.19 Pressure Distribution When H/D is Varied.....	109
5.20 Pressure Distribution When v is Varied.....	111

LIST OF SYMBOLS

- A = cross-sectional area, or Jenike's strain energy parameter
 A_c = area of horizontal cross-section of the vertical part of bin
 B = Jenike's strain energy parameter, or constant for Reimbert's equation
 $[B]$ = matrix of differential operator relating displacement/velocity field to strain field
 $[C]$ = constitutive matrix
 $[C]^e$ = elastic constitutive matrix
 C_{ijkl} = constitutive tensor
 D = bin diameter
 E = Young modulus
 EYL = effective yield line
 f = yield function
 f'_c = unconfined yield strength
 f_{cu} = uniaxial compressive strength
 $F_i, \langle F \rangle$ = body force field in tensor and matrix form
 F_s = force in spring for one radian sector
 $F_T, \langle F_T \rangle$ = friction force and its vector
 F_x, F_y = horizontal and vertical component of friction force
 g = potential function
 H = contained material height or silo height
 h_1 = height of material cone

I_1, J_2 = stress invariants
 k = ratio of pressure σ_θ and σ_r (related to Janssen's K factor), or Drucker-Prager Constant for failure surface
 k_{BE} = stiffness of boundary element
 K = Janssen's constant, ratio of horizontal to vertical pressure
 $[K]$ = structure stiffness matrix
 $[K_R]$ = element stiffness matrix
 $[K_{BE}]$ = boundary element stiffness matrix
 λ = denotes length
 M = Jenike's strain energy parameter
 N = Jenike's strain energy parameter
 $[N]$ = matrix of interpolation function
 p = horizontal pressure
 P = concentrated normal force per unit length, or perimeter of cylindrical portion of bin
 q = vertical pressure
 q_n = co-efficient in calculation of vertical force in hopper
 $q_i, \langle q \rangle$ = equilibrating load vector
 Q_c = total vertical load across solids in cylindrical portion of bin at transition
 Q_n = total vertical force across solid in hopper
 r = radial distance, or radius, or horizontal coordinate

$\langle r \rangle$ = displacement/velocity field, or d.o.f. of structure
 $\langle R \rangle$ = load vector
 S_{ij} = deviatoric stress tensor
 S = nondimensionalized stress parameter
 S_i = nondimensionalized initial pressure parameter
 S_f = nondimensionalized flow pressure parameter
 $T_i, \langle T \rangle$ = surface traction field in tensor and matrix form
 u = displacement/velocity in horizontal direction
 v = displacement/velocity in vertical direction, or shear stress
 V = friction force per unit length, or volume
 w_T = tangential component of displacement/velocity
 w_n = normal component of displacement/velocity
 W = strain energy or work
 W_I = internal work
 W_E = external work
 x = Jenike's transformed co-ordinate
 z = vertical coordinate, or Reimbert's vertical distance from base of cone, or vertical distance from free surface of material
 z_o = depth of switch location
 α = coefficient of compressibility of solid material, or Drucker-Prager constant for failure surface.
 γ = unit weight of material
 δ = effective angle of internal friction, or denotes variation

Δ = denotes increment
 ϵ, ϵ_{ij} = denotes strain and strain tensor respectively
 $\epsilon_v, \epsilon_n, \epsilon_c$ = vertical, horizontal, and hoop strain respectively
 ϵ_e pr ϵ^e = elastic strain component
 ϵ^p = plastic strain component
 ϵ_{ep} = elastic-plastic strain
 ϵ^0 = initial strain
 θ' = hopper slope with vertical
 θ_s = spring inclination with horizontal
 θ_m = angle of similarity
 λ = scalar function
 ν = Poisson's ratio
 π = an irrational number denoting the ratio of circumference of a circle to its diameter
 σ, σ_{ij} = denotes stress and stress tensor respectively
 σ_1, σ_2 = major and minor principal stresses
 σ_r = stress or pressure in radial direction
 σ_θ = stress or pressure normal to σ_r
 σ_T = tangential stress
 $\sigma_v, \sigma_n, \sigma_c$ = vertical, horizontal or normal, and hoop pressure respectively
 σ_m = mean normal stress
 τ_m = mean shear stress
 ϕ = angle of internal friction of material
 ϕ' = angle of wall friction
 $()^0$ = denotes initial quantities

$()^T$ = denotes transpose

$(\bar{})$ = denotes prescribed quantities

$(_)$ = denotes nodal quantities

CHAPTER 1 - INTRODUCTION

1.1 Silo and History

Storing and handling of bulk materials are essential aspects of grain, chemical and mining operations. For the last twenty years, these industries have explored the use of silos of increasing height, diameter and storage capacity. A silo is a deep bin, used to store and to feed bulk material, when required, at some specified rate. A thorough understanding of the flow characteristics of the contained material, the flow pattern, which develops as a result of discharge of material, and the lateral pressure exerted on the silo wall during flow of contained material are essential for designing an economical and reliable silo structure, having a long operational life.

The lateral pressure exerted by stored materials on silo walls has been under study for the past hundred years. Before 1860, designers assumed that a granular material behaves as a quasi-liquid and exerts pressures similar to hydrostatic pressures. This assumption overestimated the horizontal static pressure and bottom pressure, and did not account for the friction between the stored solid material and the silo wall. Issac Roberts in the early 1880's, conducted experiments on a bin model and concluded that the vertical and lateral pressures of a grain silo did not increase after the material depth reached twice the smaller cross sectional dimension. The friction between

stored solid material and the wall transferred the weight to the wall through the height.

In 1885, H.A. Janssen developed a method to calculate granular material pressures on the silo wall and bottom. Airy (1898) proposed an alternative method of computing pressure. Toltz (1897), Bovey (1904), and Ketchum (1909) conducted tests and found that the static pressures compared favourably with Janssen's predictions while the dynamic pressure during withdrawal of granular material showed an increase up to 10%. That initial period of growth in silo research was characterised by experimental precision and great clarity of formulation.

The observation of early investigators that bin pressures were not constant but varied between the initial condition of charging and the condition of flow, was confirmed experimentally by Shumsky (1941), Bernstein (1947), Reimbert (1956), Bergau (1959), Kovtun and Platonov (1959), Kim (1959), Pieper and Wenzel (1964), Turitzin (1963), and Balnchard and Walker (1966). Shumsky, Pieper and Wenzel, and Walker reported that further refining the testing techniques showed that not only flow pressures exceeded the initial pressures, but certain undefined conditions led to high peak loads which occurred not at the base of the silo but at some higher location in the structure.

These results indicate that an active pressure develops during charging of the solid material into a bin, whereas a

passive pressure develops during flow of the material from the bin [Kottler (1899), Ohde (1950), Jenike (1954), Nanninga (1956), Pieper, Mittelman and Wanzel (1964), Pieper, Schnelle and Wenzel (1965), Walker (1966)].

Nanninga reported that at the plane of transition from an active pressure field in the upper part of the bin to a passive pressure field in the lower part, an overpressure at the wall is required to maintain equilibrium of the flowing mass.

Since 1965, excellent experimental and theoretical work have been reported. One of the most important silo developments in the last two decades is the increased understanding of flow characteristics of the stored solid material. Johanson (1964) used the method of characteristics to determine the stress in converging flow channels. Walker (1966) and Walters (1973) developed methods for calculation of flow pressures. Jenike et al. (1968) defined the concepts of mass flow and funnel flow in silos, and derived differential equations for mass flow. Jenike et al. (1973) developed analytical methods for dealing with both mass and funnel flow, based on an energy approach. Claque and Wright (1973) and Bransby et al. (1973) experimentally measured the pressures developed during mass flow. Johanson (1965) and Williams (1974) developed formulas for computing discharge rates from a mass flow conical hopper. In 1977 the American Concrete Institute developed its first code of practice entitled

"Recommended Practice for Design and Construction of Concrete Bins, Silos, and Bunkers for Storing Granular Materials (ACI 313-77)".

Presently, investigators are developing and modifying existing theories for more precise prediction of flow and pressure. Several finite element models have been developed to predict the behavior of flowing mass in silos, and the pressure exerted on the silo wall. Bishara and Chandrangsou (1978) developed a finite element model capable of handling a nonlinear viscoelastic material. Jofriet and Dickinson (1984) developed a finite element model for a flat bottom silo. Eibl and Häussler (1984) have formulated a finite element model for a mass flow silo using an elastic viscoplastic constitutive law.

1.2 Scope and Objective of Thesis

The objectives of this thesis can be summarized as:

1. To review classical theories used by different design codes for calculating wall pressures imposed by the contained solid, the finite element models developed by different research groups, and full scale silos test results.
2. To develop a finite element model and program (FEPILS) for mass flow axisymmetric silos, using an elastic perfectly plastic material model and accounting for wall friction.
3. To run sample problems and investigate the pressure

and stress distribution using program FEPILS.

4. To compare these pressures and stresses with the classical theories and methods of analysis.
5. To investigate the influence on pressure distribution, when the angle of internal friction of material, angle of wall friction, hopper geometry, height of silos, and Poisson's ratio of the contained granular solid materials vary.

1.3 Organization of Thesis

Chapter 2 is divided into three parts. Part one contains a review of classical theories with emphasis on Janssen's, Reimbert's and Jenike's theories. Part two of this chapter discusses the finite element method of analysis developed by different research groups. The last part of this chapter reviews the field measurements of full scale silos.

In Chapter 3 a finite element model for incremental analysis of axisymmetric silos is presented. Friction forces and the associated boundary conditions are formulated. Numerical technique for solution of friction problem is described.

Chapter 4 discusses the type of material and failure surface used to represent the behavior of granular solid material.

A finite element program for investigation of loading on axisymmetric silos (FEPILS) is described in Appendix A.

The solution technique incorporated in the program, which includes the numerical method adopted for loads and friction forces are discussed. The incremental implementation of the plastic model is also discussed in this chapter.

In Chapter 5 sample problems are analyzed to investigate the capability of program FEPILS. The results of the analyses are compared with classical theories. A set of problems is run varying the angle of internal friction, angle of wall friction, hopper geometry, height of silos and Poisson's ratio of contained material to investigate their effect on pressure distribution.

Chapter 6 contains summary and conclusions.

CHAPTER 2 - THEORY AND ANALYSIS

2.1 Static Pressure Theories

2.1.1 Introduction

The magnitude and distribution of pressures that are exerted by the contained material on silos are major concerns to design engineers. The pressures that are exerted by the contained material during filling are considerably different from those during discharge. Pressures that occur prior to withdrawal of materials are called static pressures or initial pressures, and those that occur whenever the material is being withdrawn through the discharge outlet are called flow pressures or dynamic pressures. Despite the developments of the last two decades in understanding the flow properties and the pressures exerted by ensiled material in silos, many codes around the world still use Janssen's and Reimbert's static theories. Since Janssen (1895) and Reimbert (1956) many researchers have worked to refine and improve these theories. The Janssen's theory and Reimbert's theory are discussed in detail because they are the basis of all current design codes.

2.1.2 Janssen's Theory

Janssen based his theory on the following assumptions.

1. Vertical pressures are uniform over any horizontal cross section of a bin. These pressures vary only

in the vertical direction.

2. Horizontal pressures are uniform over the perimeter of a cross section and vary only in the vertical direction.
3. The ratio of horizontal pressures to vertical pressures, K , is constant throughout the height of material.
4. The shear stress at the wall is a linear function of the horizontal pressure.

The free body diagram for a material slice at depth Z is shown in Figure 2.1. Vertical equilibrium of the body forces and stress resultants of the free body yields the following differential equation.

$$\frac{dq}{dZ} = \gamma - \frac{\mu' K q}{R} \quad (2.1)$$

Introducing a normalizing stress parameter, $S = q/R\gamma$, Eq. 2.1 is written as

$$\frac{dS}{dZ} = \frac{1 - \mu' K S}{R} \quad (2.2)$$

for which a solution exists in the form

$$1 - \mu' K S = e^{-\mu' K (Z/R)} \quad (2.3)$$

subject to the requirement that $S = 0$ when $Z = 0$.

Consequently the average vertical static pressure q at depth

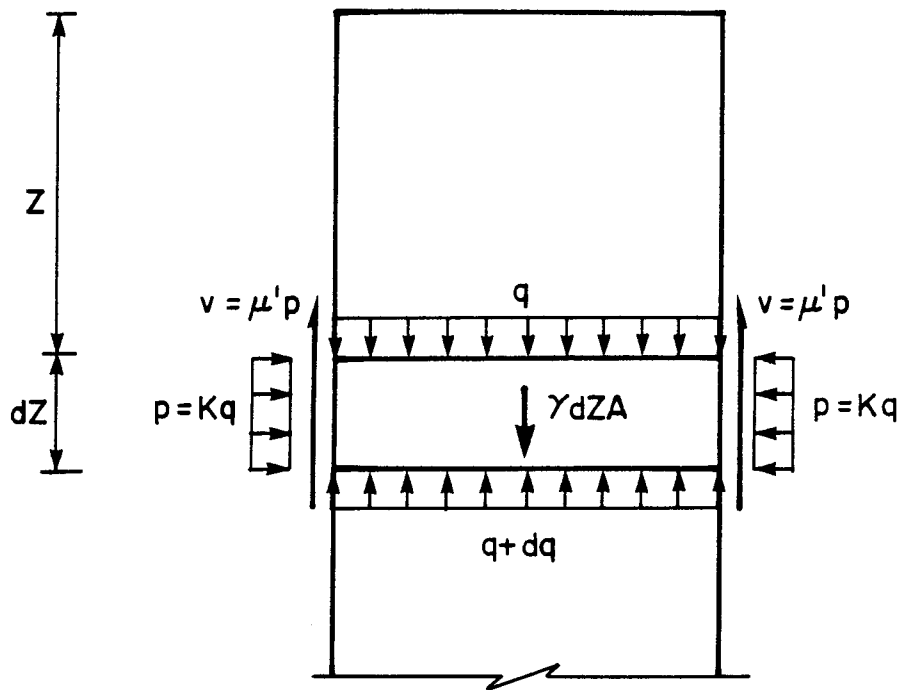


Fig. 2.1 The Free Body Diagram for Janssen's Material Slice

z below the material surface is given by

$$q = \frac{\gamma R}{\mu' K} [1 - e^{-\mu' K Z / R}] \quad (2.4)$$

The ratio of vertical to horizontal pressure, K, is independent of magnitude of pressure, so that the lateral unit pressure p is given by

$$p = Kq = \frac{\gamma R}{\mu'} [1 - e^{-\mu' K Z / R}] \quad (2.5)$$

Janssen's theory is applicable to axisymmetric and two dimensional (plain strain) problems, because symmetry requires that no shear stress occurs on a plane orthogonal to the radial direction. However this theory can be applied to unconventional cross sections, with some loss in accuracy (Fintel, 1974).

It is apparent from Eq. (2.5) that as depth z increases, the lateral static pressure, p, on the silo wall asymptotically approaches:

$$p = \gamma R / \mu' \quad (2.6)$$

which is the maximum lateral pressure, corresponding to a vertical pressure in which the wall friction force exactly balances the additional weight of the material at an infinite depth.

2.1.3 Reimbert's Theory

Reimbert's theory is based on experimental work conducted on a full scale silo in 1954 (Reimbert 1955). Many silo design codes recommend this theory as an alternate to Janssen's theory for computation of static pressures. Fig. 2.2 reveals graphically the various asymptotes used by Reimbert for his derivation.

Reimbert defines the total vertical load at any depth Z as Q_T , if there is no wall friction acting on the material in the silo.

$$Q_T = Q_O + \gamma AZ \quad (2.7)$$

where $Q_O = \frac{\gamma Ah_1}{3}$ is the weight of the conical surcharge. This is shown in Fig. 2.2 as Curve I. He further defines Q_w as that component of vertical wall force transferred to the silo wall by friction. This force increases from zero at the free surface of the material to an asymptote parallel to Curve I, because at great depths, the weight of the material is exactly balanced by wall friction. This is shown by Curve II, which is tangent to Z -axis at $Z=0$. Its asymptote is at an angle γA from Z axis and has an origin at $-(Q_{\max} - Q_O)$, where Q_{\max} is the maximum vertical force. The difference between the values of Curve I and Curve II yield Curve III which is the variation of lateral wall force with depth. Curve II can be represented by an expression of hyperbolic form as

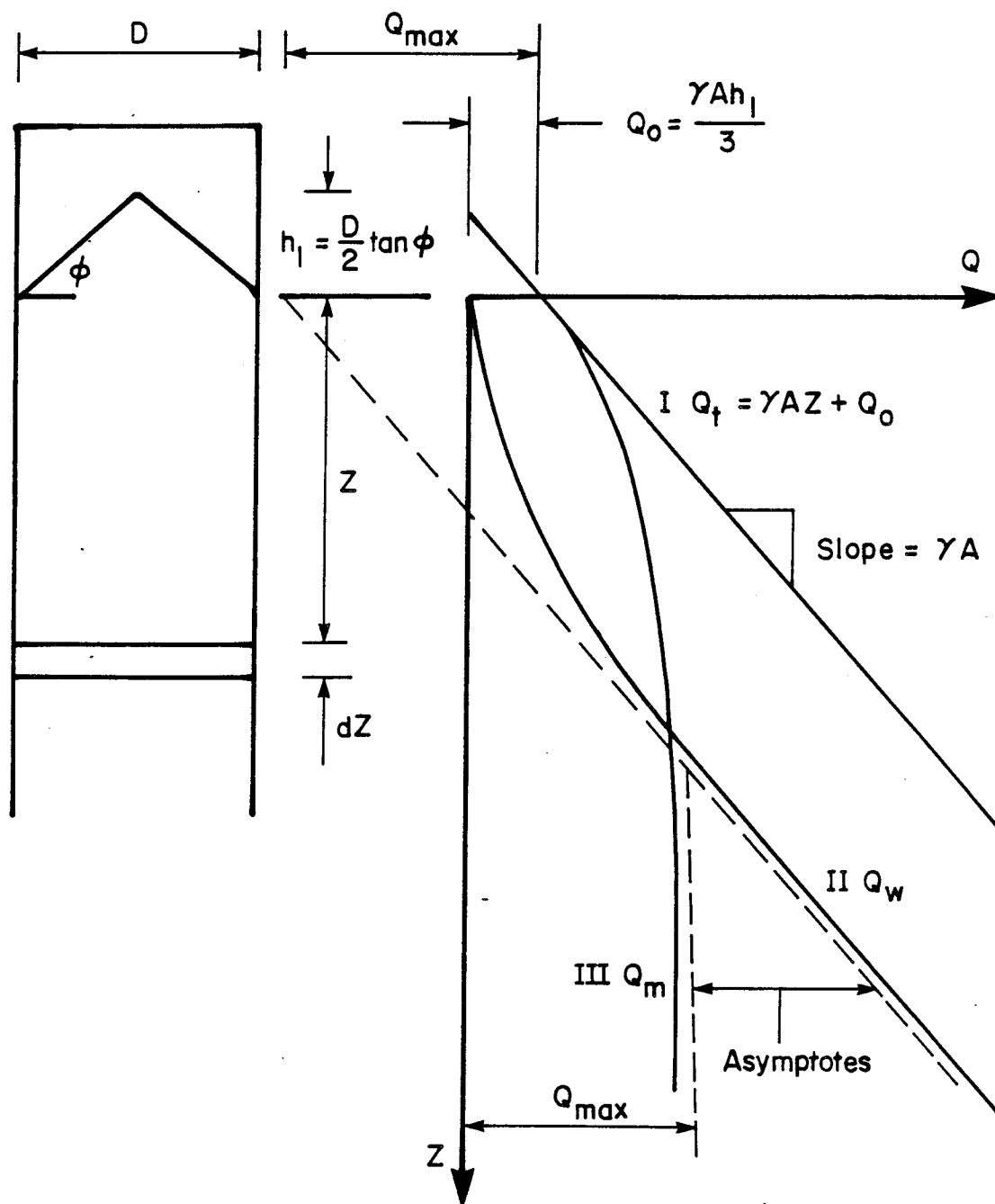


Fig. 2.2 Reimbert's Distribution of Material Weight

$$Q_w = \frac{e\gamma A Z^2}{eZ + f} \quad (2.8)$$

Satisfying necessary boundary conditions, the coefficients e and f can be determined and Eq. 2.8 takes the following form

$$Q_w = \frac{\gamma A Z^2}{Z + B} \quad (2.9)$$

$$\text{where } B = \frac{Q_{\max} - Q_o}{\gamma A} = \frac{R}{\mu' K} - \frac{h_1}{3} \quad (2.10)$$

Differentiating Eq. 2.9

$$dQ_w = \frac{\gamma A [Z^2 + 2BZ] dz}{(Z + B)^2} \quad (2.11)$$

This expression can be equated to the lateral static pressure at depth Z , which yields

$$pP\mu' dz = \frac{\gamma A [Z^2 + 2BZ] dz}{(Z + B)^2} \quad (2.12)$$

Hence

$$p = \frac{\gamma A}{P\mu'} \left[1 - \frac{1}{(Z/B + 1)^2} \right] \quad (2.13)$$

Both Janssen's and Reimbert's formulas for pressure have similar asymptotes as Z approaches ∞ . Whereas Janssen's solution assumes an exponential form, Reimbert's solutions takes a hyperbolic form. In addition Reimbert's theory

accounts for the surcharge of the material which is commonly found at the top of ensiled materials under static conditions.

2.1.4 Discussion

Lateral pressures on silo walls under static or filling conditions can be predicted reasonably well from Janssen's and Reimbert's methods. However experimental evidence shows that pressures during flow of granular solid materials can be greater than the static pressures. Recent Codes of Practice recognize these overpressures and recommend that pressures on silo walls be calculated by Janssen's or Reimbert's method and then multiplied by an "overpressure factor" to obtain design pressures.

Some investigators have examined Janssen's work critically, and attempted to refine his theory under relaxed assumptions. Jenike, Johanson and Carson (1973) pointed out that Janssen's formula is a lower bound on the average pressures, and not necessarily the actual pressure on silo walls. Bagster (1971) suggested that the common interpretation of Janssen's K factor as being $(1-\sin\phi)/(1+\sin\phi)$ is erroneous and that it should vary between that and $(1-\sin^2\phi)/(1+\sin^2\phi)$. Dabrowski (1965) and Walker (1966) stated a similar conclusion. Walker (1966) reported that the principal stresses at the bin centre are not equal to the principal stresses in the wall vicinity. He also stated that the compaction of loaded materials below

charging materials causes subsidence and frequent full mobilization of wall friction. Lavin (1970) noted that the vertical pressure is not uniform over the horizontal cross-section, and analyzed the vertical equilibrium of a differential ring element (as opposed to Janssen's disc shaped element). His solution shows agreement with the limiting pressure predicted by Janssen's equation. The modified-Janssen solution given by Walker (1966) deals with this assumed cross-sectional nonuniformity by describing the variation of K over the cross-section. Walker's solution can be thought of as a smoothed approximation of Lavin's exact analysis.

A numerical comparison of different methods of pressure calculation is presented in Figure 2.3, for a particular silo geometry, and material properties.

2.2 Flow Pressure Theories

2.2.1 Introduction

Recent studies by Walker (1966), Walters (1973), Jenike et al. (1968-1973) and many other investigators have clearly shown that pressure occurring during emptying of silos, under certain circumstances, substantially exceed the static pressures calculated by Janssen's or Reimbert's methods. Theimer (1969) and Sadler (1976, 1980) described a number of bin failures caused by overpressures associated with flow conditions among other factors. Flow theories that account for these overpressures have been developed by Walker,

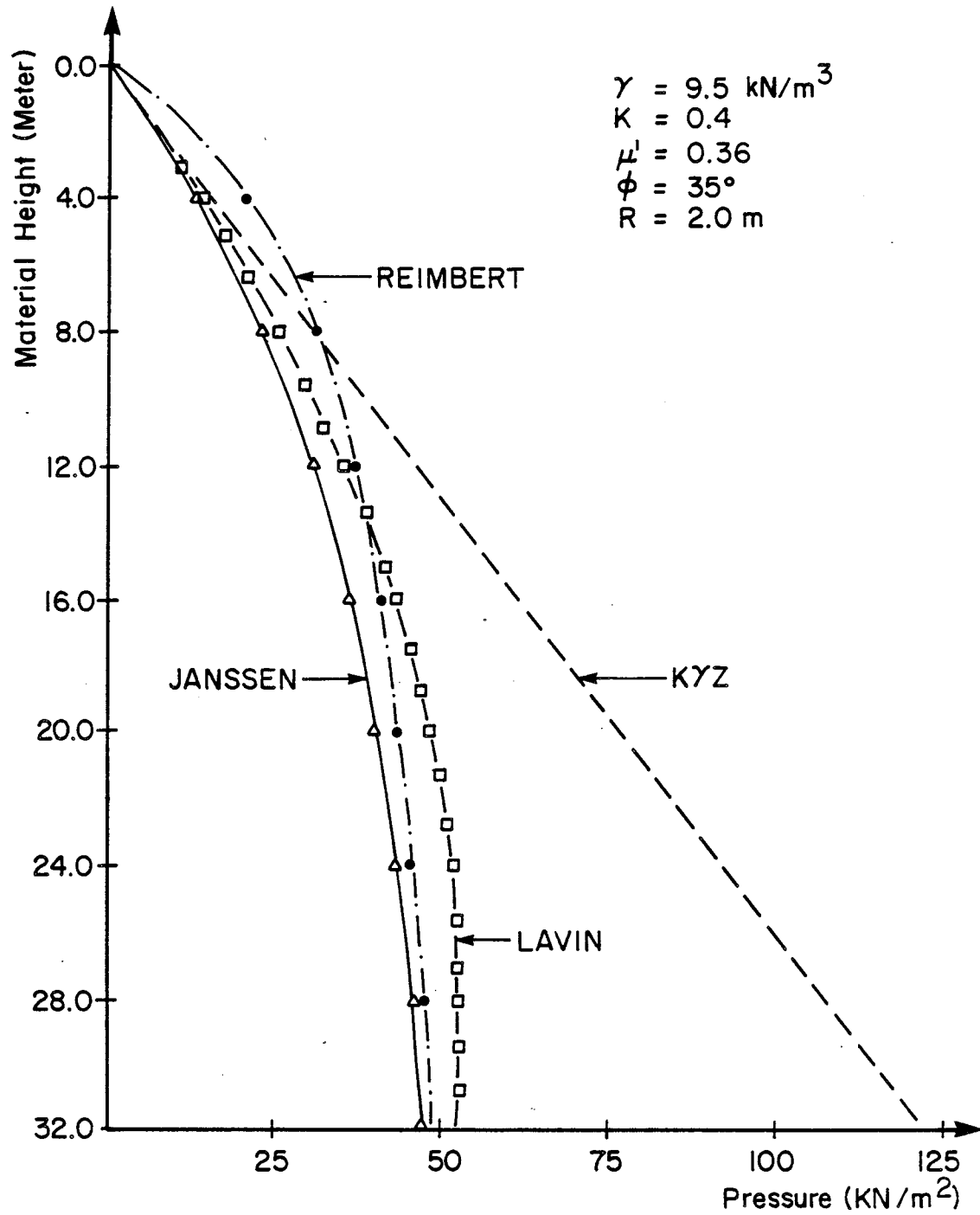


Fig. 2.3 Comparison of Different Methods of Pressure Calculation

Walters and Jenike and Johanson.

2.2.2 Flow Pattern

A knowledge of the flow characteristics of granular solids and the flow pattern which may develop in a silo is essential for understanding the magnitude and distribution of pressures on a bin wall. Two basic flow patterns have been identified by Jenike et al. (1968).

Funnel Flow

This type of flow occurs in bins with a flat bottom or with a shallow or rough hopper offering great resistance to the flowing material. In these cases flow may occur through a channel formed within stagnant material. The channel is usually conical in shape, having lower diameter equal to the effective dimension of the outlet and increases in diameter as it extends upwards. In tall bins or silos, the channel boundaries may expand to intersect the vertical wall at a point defining an effective transition to mass flow (Fig. 2.4). Bins exhibiting funnel flow are common in industry and are least costly. This type of flow is disadvantageous when handling materials susceptible to deterioration. In addition, the formation of ratholes and stable arches may occur.

Mass Flow

Mass flow occurs in bins with sufficiently steep and smooth hoppers, adequate outlet size and where the entire volume of solids is flowing with no stagnant or dead zones. In mass flow bins the flow channel boundary coincides with the wall and hopper surfaces, as shown in Figure 2.5. In general mass flow has the following characteristics:

1. Uniform flow.
2. The bulk density of the solid is constant, and independent of the head of stored solid.
3. Pressure across any horizontal cross section is relatively uniform.
4. There are no dead regions within the bin, hence there is a minimum of consolidation at rest.

Jenike (1964, revised 1976) provides a meaningful criteria for predicting gravity flow or no-flow of solids in a bin. He states that gravity flow will occur in a channel if the yield strength which the solid develops as a result of the action of consolidating pressure is not sufficient to support an obstruction to flow.

As an element of solids flows downwards, it compacts under a major consolidating stress, σ_1 acting within the bin, and develops unconfined yield strength, f'_c . For an obstruction to fail, the stresses in an obstruction must reach the yield strength at the critical location. The major stress that acts on the abutment of an arch has been

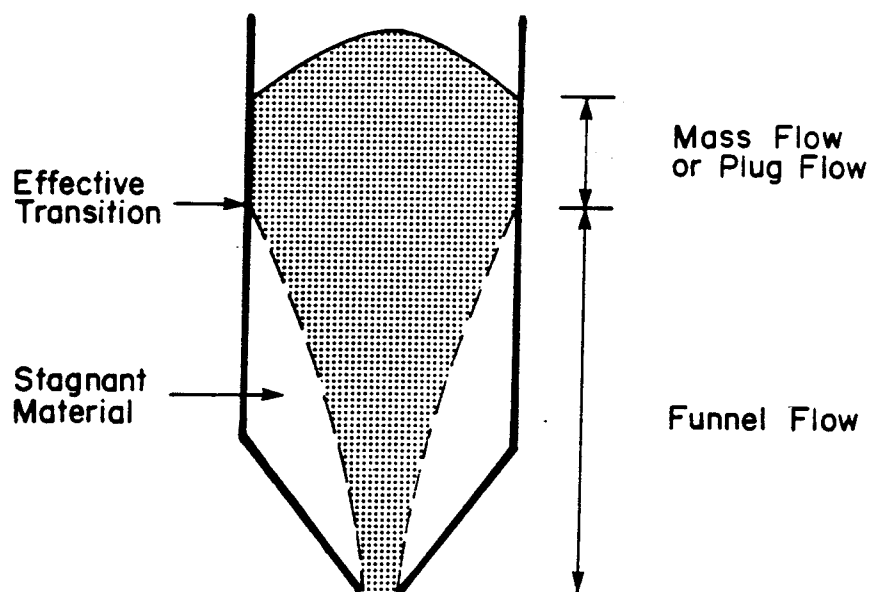


Fig. 2.4 Funnel Flow Below an Effective Transition

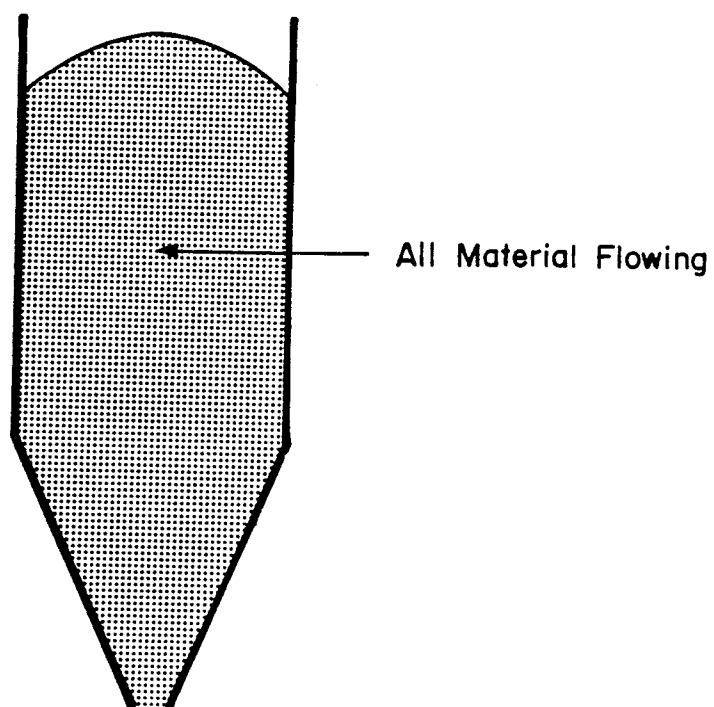


Fig. 2.5 Mass Flow

shown to be directly proportional to Span B of an arch. The flow criteria is expressed by

$$\bar{\sigma}_1 > f'_c \quad (2.14)$$

Jenike (1960) has shown that the stress, $\bar{\sigma}_1$, acting at the abutments of an arch, can be expressed by

$$\frac{\bar{\sigma}_1}{\gamma B} = \frac{1}{H(\theta)} \quad (2.15)$$

where γ = bulk density

B = diameter of circular opening

$H(\theta)$ = a function of hopper slope measured from the vertical.

The unconfined yield strength, f'_c , is determined by a shear test under appropriate consolidating stress. In all of Jenike's theories discussed subsequently a flow situation is assumed to exist.

2.2.3 Jenike's Theories

Jenike and Shield (1959) assumed that a bulk solid can be represented by a rigid-plastic coulomb solid. Such a solid is characterized by an effective yield locus (EYL) that defines the limiting shear strength under any normal stress (Fig. 2.6). Plotting shear stress, τ , and normal stress, σ , the yield locus for a coulomb solid intersects the τ axis at a value of τ defined as the cohesion, c , and

has a slope equal to the angle of internal friction, ϕ . Jenike and Johanson (1968) in their analysis of pressure fields assumed that in the plastic region the solid is isotropic, frictional, cohesive and compressible. During incipient failure the bulk solid expands and during steady flow it can either expand or contract. The state of stress at any point is independent of time and is unaffected by velocity changes. As an element of solid flows through a channel, shown in Fig. 2.7, the major consolidating stress σ_1 and the minor consolidating stress σ_2 on the element change and continuous shear deformation occurs.

When the material stops flowing, it is assumed that these stresses remain. The material gains strength at a stationary condition under these stresses and resists the flow of solids when the bin outlet is reopened. For any stress condition represented by a Mohr circle tangent to the locus, the bulk solids are at yield, and the major and minor consolidating stresses at this condition are defined by intersection of the circle with the σ axis (Fig. 2.6).

Jenike (1954), Walker (1966) and Handly and Perry (1968) have demonstrated experimentally and Smoltczyk (1953) and Jenike (1961) have shown analytically that pressures within a solid contained in a hopper have a tendency to decrease towards zero at the vertex of a hopper. A radial (meridional) pressure field is said to occur, when the pressure decreases linearly, and the pressures along a given ray are proportional to the distance from the vertex. It is

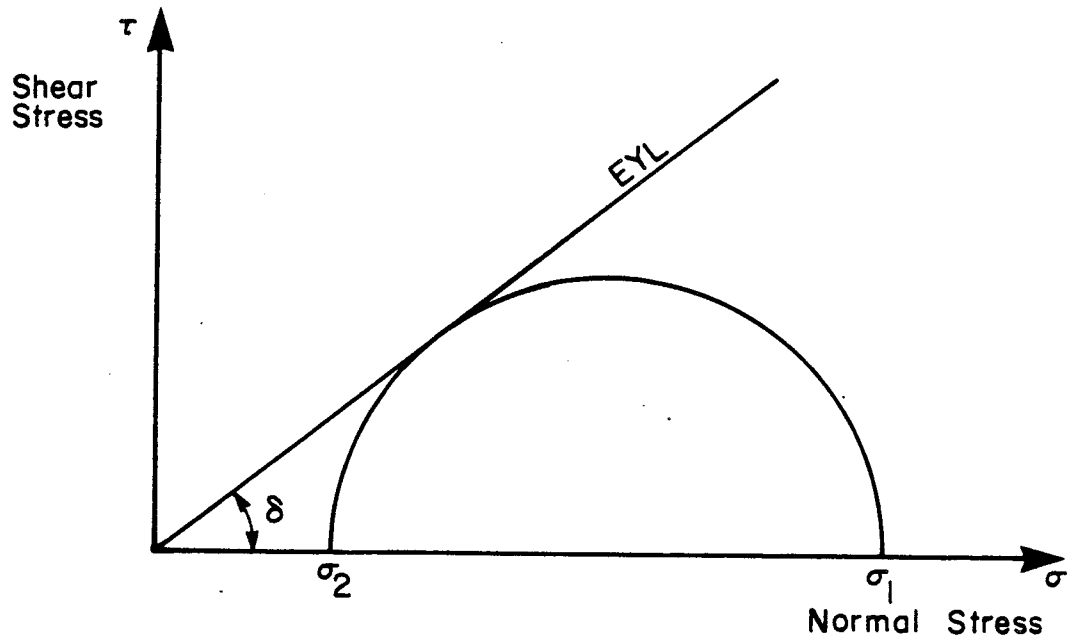


Fig. 2.6 Yield Locus of Coulomb's Solid

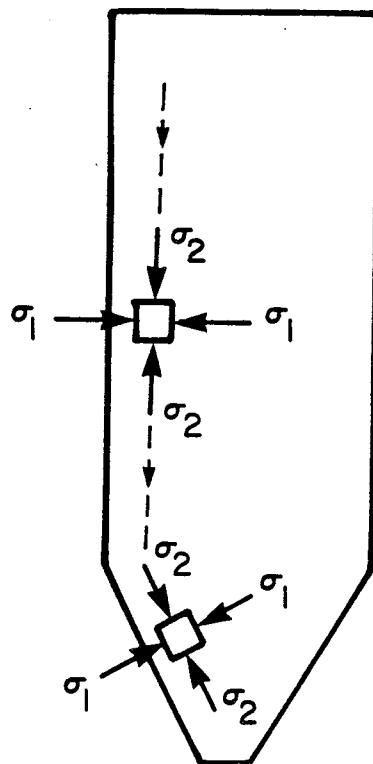


Fig. 2.7 Stress on an Element Flowing Through Bin and Hopper

apparent that a radial field cannot extend all the way upward to a free surface, and is topped off by a compatible pressure field decreasing upwards towards the free surface. At the interface, these two pressure fields do not match and a disturbed radial stress field develops, which consists of a wave of overpressure and underpressure superimposed on radial pressure; the wave decays rapidly towards the vertex of the hopper.

When an empty bin with a closed outlet is charged, the material contracts and slips along the wall. In the cylindrical part solids contract vertically only, and a plastic-active pressure field develops. In the hopper the material contracts both vertically and horizontally as slip occurs along the wall. As a result an elastic-active pressure develops because it does not reach the limiting or plastic state. Major principal stresses are assumed to act in vertical or close to vertical direction as shown in Fig. 2.8a. Pressure, p , which acts on the wall of bin increases from the top somewhat according to Janssen's formula, goes through a sharp change at the transition to hopper, and decreases towards zero at the vertex.

In a mass flow bin, when the outlet is opened the solids must contract horizontally and expand vertically in order to flow in the hopper. This causes the major stress to act in a direction close to the horizontal, forming what is defined as a plastic-passive pressure field, as shown in Fig. 2.8b.

Nanninga (1956) was the first to observe that at the transition from active to passive pressure fields, equilibrium of the mass requires an overpressure to occur. Jenike and Johanson (1968) and Walters (1973) postulated that a large transient "switch" pressure develops when the flow is initiated in a bin. During initial loading an active stress field is generated. When discharge begins, the support of the solid at the outlet is removed. The unsupported solid above the outlet expands downward. This reduces the vertical pressure within the solid in that region and causes a switch to a passive pressure field; the major principal stress now arches across the outlet. As the flow continues, the region of flow expands into the hopper, and the switch travels upwards, to a point where the hopper intersects the vertical section of the bin in a mass flow bin.

The stress conditions when the switch is at a height, Z , is shown in Fig. 2.8b. Below the switch, the pressures are in a passive (dynamic) state and smaller flow pressures develop. Above the switch the solids are still in an active state and initial pressures prevail. The material at the transition between two pressure fields is no longer supported by the flowing solids below, and the equilibrium of forces results in an additional pressure at the region of the switch.

Jenike's three major contributions to mass flow theory lie in the areas of determining the plastic stress field in

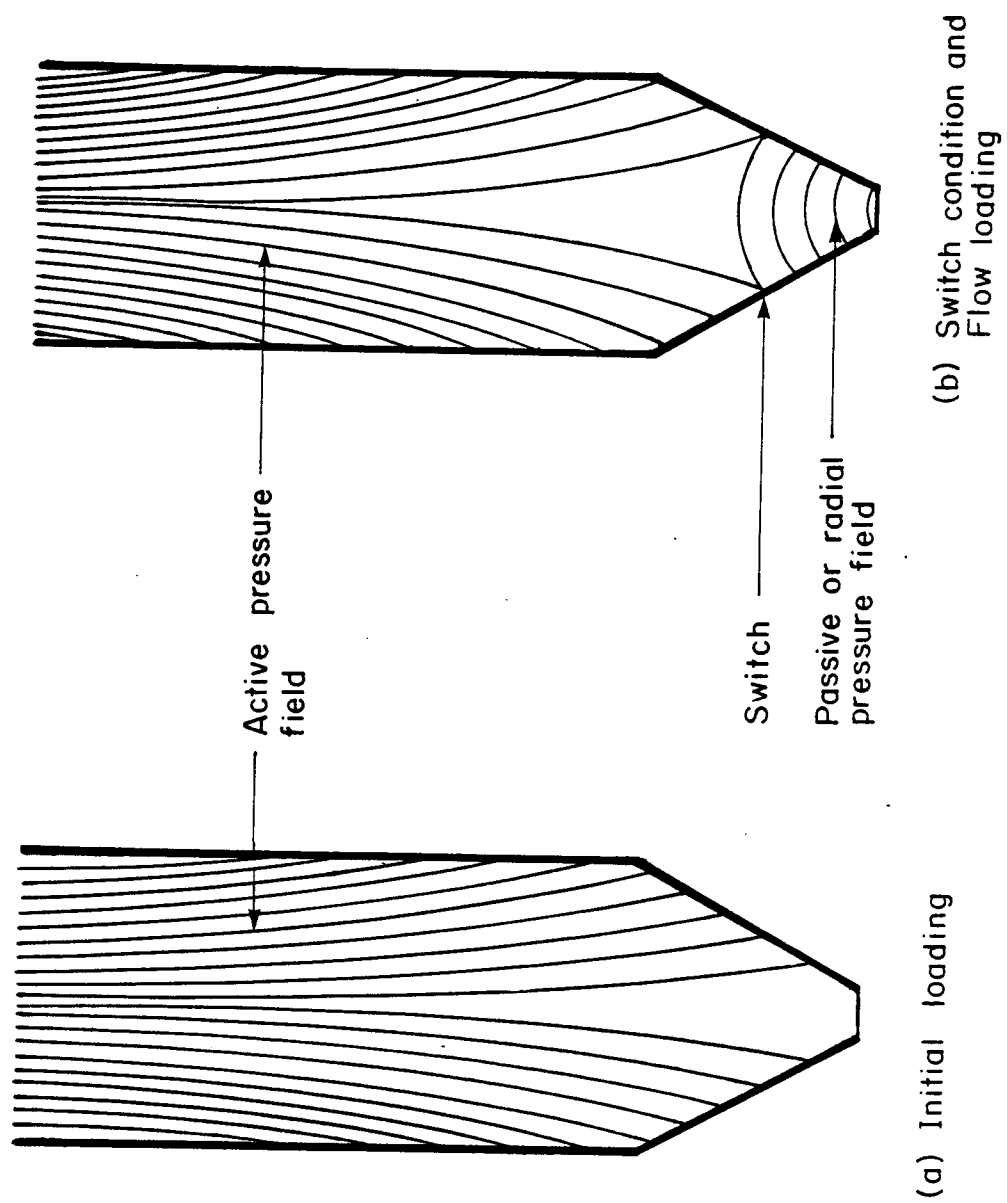


Fig. 2.8 Mass Flow Loadings

the hopper during flow, the determination of the magnitude of the major transition pressure at the juncture of the hopper and wall and finally his strain energy theory which describes the intermittent switch loads which might occur during flow on silo walls. Jenike claims that this theory accounts for the overpressures known to occur during flow of ensiled material.

In the following the basic assumptions for all three theories are discussed and results are summarized.

Stress Field in the Mass Flow Hopper: Jenike and Johanson (1968) presented an analytical method for calculating initial, flow, and switch pressures in a bin hopper with no vertical surcharge. He considered the equilibrium of an element of solid material in converging channel as shown in Fig. 2.9 and derived pressure fields for both plain strain and axisymmetric channels. The assumptions made are:

1. The solid material is nonlinear elastic during initial conditions and plastic during flow conditions.
2. Under both initial and flow conditions, a solid is assumed to slip at the walls. Hence the kinematic angle of wall friction, ϕ' , is fully developed.
3. A radial stress field is assumed which increases linearly with coordinate ray, r , from vertex of channel and is defined as

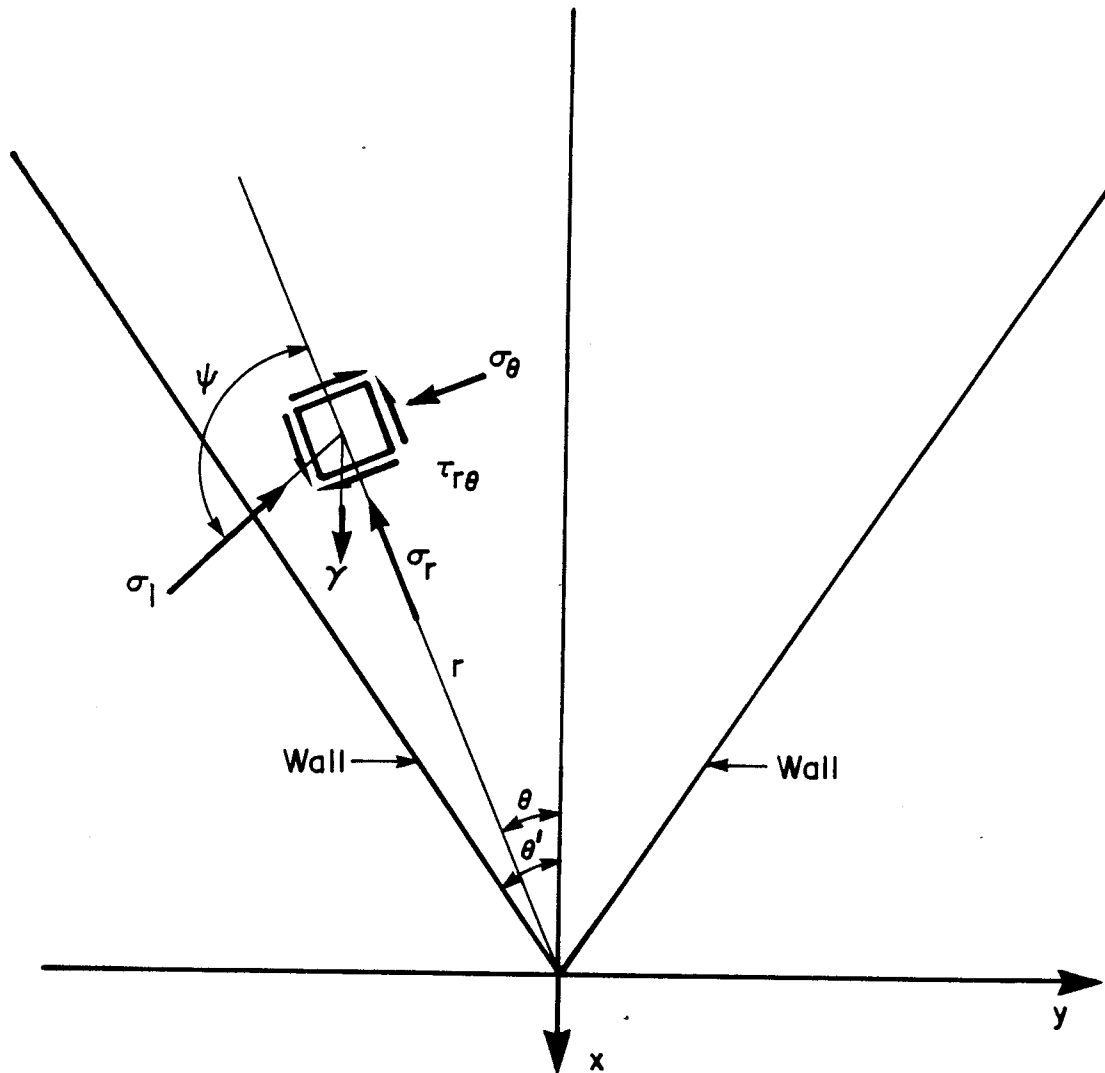


Fig. 2.9 Stress on an Element of Solid

$$\sigma = \gamma r S_i(\bar{\theta}) \quad (2.16)$$

for initial stress fields and

$$\sigma = \gamma r S_f(\theta) \quad (2.17)$$

for flow pressure fields

4. The ratio k , related to Janssen's K factor, defined as

$$k = \frac{\sigma_\theta}{\sigma_r} = \frac{1 + v(m + \alpha)}{1 + \alpha + v(m - \alpha)} \quad (2.18)$$

in which σ_r is the pressure in radial direction and σ_θ is the pressure normal to σ_r . The coefficient $m=0$, for plane strain and $m=1$, for axisymmetric case, α and v are the coefficients of compressibility of solid and Poisson's ratio respectively.

5. In flow pressure fields the principal stresses σ_1 and σ_2 are assumed to satisfy an effective yield locus (Jenike and Shield, 1959) defined as

$$\frac{\sigma_2}{\sigma_1} = \frac{1 - \sin \delta}{1 + \sin \delta} \quad (2.19)$$

where δ is an effective angle of internal friction.

On the basis of the above assumptions the differential equations have been derived for initial and flow pressure fields. The wall pressures in mass flow hoppers are assumed to have a triangular distribution as shown in Figs. 2.10a and 2.10b, when there is no surcharge. The location of the switch is uniquely defined for a given hopper configuration and solids material properties.

The peak initial pressure, p_1 , is derived as

$$p_1 = \frac{\gamma D}{1 + m i_1} \frac{1}{2(\tan \theta' + \tan \phi')} \quad (2.20)$$

in which i_1 is the relative position of peak initial pressure, and is a function of k , θ' and ϕ' .

The peak flow pressure is obtained from

$$p_2 = \frac{\gamma D}{1 + m i_2} \frac{1}{2(\tan \theta' + \tan \phi')} \quad (2.21)$$

in which i_2 is the relative position of peak flow pressure, and is a function of θ' and ϕ' . The magnitude of concentrated load at the location of switch is obtained by calculating the force equivalent to the shaded area shown in Fig. 2.10c. This force is required to maintain equilibrium of the mass of solid and acts normal to the wall,

$$P = \gamma D^2 FG \quad (2.22)$$

in which $F = 1/4 \sin \theta' (\tan \theta' + \tan \phi')$ and G is a function

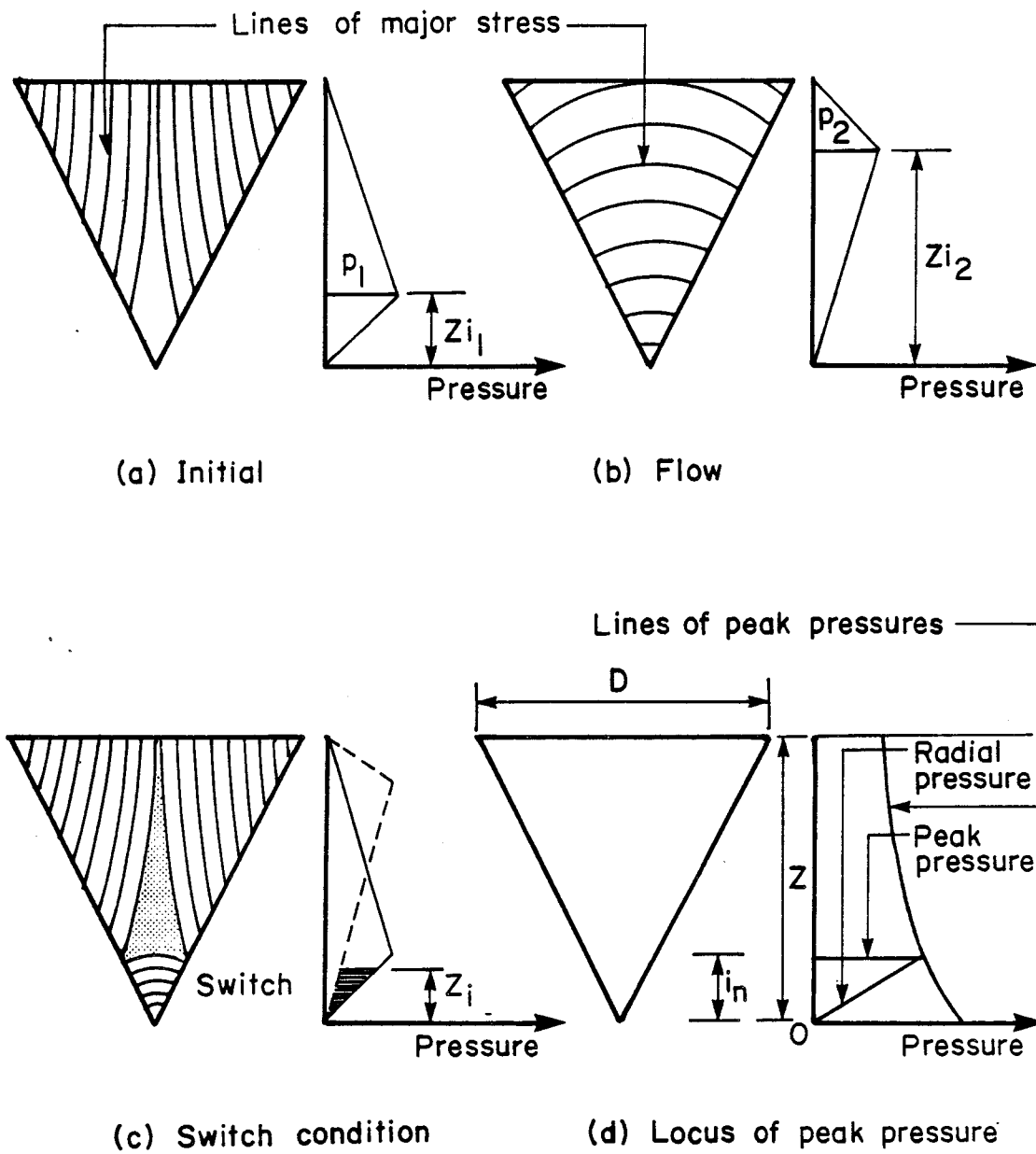


Fig. 2.10 Radial Pressure Field in Hopper

of m , i_1 , i_2 and i , the relative position of the switch.

Overpressure at Transition in Mass Flow Bins: Jenike and Johanson (1969) derived an expression for the concentrated force at the transition from the vertical part to the hopper of a bin. This force, P , occurs during the flow of a material from a bin with the vertical surcharge on hopper [See Fig. 2.11]. The vertical surcharge exerts a vertical load, Q_c , on the solids in the hopper at the transition. This can be expressed by Janssen's equation as

$$\frac{Q_c}{A_c} = q = \frac{\gamma R}{\mu' K} [1 - e^{-\mu' K Z / R}] \quad (2.23)$$

The total vertical force across a conical channel during flow has been computed for a radial pressure field by Jenike (1961) as

$$Q_n = q_n \gamma D^{2+m} L^{1-m} \quad (2.24)$$

where q_n is coefficient for vertical force in a mass flow hopper and is a function of δ , θ' , ϕ' and coefficient m . $n=1$ for initial loading and, $n=2$ for flow loading. The normal force P and frictional force V are assumed to balance the difference between Q_c and Q_n . For a cylindrical channel P and V are given per unit length of the circumference as

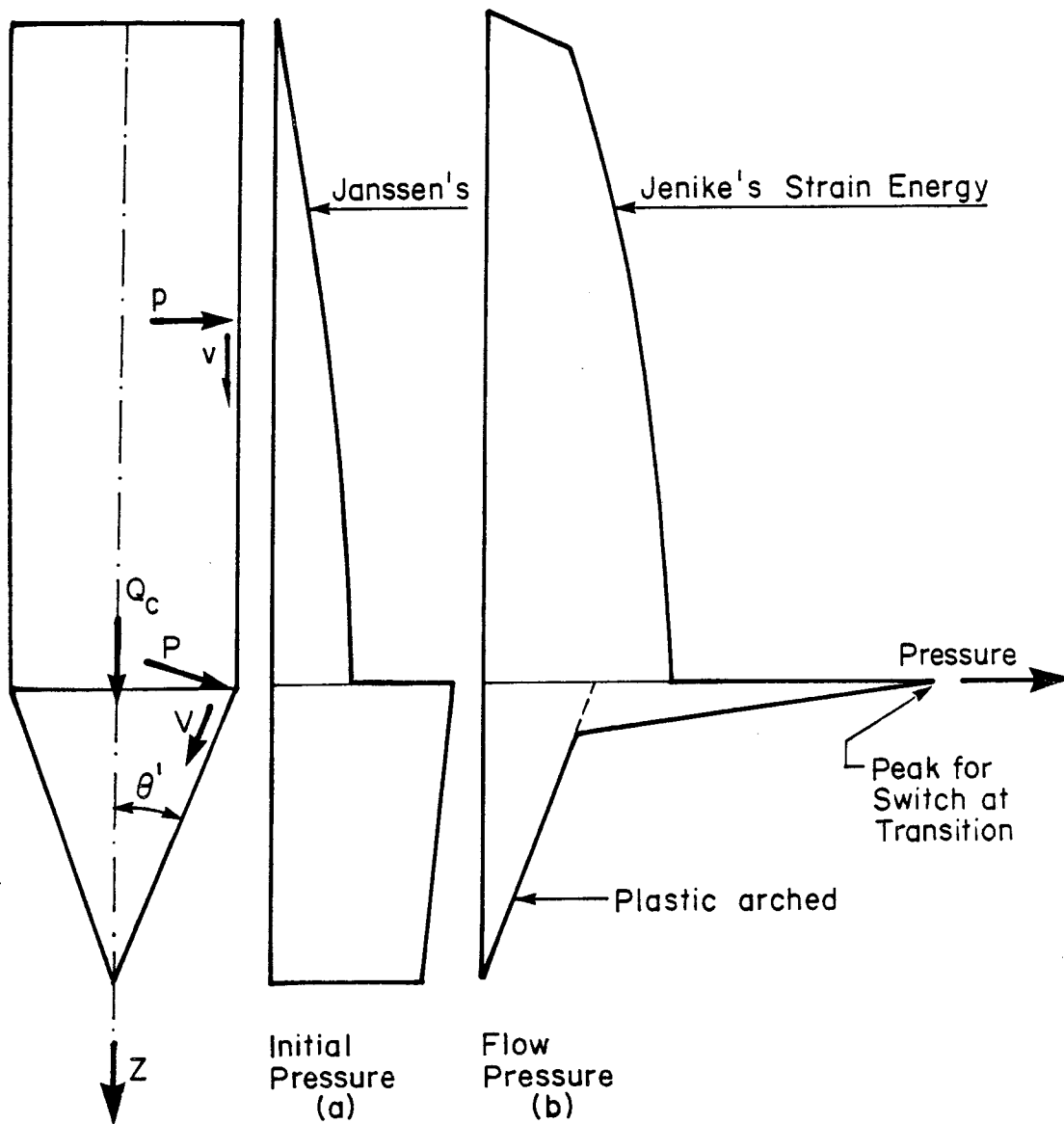


Fig. 2.11 Pressure Distributions in Mass-Flow Bins

$$P = \frac{Q_c - Q_n}{\pi D (\sin \theta' + \cos \theta' \tan \phi')} , \quad (2.25)$$

$$V = P \tan \phi' \quad (2.26)$$

Jenike et al. (1973) suggested that this force, P , can be distributed over $0.3D$ slant distance of hopper wall below transition.

Jenike's Strain Energy Theory

Jenike et al. (1973 Part 2) measured wall pressures on model bins handling sand and coke. They observed widely varying pressure fluctuations in the cylindrical portion during flow, attributed to the very slight imperfection in the shape or finish of the bin cross section. They found that the flow pressures were similar to the Janssen's pressure field, in a diverging channel of 0.5 degree, while introduction of ledges or by using a 0.5 degree converging channel, local pressures often exceeded Janssen's pressure distribution by a factor of two to three. Patches of thin boundary layers form and dissolve intermittently at the walls of cylinder due to imperfection in the shape of bin. The formation of a layer causes a switch from Janssen's to a passive stress field, and the dissolution of the layer causes a switch back to Janssen's.

An envelope enclosing the expected peak pressures at various vertical locations defines an upper bound solution to pressure. Jenike et al. (1973 Part 2) indicated that

initial wall pressures on the cylinder in a mass flow bin can be well represented by Janssen's theory. During flow, however, it gives a lower bound to the maximum wall pressure. Bins with surface imperfections can be designed on the basis of an upper bound pressure. The upper bound on the wall pressure was developed by Jenike et al. through minimizing the recoverable strain energy. The assumptions made are

1. The switch is assumed to occur at some level Z , above this level, Janssen's field is assumed to prevail while below this level a passive stress field prevails.
2. The vertical pressure is constant over any cross section.
3. Kinetic energy terms are small compared to strain energy terms and are neglected. Further, the vessel is assumed rigid and both the modulus of elasticity, E , and Poisson's ratio, ν , are assumed constant.

Jenike et al. postulated that energy is dissipated at maximum rate during flow of solids; hence, the recoverable part of energy within the flowing mass tends towards a minimum. For a slice of solid of height, dZ , the recoverable strain energy, neglecting shear strain is

$$dW = -AdZ \left[\int_{\epsilon_v} \sigma_v d\epsilon_v + \int_{\epsilon_n} \sigma_n d\epsilon_n + \int_{\epsilon_p} \sigma_c d\epsilon_c \right] \quad (2.27)$$

The recoverable part of the differential strains are

$$d\varepsilon_v = \frac{d\sigma_v}{E} - \nu \frac{d(\sigma_n + \sigma_c)}{E}, \text{ etc.} \quad (2.28)$$

where σ_v , σ_n , and σ_c are vertical, horizontal and hoop pressures and ε_v , ε_n , and ε_c are corresponding strains.

A passive stress field is assumed in terms of a stress parameter, S , and two lateral coefficients K and K_3 , as follows.

$$\sigma_v = R\gamma S \quad (2.29a)$$

$$\sigma_n = KR\gamma S \quad (2.29b)$$

$$\sigma_c = K_3 R\gamma S \quad (2.29c)$$

where R is the hydraulic radius and γ is the specific weight of solid material. For an axisymmetric case $\sigma_c = \sigma_n$ and hence $K_3 = K$.

Setting the first variation of the strain energy expression to zero, the governing differential equation is extracted. The general solution to this differential equation has the following form

$$S = Ae^x + Be^{-x} + N \quad (2.30)$$

in which

$$x = \frac{\mu'(z - z_o)}{(2 - 2\nu)^{m/2} R} \quad (2.31a)$$

$$N = \frac{2\nu}{\mu'(2 - 2\nu)^{(1-m)}} \quad (2.31b)$$

where z_o is the location of the switch. The essential and natural boundary conditions can be used to solve for constants A and B. Knowing constants A, B and N, the stress parameter can be found at any location, z , below the assumed instantaneous switch, z_o . The pressure on cylindrical portion of wall can be calculated from Eq. 2.29b.

Funnel Flow Bins

The initial pressure in a funnel flow bin can be represented by Janssen's pressure field all the way down to the outlet. When the outlet is opened flow starts through a channel formed within a stagnant mass of solids. The flow channel is conical expanding upward from the outlet. If the bin is sufficiently tall the flow channel intersects the cylindrical wall. Above this level, referred to as the effective transition, mass flow occurs.

At the level of the effective transition a switch occurs from the cylindrical pressure field, which may be a Janssen's field or a Jenike's upper bound strain energy field to a converging pressure field within. A peak pressure develops at the level of the switch. Jenike et al. (1973 Part 4) have suggested methods for calculating these

pressures and the location of the switch.

2.3 Finite Element Analysis

The developed codes of practice for determination of design loads on bins are mainly based on operating experience, pressure measurements in full size silos and pressure theories (Janssen's and Reimbert's) representing best fit test data. These theories have not been able to describe the complex behavior of flowing solids in a qualitative or a quantitative manner.

During recent years, with increasing size of silos, the uncertainty has increased by the occurrence of considerable damage to these structures.

The finite element method provides a rational technique for evaluating the pressures on the silo walls and stresses within the ensiled material. Many research groups are using the technique to reach a reliable and rigorous understanding of the silo problems. In the following the work of the three main groups is discussed.

2.3.1 The Ohio State University Group

Bishara et al. (1976) presented constitutive laws for some ensiled farm products and a finite element analysis of silage-silo interaction in a top unloading axisymmetric silo structure. It is assumed that silage is an isotropic piecewise-linear viscoelastic material contained in an elastic cylinder. The silage mass is divided into laminae,

representing the sequence of loading. The friction forces along the material-wall interface has been modeled as a force boundary and assumed to remain unchanged during each time interval. They are calculated from radial stress, at the end of previous interval, in the silage element next to the wall. The analysis of a 24' x 70' top unloading silos, with 20 silage laminas filling at 0.5 days interval, showed a highest pressure to occur at 4' above the floor. There is considerable difference between Janssen's and the finite element pressure curves. To avoid the commulative error resulting from the piecewise linear approach Karoon and Bishara (1978) developed a nonlinear finite element method using the Newton-Raphson iteration technique, based on the Lagrangian description of motion. To demonstrate the applications of developed finite element model, the same silo was analyzed. The result showed the highest pressure just after filling at 7.5 feet above the silo floor. The lateral pressure obtained is higher than that predicted by piecewise linear viscoelastic finite element formulation. The magnitude of the maximum lateral pressure decreases by almost 60% when the coefficient of friction, μ' , increases from $\mu' = 0.0$ to $\mu' = 0.4$. Bishara et al. (1983) generalized the constitutive law for granular materials and adopted the finite element program developed by Karoon and Bishara (1978), with special provision to allow for slip-stick phenomenon at the silo wall and material interface. A 24' x 70' silo filled with dry sand was used to demonstrate

the performance of finite element program. For depth of ensiled material not exceeding the diameter, the lateral pressures obtained from the developed method lie between Janssen's and Reimbert's solutions. Below that depth the pressures exceed Janssen's values by 20 to 25 percent and Reimbert's by about 10 to 15 percent. The average vertical pressure lies between Janssen's and Reimber's predicted value. However, the analysis shows that the vertical pressure distribution is parabolic over the silo cross section, with a maximum at the centre and a minimum at the silo wall. This nonuniform distribution reflects the effect of wall friction. Reimbert's and Janssen's methods do not take into account the nonuniformity of vertical pressure in their calculation.

El-Azazy (1982) modified the program developed by Beshara et al. (1978) to account for pressure during bottom unloading of farm silo by Flail unloaders. The program was further modified to simulate dome formation above the cavity created by the unloader, and the collapse of this dome. A modified Druker-Prager failure criteria was used for ensiled material. The results show that the lateral pressure at the level of dome formation, during unloading is double that during static conditions, and there is a drastic decrease in its value to near zero immediately above this level.

2.3.2 University of Guelph Group

Jofriet et al. (1977) analyzed the static pressure

exerted by a granular material on a cylindrical structure. Friction along the wall/material interface was incorporated in the model. The solution obtained was comparable to Janssen's theory, except near the bottom of cylinder. Jofriet et al. (1980) carried out a number of finite element analyses of whole-plant corn silos to investigate the effect of silo geometry and wall friction on lateral wall pressure and the proportion of vertical load carried by the wall. They assumed a linear elastic isotropic material and a rigid cylindrical boundary. The analysis has been carried out in a number of steps to simulate the filling procedure. For each solution step additional layer is added. The coordinates, the density and the elastic moduli are updated after every step.

The results of these analyses indicate that the lateral pressure increases with the decrease in aspect ratio of the silo. This trend is also predicted with Janssen's formula. It also shows an increase in lateral pressure with a decrease in the coefficient of wall friction. This is of course a result of increased vertical pressure and decreased total vertical load transmitted to the wall.

Jofriet and Dickinson (1984) developed a finite element model based on isotropic linear elastic material behavior, for a bottom-unloading farm silo. In this study the effects of base constraints, formation of arch and cavity size, coefficient of wall friction and lateral pressure ratio on the lateral wall pressure were investigated. The cavity

shape is axisymmetric and the material behavior is uniform with respect to depth in lower region. The stress distribution after formation of arch or cavity is independent of the past history of the material, and the unloading process is sufficiently slow, hence the dynamic effects can be neglected. Rigid constraints are used at the wall in the radial direction, and the vertical shear force in the wall is equal to the product of coefficient of friction and corresponding radial reaction, acting vertically upward.

The analysis of a 6 m diameter and 20 m height silo indicated that arching of the material at the cavity causes higher radial pressures on the lower region of the silo walls, than those experienced without the cavity. The material starts flowing only when the local stress state exceeds the strength of the material. It is also observed that above a height equal to the diameter, the effect of arching is negligible. The overpressure becomes more concentrated with increase in the size of cavity and the peak pressure at the base increases exponentially with linearly increasing cavity size. The lateral wall pressure decreases with increasing coefficient of wall friction, which is also indicated by Janssen's solution. The pressure ratio, K , has a negligible effect on the overpressures at the base.

2.3.3 University of Karlsruhe Group

Eibl et al. (1984) presented a nonlinear finite element analysis simulating discharge through a mass-flow silo, assuming that a granular solid during discharge exhibits a solid-like and fluid-like behavior and using an incremental viscoplastic constitutive law. Large deformations, and mass properties are formulated in the context of an Eulerian frame of reference. The following basic assumptions lead them to the formulation of finite element model.

1. Cauchy stress σ^* is divided into a rate independent part σ_s^* and a rate dependent part σ_v^* i.e.

$$\sigma^* = \sigma_s^* + \sigma_v^* \quad (2.32)$$

2. The rate independent part is defined by the elastic-plastic law proposed by Lade (1977) as

$$\Delta \sigma_s = H \Delta \varepsilon_{ep} \quad (2.33)$$

3. Strain tensor $\Delta \varepsilon_{ep}$ has been divided into an elastic component $\Delta \varepsilon_e$, a plastic contractive component $\Delta \varepsilon_c$ and a plastic expansive component $\Delta \varepsilon_p$, such that

$$\Delta \varepsilon_{ep} = \Delta \varepsilon_e + \Delta \varepsilon_c + \Delta \varepsilon_p \quad (2.34)$$

4. An isotropic hypoelastic law with stress dependent Young's modulus E , and constant Poisson's ratio, ν ,

are used to define the elastic component

$$\Delta \varepsilon_e = E \Delta \sigma_s \quad (2.35)$$

5. The plastic contractive component due to volumetric compression is determined by an associated flow rule. The plastic expansive component due to increase in deviatoric stresses, is obtained from a nonassociative flow rule.

$$\Delta \varepsilon_c = \Delta \lambda_c \frac{\partial f_{co}}{\partial \sigma_s} \quad (2.36a)$$

$$\Delta \varepsilon_p = \Delta \lambda_p \frac{\partial g}{\partial \sigma_s} \quad (2.36b)$$

where $\Delta \lambda_p$ and $\Delta \lambda_c$ are monotonically increasing positive scalars determined from plastic work functions.

6. The yield surface, f_{co} , may expand infinitely in the principal stress space, while the expansive yield surface, f_{ex} , has been limited by a surface, η . The elastic-plastic strain increment is thus given by

$$\Delta \varepsilon_{ep} = E \Delta \sigma_s + \Delta \lambda_c \frac{\partial f_{co}}{\partial \sigma_s} + \Delta \lambda_p \frac{\partial g}{\partial \sigma_s} \quad (2.37)$$

7. The rate dependent part of Cauchy stress is defined by a relation of a form analogous to the

incompressible Newtonian fluid, in terms of a material parameter called viscosity number.

8. The boundary conditions imposed on the problem are,

a) Velocity normal to bin wall is zero, $v_n = 0$

b) Velocity tangential to the normal is such that,

$$v_t = 0 \text{ if } \sigma_t < \tan \phi' \cdot \sigma_n, \text{ otherwise}$$

$$\sigma_t = \tan \phi' \cdot \sigma_n.$$

c) At the outlet $\sigma_n = \sigma_t = 0$

On the basis of above assumptions and the principle of virtual velocities the problem has been formulated in Eulerian frame of reference. Analysis of two plain strain silos, with different geometric configurations have been carried out under static conditions. The wall pressures obtained were found to be less, but close to the experimental results given by Motzkus (1974). The authors did not compare their results with Janssen's and Reimbert's theory.

Flow pressures were analyzed for 6.5' x 39' plane strain silo, with a hopper inclined at 60 degree to horizontal. The results of the analysis are summarized as

1. The flow velocity in the cylindrical portion is found to be approximately constant, i.e. the solids move like a rigid body. In the hopper area, flow velocity is maximum at the silo centre and decreases

to a minimum at the silo wall.

2. Under static conditions, the direction of the major principal stresses are close to the vertical in both the cylindrical and hopper parts. When discharge begins, the direction of the major principal stress is reoriented from the vertical to the horizontal in the hopper area, while in the cylindrical area it does not change. Subsequently the magnitude of stress decreases above the outlet, and increases near the transition area between hopper and cylinder. The stress level within the cylinder area is unchanged. This stress redistribution during flow has been explained by Jenike et al. (1968), Walker (1966) and Walters (1973) as a transition from an active state of stress to a passive state of stress.
3. The lateral wall pressure in the cylindrical area increases uniformly with material depth followed by a strong increase near the transition.
4. The normal wall pressure in the hopper area increases uniformly during the initial phase of discharging. When the flow is established the pressures near the outlet decreases and a peak pressure develops near the transition.

5. During charging the material near transition is in limit state, while the rest is in plastic hardening range. Elastic behavior occurs during the initial phase of discharging, which is transmitted to the plastic hardening range in the hopper area, and then to limit states as the flow propagates.

2.4 Field Measurements

2.4.1 Simmonds and Smith (1983)

Simmonds and Smith (1983) presented an experimental study conducted on an operating reinforced concrete coal silo, owned by Fording Coal Limited in British Columbia. The objective was to quantify material overpressure within a full scale silo.

The cylindrical portion of the silo has 70 feet inside diameter, 12 inch wall thickness and rises 155.7 feet above transition. The silo has two pyramidal outlet hoppers, all of steel plate construction, as shown in Fig. 2.12. Strain gauges have been mounted on hoop reinforcement at various locations. Actual bar strain measurements were recorded as either static or continuous.

The study showed that during flow large instantaneous overpressures coincided with quasi-static overpressures of similar magnitude. At strain gauge locations 5 and 6, there were virtually no affect during discharge, also at location 4, no overpressures were observed. Therefore, the

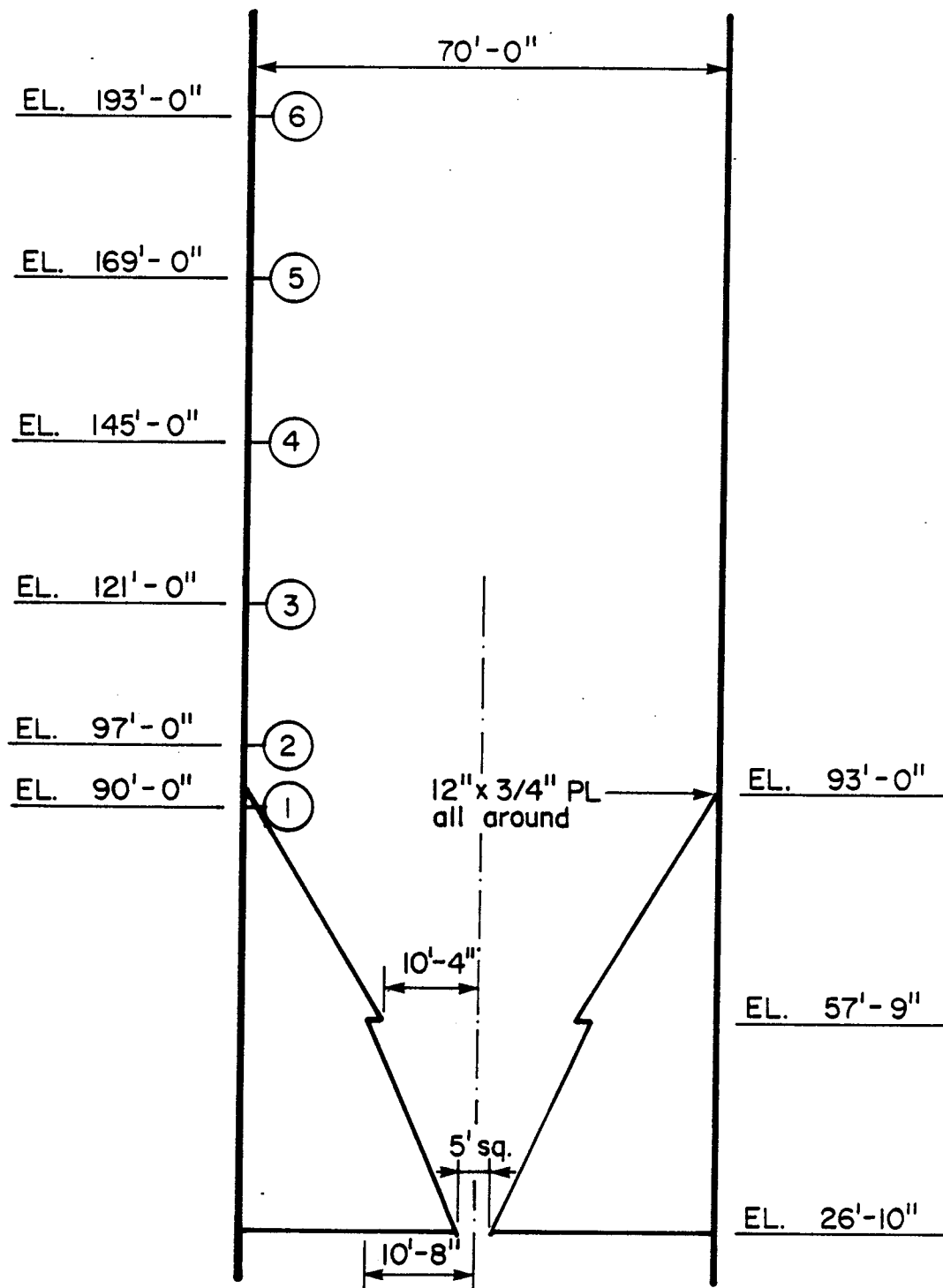


Fig. 2.12 Section of Fording Coal Silo

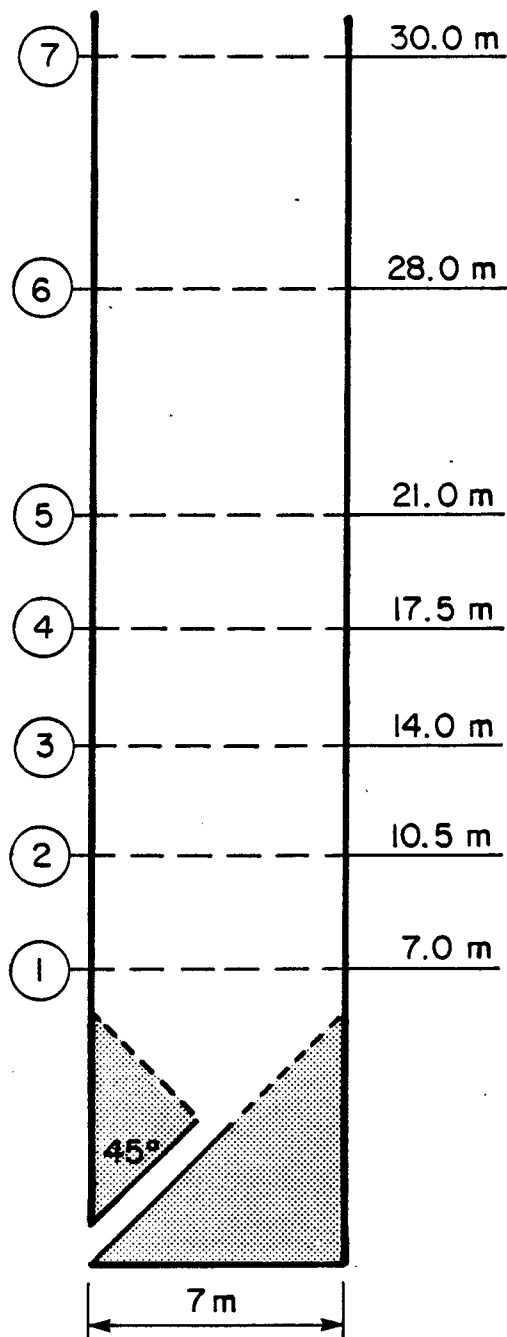
distribution of lateral pressure was close to static, from free surface of material down to a level between strain gauge locations 3 and 4.

If it is assumed that μ' does not vary greatly, K_{dy} at location 3 can be approximated by K_{st} x overpressure factor (o.p.f.). For the type of coal under study, K_{st} was close to 0.48, and with a maximum o.p.f. of 2.0, the largest measured value for K_{dy} was then close to 1.0. This is supported by Blight and Midgely (1980). Jenike's strain energy method, also, gives a value for K close to unity, when the switch location is assumed to occur at a depth greater than one diameter from free surface. It was also indicated with respect to this study that the dynamic pressures were found to be satisfactorily bounded by the strain energy predictions. Further it was observed from continuous strain record that the rate of withdrawal may influence the distribution of lateral pressures, while Pieper (1969) in a model study showed that in a silo with symmetric outlet, filling and emptying speeds have no influence.

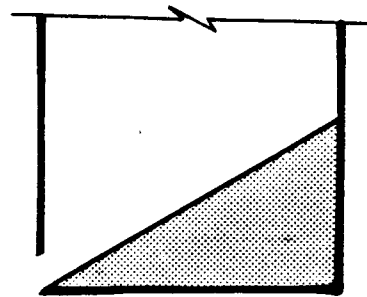
2.4.2 Technical University of Denmark (1980)

Nielsen and Kristiansen (1980) performed a full-scale test on a silo, 7 m in diameter and 46 m high, using barley as ensiled material. 36 pressure cells on the walls and 5 on the bottom were mounted in the silo, as shown in Fig.

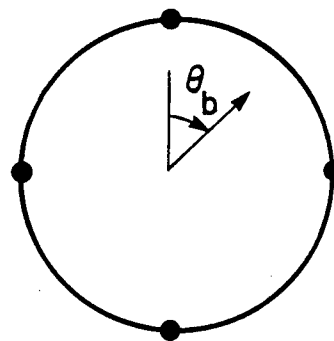
2.13. Three tests with central discharge and five with



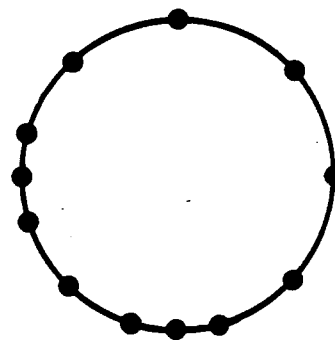
(a) Section with
centre outlet



(b) Eccentric outlet



(c) Sections 1,2,3,5,6 & 7
4 cells



(d) Section 4, 12 cells

Fig. 2.13 Section of Test Silo, Technical University
of Denmark

eccentric discharge were carried out. The test showed that the static pressure during filling and rest deviated considerably from Janssen's field. In some cases the mean values were 20% below Janssen's formula, while in others, they were up to 100% above this. During eccentric discharge, the distribution of mean values for the maximum discharge pressure was largely plane-symmetric. Except at the bottom most locations, where a considerable increase in pressure occurred at all locations. The mean values for the maximum pressures were lowest, about 1.8 times that obtained from Janssen's formula for $\theta_b = \pi/2$ and $3\pi/2$. At one point between locations 3 and 4, the pressure observed was about 2.8 times Janssen's formula for $\theta_b = 0$, and 3.2 times the Janssen's value for $\theta_b = \pi$. The maximum pressure on different locations did not occur at the same time. For central discharge the mean value of the maximum discharge pressures were axisymmetric. The maximum pressure was of approximately the same order of magnitude except that it was scattered between locations 1 and 3. Considerable deviation from the axisymmetric were ascertained in an individual test which may induce some moment in silo walls.

Significant cracks were observed at location where the largest pressures were measured as well as where the maximum deviation from an axisymmetric distribution was observed.

CHAPTER 3 - THE FINITE ELEMENT FRICTION MODEL

3.1 Introduction

The behavior of a granular material flowing through a silo is dominated by a number of variables falling into three different categories,

- i) geometric variables such as diameters, heights, and angles of hopper inclination, etc.,
- ii) material properties,
- iii) boundary conditions, such as wall friction.

The first two categories can be normally incorporated in any finite element technique. Material nonlinearities may, however, necessitate an incremental approach.

The third category projects the problem into the class of contact problems with Coloumb friction in which normal tractions are not known in advance (Campos, et al. 1982). The presence of friction forces gives rise to nonconservative forces which introduce dissipative terms in the variational formulation. With a certain loss of generality and at a risk of nonuniqueness the incremental virtual work principle may be used to describe such fields.

In the following different approaches to describe the boundary friction problem are presented. The particular approach chosen is fully developed and the finite element technique used in the rest of the study is described.

3.2 Incremental Virtual Work Formulation

Consider a mechanical system in equilibrium under a set of applied forces, T° and F° and prescribed kinematic constraints q° . The principle of virtual work states that the sum of all virtual work/rate of virtual work, δW , done by the external and internal forces existing in the system in going through an infinitesimal arbitrary virtual displacements/velocities satisfying prescribed kinematic constraints is zero i.e. $\delta W = 0$. The principle of virtual work is invariant under co-ordinate transformations and it holds good independently of the stress-strain relations of the material.

The incremental variational formulation presented here is based on small displacement/velocity field. Let the material body shown in Fig. 3.1 be divided into "k" number of elements. Let V_k be the volume of element and let $S_{\sigma k}$, S_{qk} and S_{fk} be those portions of element surfaces on which prescribed tractions, displacements/velocities and friction forces respectively are applied.

The superscript $()^\circ$ indicates initial quantities at the beginning of a load step, and the prefix $\Delta()$ denotes incremental quantities. Prescribed quantities are denoted by $(\bar{})$ and the nodal quantities are denoted by $(_)$.

When certain external forces are prescribed as acting on a deformable body, a statically admissible stress distribution is defined as one satisfying the differential equation of equilibrium in the interior of the body and the

boundary conditions.

The differential equation of equilibrium in incremental form can be written as

$$\sigma_{ij,j}^0 + \Delta\sigma_{ij,j} + F_i^0 + \Delta\bar{F}_i = 0 \quad (3.1a)$$

The symbols σ and F denote the stress tensor and the body force per unit volume vector respectively.

The stress increment tensor $\Delta\sigma_{ij}$ can be expressed in terms of the constitutive tensor C_{ijkl} and the strain increment tensor $\Delta\epsilon_{kl}$ as

$$\Delta\sigma_{ij} = C_{ijkl} \Delta\epsilon_{kl} \quad (3.1b)$$

The strain increment tensor is related to the displacement/velocity field tensor, q , as

$$\Delta\epsilon_{ij} = \frac{1}{2} (q_{i,j}^0 + q_{j,i}^0) + \frac{1}{2} (\Delta q_{i,j} + \Delta q_{j,i}) - \epsilon_{ij}^0 \quad (3.1c)$$

The mechanical boundary conditions on $S_{\sigma k}$ are defined (Pian, 1976) as

$$\bar{T}_i^0 = \sigma_{ij}^0 n_j \quad (3.2a)$$

$$\Delta\bar{T}_i = \Delta\sigma_{ij} n_j \quad (3.2b)$$

in which T and n are the surface tractions and the unit

vector normal to the surface respectively. The displacement/velocity boundary conditions on S_{qk} are written as (Pian, 1976)

$$q_i^0 + \Delta q_i = \bar{q}_i^0 + \Delta \bar{q}_i \quad (3.3)$$

Since the initial and prescribed quantities do not vary, the first variation of Eqs. 3.1c and 3.3 are

$$\delta \Delta \epsilon_{ij} = \frac{1}{2} (\delta \Delta q_{i,j} + \delta \Delta q_{j,i}) \quad (\text{on } V_k) \quad (3.4a)$$

$$\delta \Delta q_i = 0 \quad (\text{on } S_{qk}) \quad (3.4b)$$

Let the body in the initial equilibrium configuration be given an infinitesimal virtual displacement/velocity $\delta \Delta q_i$, subject to the conditions of Eq. 3.4b. The virtual work, δW_I , of the internal forces and the virtual work, δW_E , of the external forces are expressed as

$$\delta W_I = \sum_k \left\{ \int_{V_k} (\sigma_{ij}^0 + \Delta \sigma_{ij}) \delta \Delta \epsilon_{ij} dV + \int_{S_{fk}} |\sigma_T^0 + \Delta \sigma_T| |\delta \Delta q_T| dS \right\} \quad (3.5a)$$

$$\delta W_E = \sum_k \left\{ \int_{V_k} (\bar{F}_i^0 + \Delta \bar{F}_i) \delta \Delta q_i dV + \int_{S_{\sigma k}} (\bar{T}_i^0 + \Delta \bar{T}_i) \delta \Delta q_i dS \right\} \quad (3.5b)$$

The symbols σ_T and q_T denote, respectively, the tangential friction forces and the tangential displacements/velocities.

The principle of virtual work can be written as

$$\delta W_I - \delta W_E = 0 \quad (3.6)$$

Substituting δW_I and δW_E from Eqs. 3.5 and rearranging

$$\begin{aligned} & \sum_k \left\{ \int_{V_k} \Delta \sigma_{ij} \delta \Delta \epsilon_{ij} dV + \int_{Sf_k} |\sigma_T^0 + \Delta \sigma_T| |\delta \Delta q_T| dS \right. \\ & \left. - \int_{V_k} (\bar{F}_i^0 + \Delta \bar{F}_i) \delta \Delta q_i dV - \int_{S\sigma_k} (\bar{T}_i^0 + \Delta \bar{T}_i) \delta \Delta q_i + \int_{V_k} \sigma_{ij} \delta \Delta \epsilon_{ij} dV \right\} = 0 \end{aligned} \quad (3.7)$$

The first term and the third to fifth terms on the left hand side of Eq. 3.7 give rise to the usual finite element matrices (Elwi and Murray, 1980 and Bathe, 1982) in the following manner. Let the displacement/velocity field be described in terms of nodal quantities by

$$\{\Delta q\} = [N] \{\Delta \underline{q}\} \quad (3.8)$$

where $[N]$ is a matrix of shape functions and $\Delta \underline{q}$ is the set of nodal displacement/velocity increments.

Using Eq. 3.4a the strain increment field may be written as

$$\{\Delta \epsilon\} = [B] \{\Delta \underline{q}\} \quad (3.9)$$

where $[B]$ is the usual differential operators matrix. Using Eqs. 3.1b, 3.8 and 3.9, the first and third to fifth terms of Eq. 3.7 may be written as

$$\langle \delta \Delta q \rangle = \sum_k [K_k] \{\Delta q_k\} \quad (3.10a)$$

$$\langle \delta \Delta q \rangle = \sum_k (\{\bar{F}_k^0\} + \{\Delta \bar{F}_k\}) \quad (3.10b)$$

$$\langle \delta \Delta q \rangle = \sum_k (\{\bar{T}_k^0\} + \{\Delta \bar{T}_k\}) \quad (3.10c)$$

$$\langle \delta \Delta q \rangle = \sum_k \{Q_k\} \quad (3.10d)$$

where,

$$\{K_k\} = \int_{V_k} [B]^T [C] [B] dV \quad (3.11a)$$

$$\{\bar{F}_k^0\} + \{\Delta \bar{F}_k\} = \int_{V_k} [N]^T \{\bar{F}^0\} dV + \int_{V_k} [N]^T \{\Delta \bar{F}\} dV \quad (3.11b)$$

$$\{\bar{T}_k^0\} + \{\Delta \bar{T}_k\} = \int_{S_{\sigma_k}} [N]^T \{\bar{T}^0\} dS + \int_{S_{\sigma_k}} [N]^T \{\Delta \bar{T}\} dS \quad (3.11c)$$

$$\{Q_k\} = \int_{V_k} [B]^T \{\sigma^0\} dV$$

representing the element stiffness matrix, the element body force vector, the surface tractions vector and the equilibrating loads vector.

The second term in Eq. 3.7 represents the virtual work associated with friction forces. It may be represented in several ways.

- a) a boundary layer of thin solid element with specific material properties
- b) a boundary integral in which σ_T is a linear function of σ_n , where σ_n is the normal pressure.
- c) an iterative process in which friction forces are derived as a linear function of boundary reactions.

In all three representations Coloumb type friction is assumed. The first approach requires a specific formulation, not available in the present program FEPARCS5 (Elwi and Murray, 1980) which forms the base of program FEPILS (FEPILS is an acronym for Finite Element Program for Investigation of Loading on Silos). The second approach results in an unsymmetric stiffness matrix. The third approach requires iterations, but is straight forward and can be readily implemented. This is the approach chosen for the current study.

3.3 The Friction Force Formulation

The friction forces develop along the contact surface between the material and the wall as the solid material moves in the silo. The contact surface has been defined as the friction boundary surface, S_{fk} . If the forces normal to the friction boundary, R_N , are known, the tangential friction forces, F_T , can be obtained using Coloumb's friction law. The normal forces can be determined by providing essential boundary conditions in terms of linear springs on the friction surface. These springs have very

high stiffness as compared to the stiffness of the material.

Let the spring element be defined at point B on the friction surface, as shown in Fig. 3.2a. The spring may have any orientation in the r-z plane, where r and z denote the horizontal and vertical coordinates respectively.

Let the virtual work/rate of virtual work associated with the spring element be written as

$$\delta W_I = \delta W_n F_s \quad (3.12)$$

where δW_n is the virtual displacement/velocity normal to the boundary surface and F_s is the force in the spring for a one radian section written as

$$F_s = W_n k_{BE} r/\ell \quad (3.13)$$

where k_{BE} is the spring stiffness, ℓ is the length and r is the radius at the point at which boundary element is attached. If the spring is inclined θ_s to the horizontal, then the displacement/velocity component normal to the friction surface is given by (See Fig. 3.2b)

$$W_n = \langle u \ v \rangle \begin{Bmatrix} \cos \theta_s \\ \sin \theta_s \end{Bmatrix} \quad (3.14)$$

Substituting the right hand side of Eqs. 3.13 and 3.14 in Eq. 3.12, the resulting equation can be written as

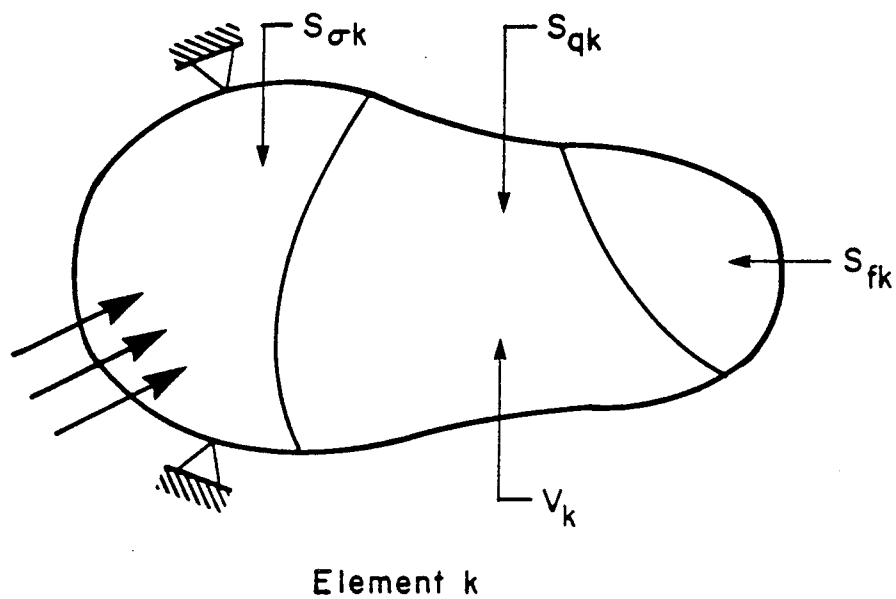


Fig. 3.1 Forces on Element k

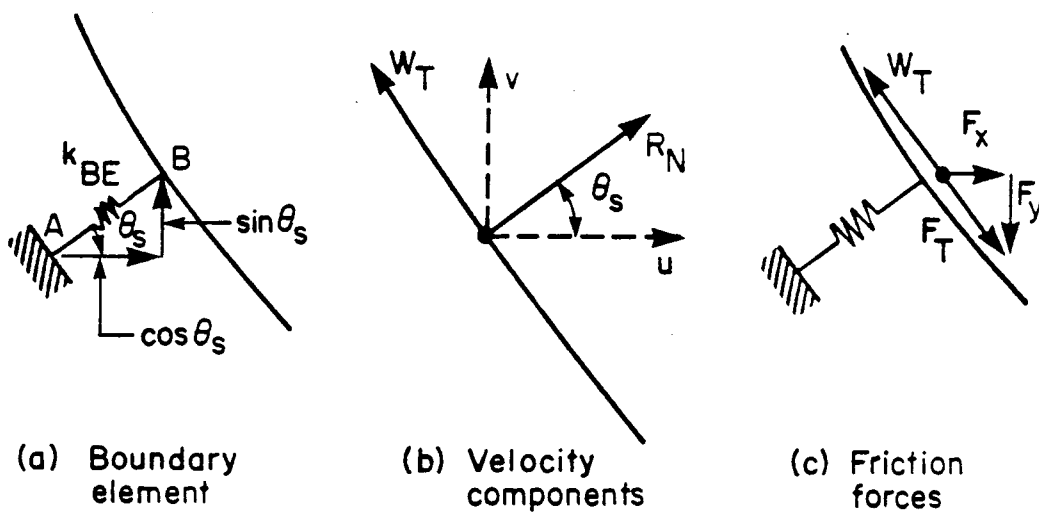


Fig. 3.2 Boundary Element and Friction Forces

$$\delta W_I = \langle \delta u \ \delta v \rangle [K_{BE}] \begin{Bmatrix} u \\ v \end{Bmatrix} \quad (3.15)$$

where $[K_{BE}]$ is the stiffness matrix of the boundary element and is written as

$$[K_{BE}] = \begin{bmatrix} \cos^2 \theta_s & \cos \theta_s \sin \theta_s \\ \cos \theta_s \sin \theta_s & \sin^2 \theta_s \end{bmatrix} k_{BE} r \quad (3.16)$$

This stiffness matrix is added to the stiffness coefficients of the node at which the spring element is attached.

The reactions or normal force components are calculated by multiplying $[K_{BE}]$ by the actual displacement/velocity obtained at any stage of solution. The reactions are added to the equilibrating loads to satisfy conditions (3.4b) of variational formulation.

The friction force can be defined as the normal force multiplied by a coefficient of friction ($\tan \phi$), acting at right angle to the normal force and in a direction opposite to the movement of material body, expressed as

$$F_T = - \tan \phi * |R_N| * \frac{|W_T|}{W_T} \quad (3.17)$$

where W_T is the tangential component of displacement/velocity written as

$$W_T = \langle u \ v \rangle \begin{Bmatrix} -\sin \theta_s \\ \cos \theta_s \end{Bmatrix} \quad (3.18)$$

and the normal force, R_N , is defined as

$$R_N = k_{BE} \times W_n \quad (3.19)$$

in which k_{BE} is the stiffness of the spring element. The horizontal and vertical component of friction force are

$$\langle F_x \ F_y \rangle = F_T \langle -\sin \theta_s \ \cos \theta_s \rangle \quad (3.20)$$

3.3.1 Solution Technique

In the strategy adopted to include friction forces, it is assumed that the normal and hence the friction forces on the friction surface is not known in advance. An iterative scheme can be developed to incorporate the friction forces in a general finite element program for the analysis of a problem without friction.

The algorithm for the analysis of such problems which have friction along the contact surface between material and silo wall is briefly described in the following. First, a finite element approximation of the problem without friction forces is obtained. The object is to get an approximate normal force and hence friction force, which may be employed later for a problem with the friction forces prescribed on friction boundary surface. Having calculated the nodal displacements/velocities at nodes on which the spring element is attached, the nodal normal and friction forces are obtained using Eqs. 3.14, 3.17 to 3.19.

The horizontal and vertical components of friction

forces are obtained from Eq. 3.20. These friction forces are multiplied by an under-relaxation factor to obtain the incremental value of friction force components, which are added to the corresponding nodal values in load vector.

The problem is then resolved using the new load vector which includes a first approximation of incremental components of friction forces. This leads to new iterates of nodal displacements/velocities field, and hence new friction forces.

This process is repeated continuously, until successive solution for friction forces do not differ by a preassigned tolerance. The final result thus obtained for normal forces after convergence of friction forces is employed to obtain the flow pressure of material on silo walls. The flow chart of this solution technique is illustrated in Fig. 3.3.

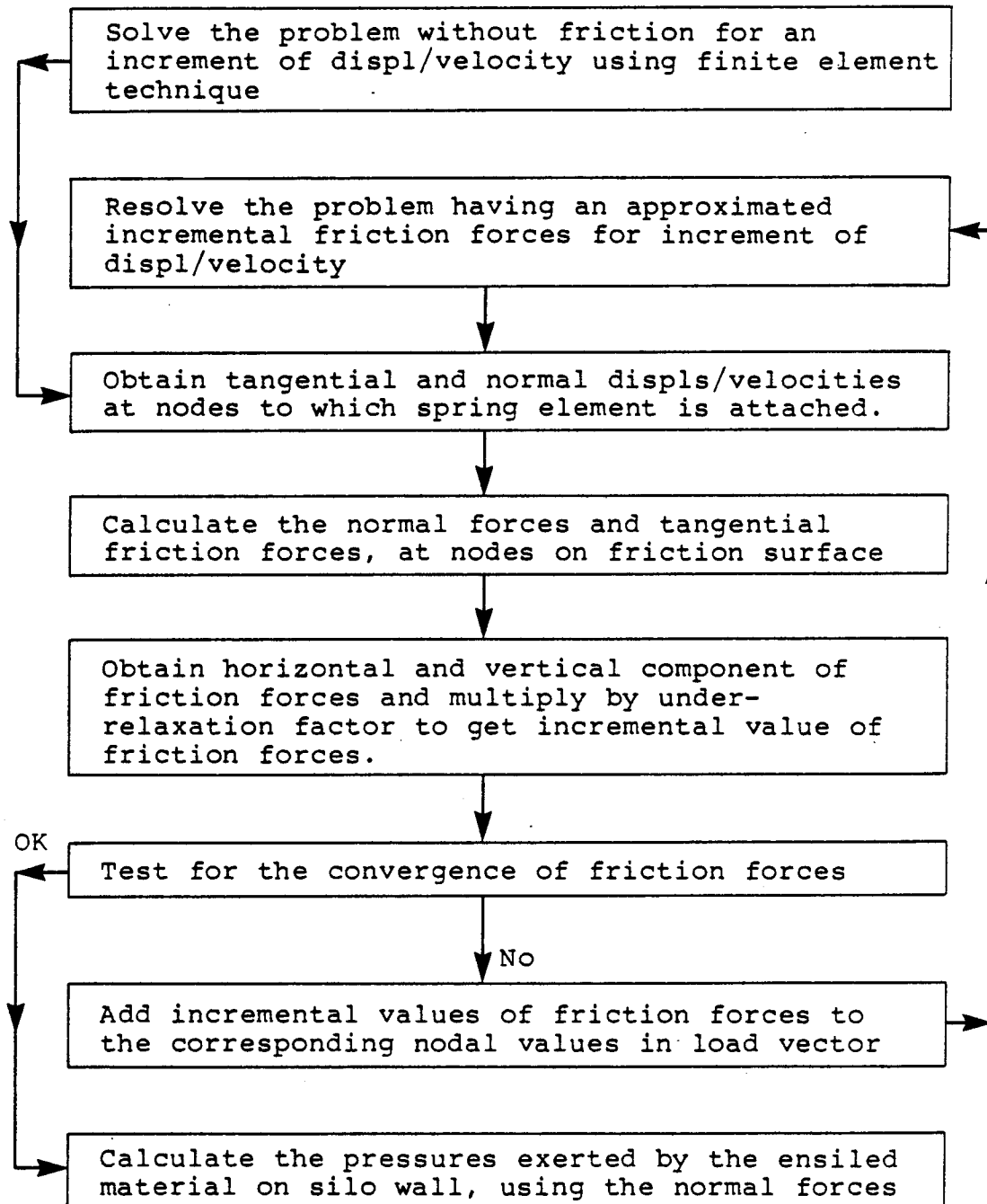


Fig. 3.3 Flowchart for Solution Scheme of Friction Force

CHAPTER 4 - MATERIAL MODEL

1.1 Introduction

Ensiled materials are often granular with or without a certain degree of cohesion. Except at certain locations, such as the outlet and free surfaces, the behavior falls in a triaxial compressive field. In such a field these materials appear to behave in a viscoplastic manner (Eibl and Häussler, 1984). The behavior is marked by several strong traits,

- i) an increase in density with increased hydrostatic stresses
- ii) an increase in shear strength with increased hydrostatic stresses, and
- iii) a marked dilatancy observed when the shear strength is achieved and plastic flow commences.

The scope of this study is directed primarily at coal type materials. Due to the current lack of information on rate dependent behavior of coal, and scarce data on density dependency, the study encompasses only elastic perfectly plastic behavior in a small displacement/velocity infinitesimal strain field. In order to model the plastic behavior taking into consideration the shear strength traits and the dilatancy effects a Drucker Prager type yield criterion (Drucker and Prager 1952) is proposed.

This failure surface can be degenerated from the five parameter curved meridian failure surface developed by

Willam and Warnke (1975), which allows better triaxial representation and may be employed in later studies.

This approach has been extensively used in the field of geotechnical engineering in modelling the properties of cohesive and granular materials. In the following the incremental stress-strain relation in matrix notation is presented.

4.2 Elastic Perfectly Plastic Model

A material body is deformed when subjected to applied forces. If upon removal of the forces the body recovers its original shape and size, then the material body is called elastic. For such a material the current state of stress depends only on the current state of deformation, i.e. stress is a function of strain. Thus the behavior of this type of material is both reversible and path independent in the sense that the stresses are uniquely determined from the current state of strain or vice versa. The deformation of material beyond the elastic limit is characterized as plasticity.

An idealized uniaxial stress-strain curve for elastic perfectly plastic materials is illustrated in Fig. 4.1. The material initially behaves linearly elastic along the path OA, i.e. the path is reversible. This is followed by a yield at point A. Once the material has reached the yield stress, σ_y , (i.e. passed point A) the path is no longer reversible. Upon unloading in this range the material once

more exhibits linear elastic behavior and follows a path parallel to OA. A permanent set of strain, ϵ^p , called plastic strain is left in the material body after complete unloading. Therefore only elastic strain, ϵ^e , can be recovered from total strain, ϵ . The stress in the material remains constant with increase in the plastic strain, beyond the yield point.

The concept of the yield point in the uniaxial case may be replaced by a yield criterion for a small (macroscopic) element of material subject to any action characterized by a tensor of applied stresses σ_{ij} .

The yield criterion and the general behavior of an elastic perfectly plastic material under a stress tensor, σ_{ij} , can be defined as follows.

1. In a nine dimensional stress space, there exists a yield surface (function of stress) defined by a yield function as

$$f = f(\sigma_{ij}) = 0 \quad (4.1)$$

f is a scalar function and $f = 0$ corresponds to the irreversible deformations. The material is elastic if

$$f < 0 \quad (4.2a)$$

and

$$df = \frac{\partial f}{\partial \sigma_{ij}} \Delta \sigma_{ij} < 0 \quad (4.2b)$$

and the material is plastic if

$$f = 0 \quad (4.3a)$$

and

$$df = \frac{\partial f}{\partial \sigma_{ij}} \Delta \sigma_{ij} = 0 \quad (4.3b)$$

It must be noted that $f > 0$, is not possible. The material is elastic until it reaches the yield limit (i.e. $f = 0$). The plastic deformation takes place without limit. For plastic flow to continue (i.e. for increase in plastic strain) the state of stress must remain on the yield surface. This is known as the criterion of loading and defined by Eq. 4.3b. Now there remains a permanent set of plastic strain, ϵ^P , when the stress intensity drops below the yield value or when the stresses are removed. This is known as the criteria of unloading defined by Eq. 4.2b.

The concept of loading and unloading has been illustrated in Fig. 4.2 where f is interpreted geometrically as a surface and σ_{ij} and $\Delta \sigma_{ij}$ as stress and stress increment vector in stress

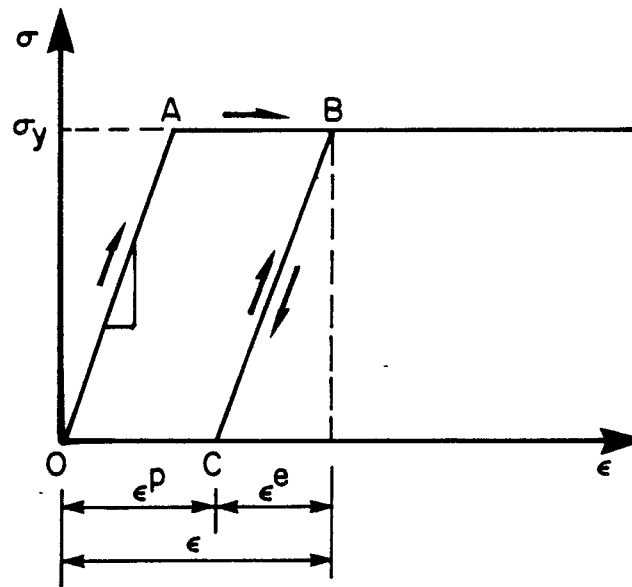


Fig. 4.1 Idealized Stress-Strain Curve

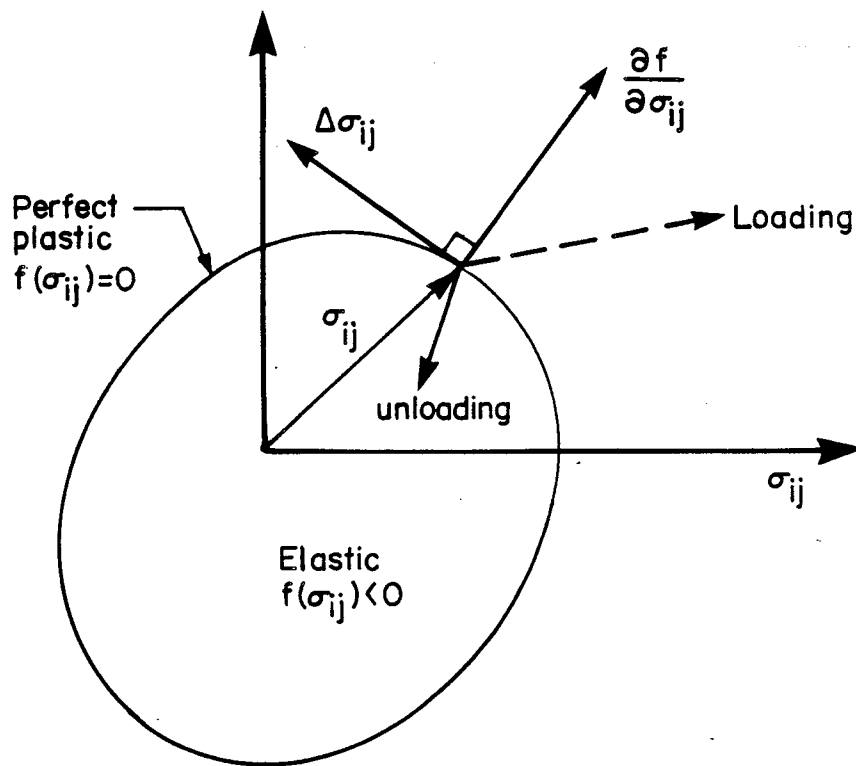


Fig. 4.2 Yield Surface and Criteria of Loading and Unloading

space. This surface is fixed for elastic perfect plastic materials.

Let the body, initially in a plastic state with stress vector σ_{ij} , be given an infinitesimal increment of stress, $\Delta\sigma_{ij}$ (additional loading). For perfect plastic materials the stress point cannot go outside the yield surface. Plastic flow occurs when the stress point is on the yield surface and the additional loading, $\Delta\sigma_{ij}$, must lie in a plane tangent to the yield surface. The additional loading $\Delta\sigma_{ij}$ produces only elastic strain, if it is directed inward from the surface f (unloading).

2. The total strain increment, $\Delta\epsilon_{ij}$, in the plastic zone of behavior can be decomposed into an elastic component, $\Delta\epsilon_{ij}^e$, and a plastic component, $\Delta\epsilon_{ij}^p$, such that

$$\Delta\epsilon_{ij} = \Delta\epsilon_{ij}^e + \Delta\epsilon_{ij}^p \quad (4.4)$$

The elastic or 'recoverable' strain increment can be related to the incremental changes of stress, $\Delta\sigma_{ij}$, by the generalized Hook's Law as

$$\Delta\sigma_{ij} = C_{ijkl} \Delta\epsilon_{kl}^e \quad (4.5)$$

3. There may not be a connection between f and the

plastic strain increment. Let there be a plastic-potential function

$$g = g(\sigma_{ij}) \quad (4.6)$$

such that

$$\Delta \epsilon_{ij}^p = \frac{\partial g}{\partial \sigma_{ij}} d\lambda \quad (4.7)$$

where $d\lambda$ is a positive scalar function, which is nonzero only when plastic deformation occurs. The equation $g(\sigma_{ij}) = \text{constant}$, defines a plastic potential surface in nine dimensional stress space. The plastic-flow vector $\Delta \epsilon_{ij}^p$ is directed along the normal to the surface of plastic potential.

If it is assumed that the plastic potential function coincides with the yield function, i.e. $f = g$, then,

$$\Delta \epsilon_{ij}^p = \frac{\partial f}{\partial \sigma_{ij}} d\lambda \quad (4.8)$$

This is called the associated flow rule. Obviously, the plastic strain increment is thus normal to the yield surface (Fig. 4.2). Eq. 4.7 with $f \neq g$ is called nonassociated flow rule.

Substituting Eq. 4.8 into Eq. 4.4 and rearranging, the elastic strain component is written as

$$\Delta \epsilon_{ij}^e = \Delta \epsilon_{ij} - \frac{\partial f}{\partial \sigma_{ij}} d\lambda \quad (4.9)$$

To obtain the stress-strain relation Eq. 4.9 is substituted for the elastic strain increment in Eq. 4.5 to obtain

$$\Delta \sigma_{ij} = C_{ijkl} \left(\Delta \epsilon_{kl} - \alpha d\lambda \frac{\partial f}{\partial \sigma_{kl}} \right) \quad (4.10)$$

Subject to the condition

- a) $\alpha = 1$ if $f(\sigma_{ij}) = 0$ and $df = 0$ i.e. σ_{ij} is on the yield surface and moving tangent to the yield surface
- b) $\alpha = 0$ if $f(\sigma_{ij}) = 0$ and $df < 0$ i.e. σ_{ij} on yield surface and unloading
- c) $\alpha = 0$ if $f(\sigma_{ij}) < 0$ i.e. σ_{ij} is inside the yield surface.

The factor $d\lambda$ is obtained by combining the stress-strain relation (Eq. 4.10) with the consistency condition (Eq. 4.3b) as follows

$$\frac{\partial f}{\partial \sigma_{ij}} C_{ijkl} \left(\Delta \epsilon_{kl} - \alpha d\lambda \frac{\partial f}{\partial \sigma_{kl}} \right) = 0 \quad (4.11)$$

rearranging and substituting, $\alpha = 1$, gives

$$d\lambda = \frac{\frac{\partial f}{\partial \sigma_{ij}} C_{ijkl} \Delta \epsilon_{kl}}{\frac{\partial f}{\partial \sigma_{ij}} C_{ijkl} \frac{\partial f}{\partial \sigma_{kl}}} \quad (4.12)$$

A general relation for stress increment is obtained by substituting $d\lambda$ from Eq. 4.12 into Eq. 4.10 as

$$\Delta \sigma_{ij} = \left[C_{ijkl} - \alpha \frac{\frac{\partial f}{\partial \sigma_{ij}} C_{ijkl} \frac{\partial f}{\partial \sigma_{kl}} C_{ijkl}}{\frac{\partial f}{\partial \sigma_{ij}} C_{ijkl} \frac{\partial f}{\partial \sigma_{kl}}} \right] \Delta \epsilon_{kl} \quad (4.13)$$

This is written in the matrix form as

$$\{\Delta \sigma\} = \left[[C]^e - \alpha \frac{[C]^e \left\{ \frac{\partial f}{\partial \sigma} \right\} \left\langle \frac{\partial f}{\partial \sigma} \right\rangle [C]^e}{\left\langle \frac{\partial f}{\partial \sigma} \right\rangle [C]^e \left\{ \frac{\partial f}{\partial \sigma} \right\}} \right] \{\Delta \epsilon\} \quad (4.14)$$

in which $[C]^e$ is the elastic constitutive matrix, $\Delta \sigma$ is the increment of stress in vector form, $\partial f / \partial \sigma$ is the gradient of the yield surface and $\Delta \epsilon$ is the increment of strain in vector form.

4.3 Failure Surface

A failure surface is described by an envelope in the stress space which defines the failure strength for any ratio of stresses.

When the stress path intersects this surface plastic flow occurs. For perfectly plastic behavior the surface does not change its configuration during plastic flow, hence the stress path describes a trajectory on the initial

surface, while the plastic strain increases continuously.

A two parameter failure surface proposed by Drucker and Prager (1952) is used in this work. This failure surface is degenerated from a five parameter surface presented by Willam and Warnke (1975).

4.3.1 Willam-Warnke Surface

The Willam-Warnke failure surface is basically a cone with curved meridians and non-circular base section, see Fig. 4.3a. The surface is conveniently represented by hydrostatic and deviatoric sections as shown in Figs. 4.3b and 4.3c.

The characteristics of this surface can be summerized in the following.

Let the mean (average) normal stress be defined as

$$\sigma_m = \sigma_{ii}/3 \quad (4.15)$$

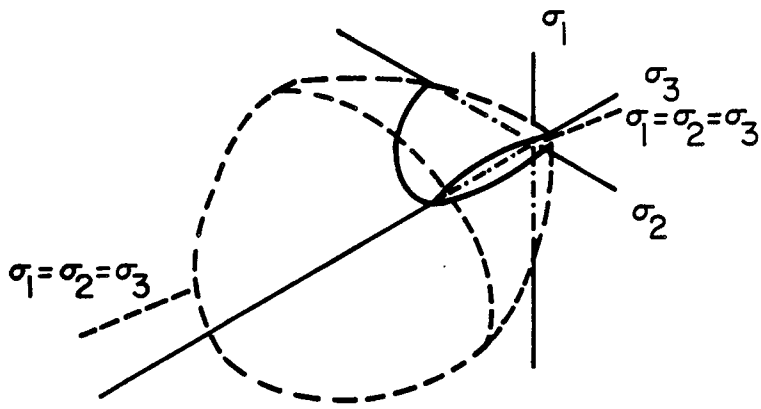
and let the mean (average) shear stress be defined as

$$\tau_m = \sqrt{S_{ij}S_{ij}}/5 \quad (4.16)$$

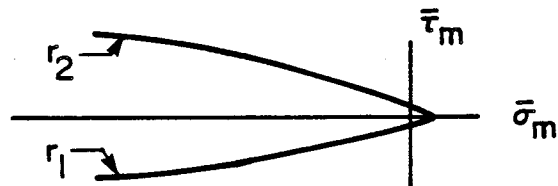
where S_{ij} is the deviatoric stress tensor defined as

$$S_{ij} = \sigma_{ij} - \sigma_{kk}\delta_{ij}/3 \quad (4.17)$$

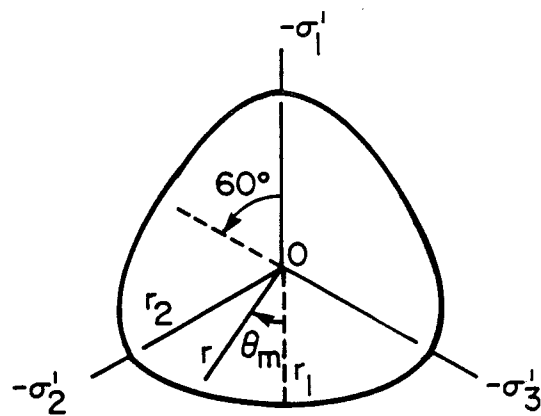
Normalizing σ_m and τ_m by uniaxial compressive strength f_{cu}



(a) General view



(b) Hydrostatic section



(c) Deviatoric section

Fig. 4.3 Willam-Warnke Failure Surface

as

$$\bar{\sigma}_m = \sigma_m / f_{cu} \quad (4.18a)$$

$$\bar{\tau}_m = \tau_m / f_{cu} \quad (4.18b)$$

The deviatoric plane ($\sigma_m = \text{constant}$) of failure surface is represented by three symmetric elliptical segments forming a closed convex and continuous curve. Hence, the surface meets the condition of symmetry, smoothness and convexity. The elliptic trace of the failure surface is described as

$$\bar{\tau}_m = r(\theta_m, \bar{\sigma}_m) \quad (4.19)$$

where θ_m is the angle of similarity and is expressed in terms of principal stresses as (Willam and Warnke, 1975)

$$\cos \theta_m = \frac{\sigma_1 + \sigma_2 - 2\sigma_3}{\sqrt{2} [(\sigma_1 - \sigma_2)^2 + (\sigma_2 - \sigma_3)^2 + (\sigma_3 - \sigma_1)^2]^{1/2}} \quad (4.20)$$

For $\sigma_1 > \sigma_2 > \sigma_3$, then $0 < \theta_m < 60^\circ$, as may be seen from Fig. 4.3c. The function $r(\theta_m, \bar{\sigma}_m)$ in Eq. 4.19 is defined as (Willam and Warnke, 1975)

$$r(\theta_m, \bar{\sigma}_m) = \frac{2r_2(r_2^2 - r_1^2)\cos\theta_m + r_2(2r_1 - r_2)[4(r_2^2 - r_1^2)\cos^2\theta_m + 5r_1^2 - 4r_1r_2]^{1/2}}{4(r_2^2 - r_1^2)\cos^2\theta_m + (r_2 - 2r_1)^2} \quad (4.21)$$

The variables r_2 and r_1 are respectively the maximum ($\theta_m = 60^\circ$) and minimum ($\theta_m = 0$) radii of the deviatoric trace of the surface (see Fig. 4.3c). These variables are assumed to be parabolic functions of the hydrostatic stress and are expressed as (Willam and Warnke, 1975)

$$r_1 = a_0 + a_1 \bar{\sigma}_m + a_2 \bar{\sigma}_m^2 \quad (4.22a)$$

$$r_2 = b_0 + b_1 \bar{\sigma}_m + b_2 \bar{\sigma}_m^2 \quad (4.22b)$$

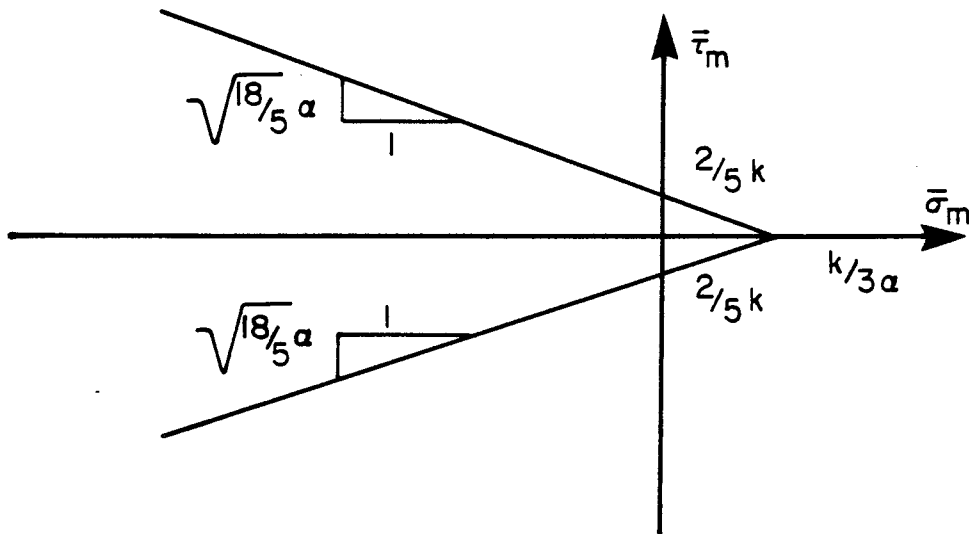
The value of the co-efficients a_0 to b_2 are chosen such that the variables r_1 and r_2 pass through a set of control points, as illustrated in Fig. 4.3b.

This surface was basically developed for concrete subjected to triaxial loading in the tension and compression regime. The values of these co-efficients for concrete materials are evaluated by Willam and Warnke (1975).

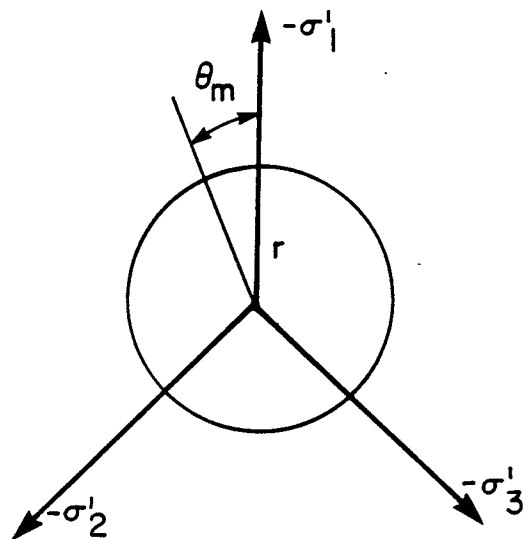
4.3.2 Drucker-Prager Surface

Drucker-Prager surface is a right-circular cone with its axes equally inclined to the co-ordinate axes in a principal stress space, as shown in Fig. 4.4. This is expressed mathematically as

$$f(I_1, \sqrt{J_2}) = \alpha I_1 + \sqrt{J_2} - k = 0 \quad (4.23)$$



(a) Hydrostatic Section



(b) Deviatoric Section

Fig. 4.4 Drucker-Prager Failure Surface

where α and k are positive material constants. I_1 and J_2 are the first stress invariant and the second deviatoric stress invariant respectively and are expressed in terms of mean normal stress, σ_m , and mean shear stress, τ_m , as

$$I_1 = 3\sigma_m \quad (4.24a)$$

$$J_2 = \frac{5}{2} \tau_m^2 \quad (4.24b)$$

Substituting Eqs. 4.24 into Eq. 4.23 and normalizing by uniaxial compressive strength gives

$$\frac{\tau_m}{f_{cu}} + \frac{18}{5} \alpha \frac{\sigma_m}{f_{cu}} - \frac{2}{5} k = 0 \quad (4.25)$$

For granular-cohesive type material the material constants are given by

$$\alpha = \frac{\tan \phi}{\sqrt{9 + 12 \tan^2 \phi}} \quad (4.26)$$

$$k = \frac{3c}{\sqrt{9 + 12 \tan^2 \phi}} \quad (4.26b)$$

where ϕ is the angle of internal friction of material and c is the cohesion.

The major disadvantage in this type of surface is that plastic volume expansion takes place at yield according to an associated flow rule which may not fit the observed values (William and Warnke, 1975). This property is known

as dilatancy.

4.3.3 Degeneration of Willam Warnke Surface to Drucker Prager Surface

The Willam-Warnke degenerates to Drucker-Prager surface of circular cone if the meridian parameters are reduced to those of identical straight lines as follows

$$a_0 = b_0 \quad (4.27a)$$

$$a_1 = b_1 \quad (4.27b)$$

$$a_2 = b_2 = 0 \quad (4.27c)$$

$$\text{and} \quad r_1 = r_2 = r \quad (4.27d)$$

in which case the deviatoric cross section is a circle.

Using Eqs. 4.8b, 4.19, 4.22 and 4.27 and noting that $\tau_m = r/\sqrt{5}$ the following expression for the meridian is obtained

$$\frac{\tau_m}{f_{cu}} = \frac{r}{\sqrt{5} f_{cu}} = a_1 + a_1 \frac{\sigma_m}{f_{cu}} \quad (4.28)$$

Comparing to the Drucker Prager failure surface, Eq. 4.23

$$a_0 = \sqrt{2/5} k \quad (4.29a)$$

$$\text{and,} \quad a_1 = -\sqrt{18/5} \alpha \quad (4.29b)$$

CHAPTER 5 - ANALYSIS AND COMPARISON

5.1 Introduction

A finite element formulation for the incremental analysis of a flowing solid material in axisymmetric silos is presented in Chapter 3. Chapter 4 describes the proposed elastic-plastic constitutive model. Program FEPILS in which the finite element model and material model proposed in Chapter 3 and 4 respectively, have been implemented as described in Appendix A. In this chapter a series of problems are analyzed using program FEPILS. Finite element model of test problems and the material properties are described. A parametric study of the material behavior is carried out. The variables investigated in this study are angle of internal friction of material, angle of wall friction, hopper slope with vertical, height to diameter ratio and Poisson's ratio. The effect of these variables on lateral wall pressure and material stresses have been examined. The results of the analyses are presented and compared with classical theories and results of finite element analysis described in Section 2.3.

5.2 Model Description

5.2.1 Description of Test Structures

A number of finite element problems are analyzed using axisymmetric silos, having a diameter of 8.0 metres, with varying height, hopper geometry, and material parameters.

The finite element idealization of three silo structures having different hopper geometry is shown in Fig. 5.1. These structures are the basis of all finite element analyses carried out in this study. Eight node isoparametric elements are used to construct each mesh of the solid element. These elements give greater flexibility in modelling the geometry of the structure and at the same time keeps the problem size reasonable. Typical spring boundary elements have been provided over the entire height of the silo to model the wall reactions and subsequently friction forces. The horizontal displacements/velocities along the axis of symmetry are suppressed.

A total of five sets of problems have been analyzed varying the parameters as follows.

Hopper Slope with Vertical: The height of the cylindrical portion of the silo is kept constant and the hopper slope with vertical is varied. The silos used for this analysis are illustrated in Figs. 5.1a to 5.1c. The height of the silos is 16.0 m and the hopper slopes with vertical are 20.56 deg., 24.78 deg. and 29.98 deg., respectively. The outlet of the silo is 2.0 m in diameter. The total height of the hopper decreases with increasing hopper inclination. Altogether, the problem has 177 nodes, 25 spring boundary elements and 48 solid elements.

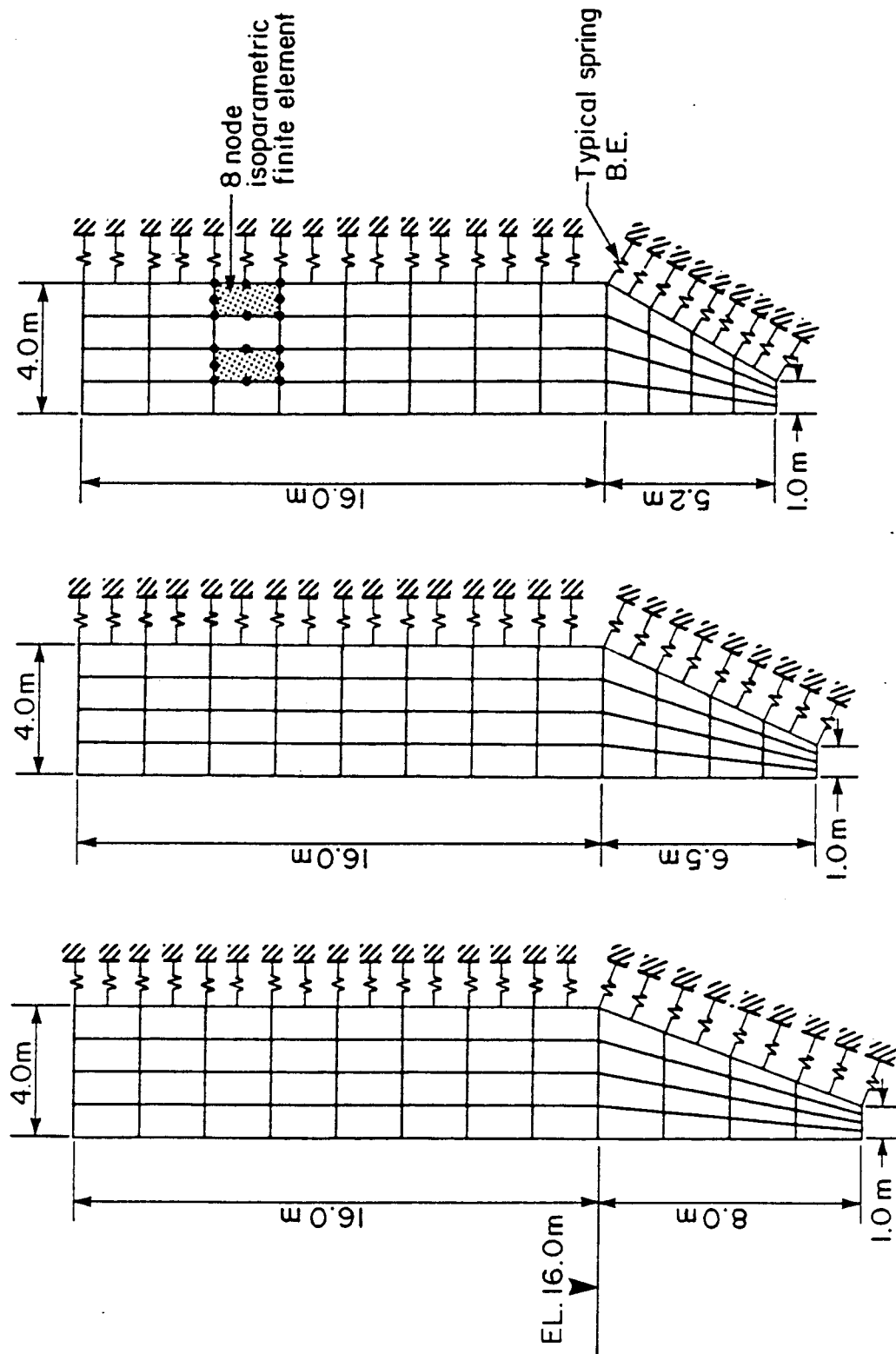
Height to Diameter Ratio: Keeping the hopper geometry

constant, the height of the cylindrical portion of the silo is increased. The ratios of cylindrical height to diameter used in this study are 2.0, 2.5 and 3.0. Fig. 5.1a shows the finite element model for the test problem with a height to diameter (H/D) ratio of 2.0. The same problem is analyzed by adding two and four rows of elements for H/D ratios of 2.5 and 3.0, respectively. Consequently four and eight spring boundary elements are added at the interface between solid material and silo wall. Therefore, 205 nodes, 56 solid elements and 29 spring boundary elements for an H/D ratio of 2.5, and 233 nodes, 64 solid elements and 33 spring boundary elements for an H/D ratio of 3.0 form the finite element models of silos.

The rest of the three sets of problems have been analyzed by varying the angle of internal friction of the material, angle of wall friction and Poisson's ratio. The silo used for all these analyses is the one illustrated in Fig. 5.1a.

5.2.2 Material Properties

The bulk density of granular materials depend on particulate properties such as size, shape, the manner of assembly of these particles and specific gravity of constitutive solids. Examination of classical theories reveal that horizontal pressure on the silo wall is a direct function of unit weight. Most granular materials have sizeable variation in unit weights. As described in Section



(c) $\theta' = 29.98^\circ$

(b) $\theta' = 24.78^\circ$

(a) $\theta' = 20.56^\circ$

Fig. 5.1 Finite Element Idealization of Silo

4.1, the scope of this study is directed at a coal type of material. Jenike and Johanson (1979) indicate that compressibility effects and moisture content can cause large variations in the unit weight of coal (from 3.34 to 10.06 kN/m³). The average unit weight of a two inch minus well graded coal is 9.5 kN/m³. This value has been chosen for determining the gravity load in this study.

Jenike and Johanson (1979) reported that for coal material passing a number 8 mesh and having a moisture content of 6%, the angle of internal friction ranges from 38° to 40°. This study uses an angle of internal friction of material of 35°, 40° and 45°. They also stated that an angle of wall friction on concrete varies from 26° to 31°. Ravenet (1980) found the angle of wall friction on a rusted steel sheet as 40°, on a corrugated steel sheet as 24°, on a polished steel sheet as 17° and on a stainless steel sheet as 8°. Problems with angle of wall friction of 25°, 20° and 15° have been investigated. There is no significant information on investigation of Poisson's ratio and modulus of elasticity of coal. From geotechnical engineering literature the average value of Poisson's ratio and modulus of elasticity for coarse sand is found to be 0.3 and 1.5×10^5 kPa. The values of Poisson's ratio used to investigate their effect on material behavior are 0.25, 0.3 and 0.35, coupled with a modulus of elasticity of 1.5×10^5 .

5.2.3 Description of the Analysis

The analysis of the finite element models described in Section A.2 is performed in two stages. In the problem preparation stage input data is read and generated, element shape functions and derivatives are calculated, column heights and addressing array of the stiffness matrix are formed, stresses, strains and material properties are initialized at all integration points, and all basic load vectors are formed.

The gravity loads are applied to the structure assuming no friction force. The increment of displacements/velocities thus obtained are used to calculate friction forces. An underrelaxation factor for friction forces, R_F , between 0.05 and 0.12, is used to calculate the increments of friction forces. These incremental values of friction forces are added to the gravity load vector, and the problem is resolved. The process is repeated until successive solutions for friction forces do not differ by a preassigned tolerance for load λ_p . The tolerance for displacements/velocities, λ_r , and loads (and friction forces), λ_p , used are 0.001 and 0.005 respectively. The number of subincrements (NI) vary from 10 to 15. The maximum number of iterations allowed per load step and for complete convergence of friction force is 30. An underrelaxation factor for displacements/velocities, R_x , used vary between 0.8 and 1.0. An initial/elastic stiffness matrix is used throughout the analysis. The nodal reaction

or normal forces obtained at the contact surface between the material and the silo wall after convergence of friction forces is used to determine the material pressure normal to the wall.

5.3 Discussion of Results

Output of the analysis from program FEPILS consists of nodal displacements/velocities, nodal friction forces and normal forces or reactions at the contact surface between the silo wall and the material, and stresses at gaussian points. Lateral wall pressures are obtained from reactions at the silo wall. Comparison of these pressures have been made with the results obtained by classical theories, discussed in Chapter 2. Stress fields within the solid material are presented, and compared with Jenike's predictions. The displacement/velocity field is presented and the effects of the coefficient of friction are discussed. A parametric study is carried out to identify the pertinent variables and to examine any visible trend in their relation to the lateral wall pressure.

5.3.1 Comparison of Pressures with Classical Theories

The lateral pressure exerted by the material on the silo wall, from finite element analysis is presented in Fig. 5.2 compared with Janssen's, Reimbert's and Jenike's pressure theories. The finite element curve is a digital approximation with linear interpolation of pressures between

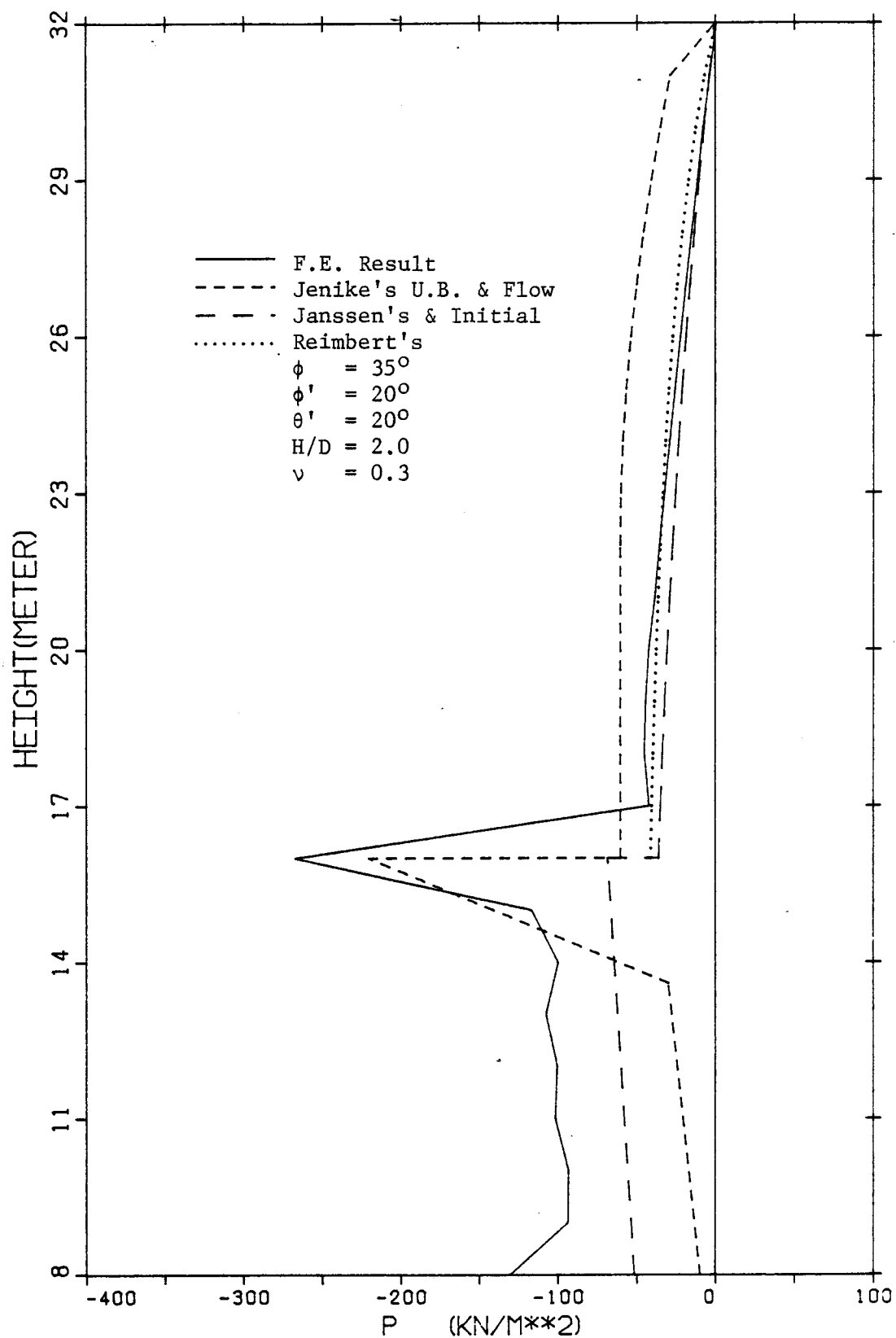


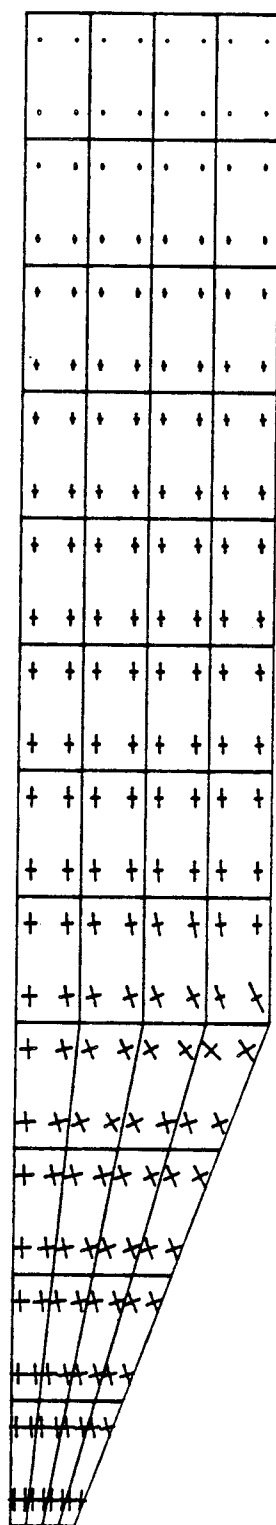
Fig. 5.2 Comparison of F.E. Results with Classical Theories

adjacent nodes. The lateral pressure obtained from the finite element analysis lies between Janssen's and Reimbert's solution, if the depth of the material from the free surface does not exceed the silo diameter. Down to this depth the analysis is on the average about 20 percent above Janssen's and 24 percent below Reimbert's solution. Below that depth down to the transition, the pressure exceeds Janssen's values by about 20 to 40 percent and Reimbert's by about 2 to 15 percent. The analysis result is about 20 to 80 percent below Jenike's upper bound solution. A sharp increase in pressure is observed at the transition from the cylindrical part of the silo to the hopper. This is defined by Jenike as the peak pressure for switch from peak or active pressure field to radial or passive pressure field at transition. The finite element solution of this peak pressure is about 20 percent above Jenike's. This peak pressure vanished at a depth less than that suggested by Jenike et al. (1973, Part 3) which is $0.3D$ slant distance of hopper wall below transition. Both initial and flow pressures in the hopper, obtained from Jenike's theory are less than the finite element prediction. The analysis result is on the average about 65 percent above his initial pressure theory and about 200 to 300 percent above radial or flow pressure theory in the hopper. Jenike assumes linear decrease in pressure from transition to zero at vertex of hopper, whereas finite element solution predicts another peak value at outlet.

Eibl et al. (1984) have suppressed normal and tangential pressures at the outlet, therefore this peak does not appear in their solution. However, their solution gives identical pressure distributions in the cylindrical part of the silo and hopper.

5.3.2 Stress Field

The resulting principal stress field of the finite element analysis, when the silo is fully charged, and the outlet is closed, is presented in Fig. 5.3. The major principal stress acts in a vertical or close to a vertical direction. Figs. 5.4 to 5.8 show the principal stresses for various hopper geometry and cylindrical height to diameter ratio, when the outlet is opened and material flows. The direction of principal stresses in the cylindrical part of silos do not change significantly, but they are reoriented in the hopper section of silos. Subsequently the magnitude of stresses decreases above the outlet and increases near the transition from the cylinder to the hopper of the silo, whereas no change in stress level is observed in the rest of the cylindrical portion of silos. Jenike et al. (1968), Walker (1966), and Walters (1973) have described this stress redistribution as the transition from an active state of stress to passive state of stress in the hopper, while active stress field is retained above transition in the cylinder of the silo. Jenike et al. (1968) assumes an arched or radial stress field in the hopper below



SCALE: 1200 M/CM
STRESS: 400.000 KPA/CM

MATERIAL DENSITY = 9.50 KN/CUM

ANG OF INT FRI = 35.00 DEG

ANG OF WALL FRI = 20.00 DEG

HOPP ANG WITH VERT = 20.56 DEG

Fig. 5.3 Stress Field When Outlet Closed and Silo Charged

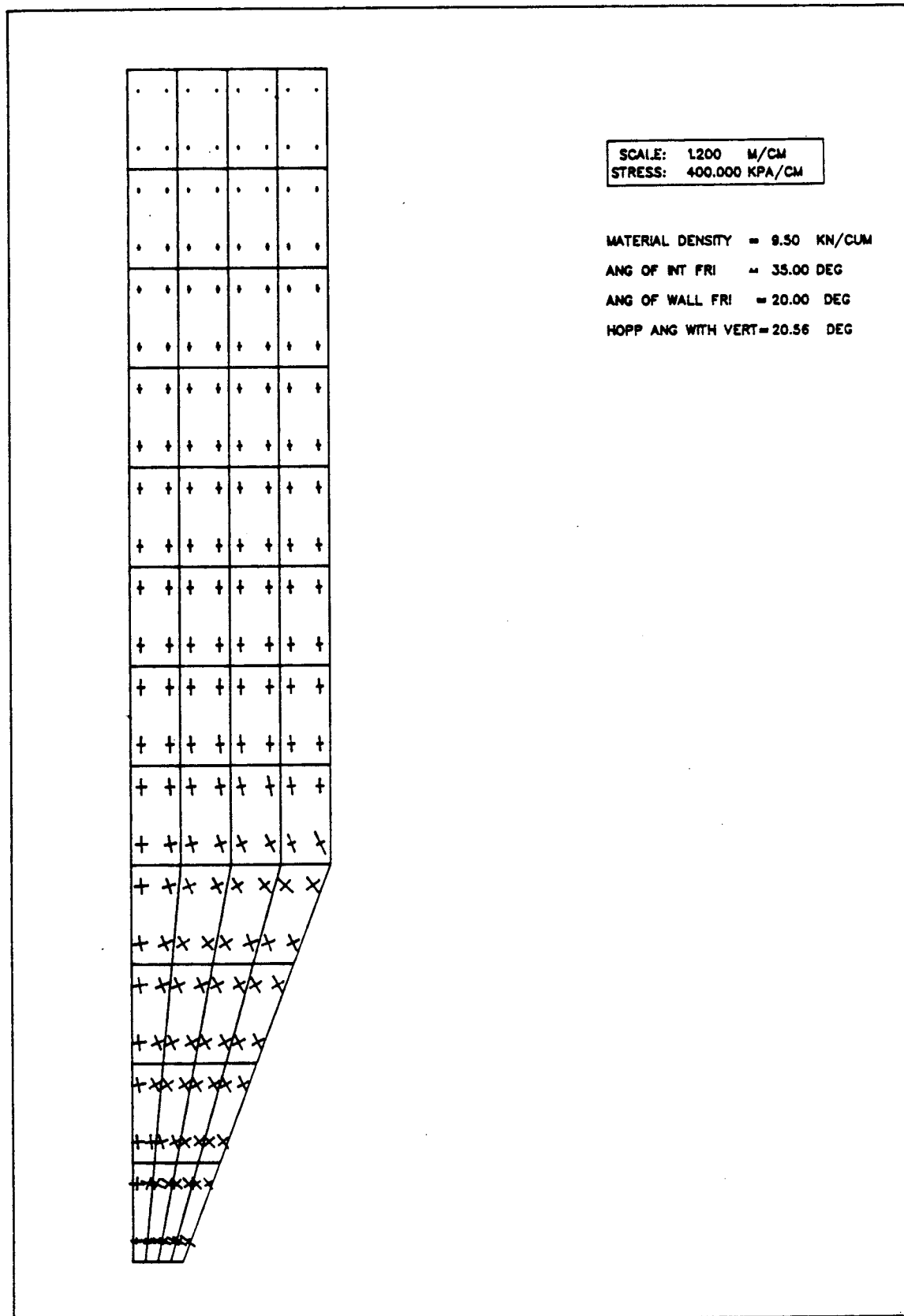


Fig. 5.4 Stress Field During Flow for $\theta' = 20.56^\circ$

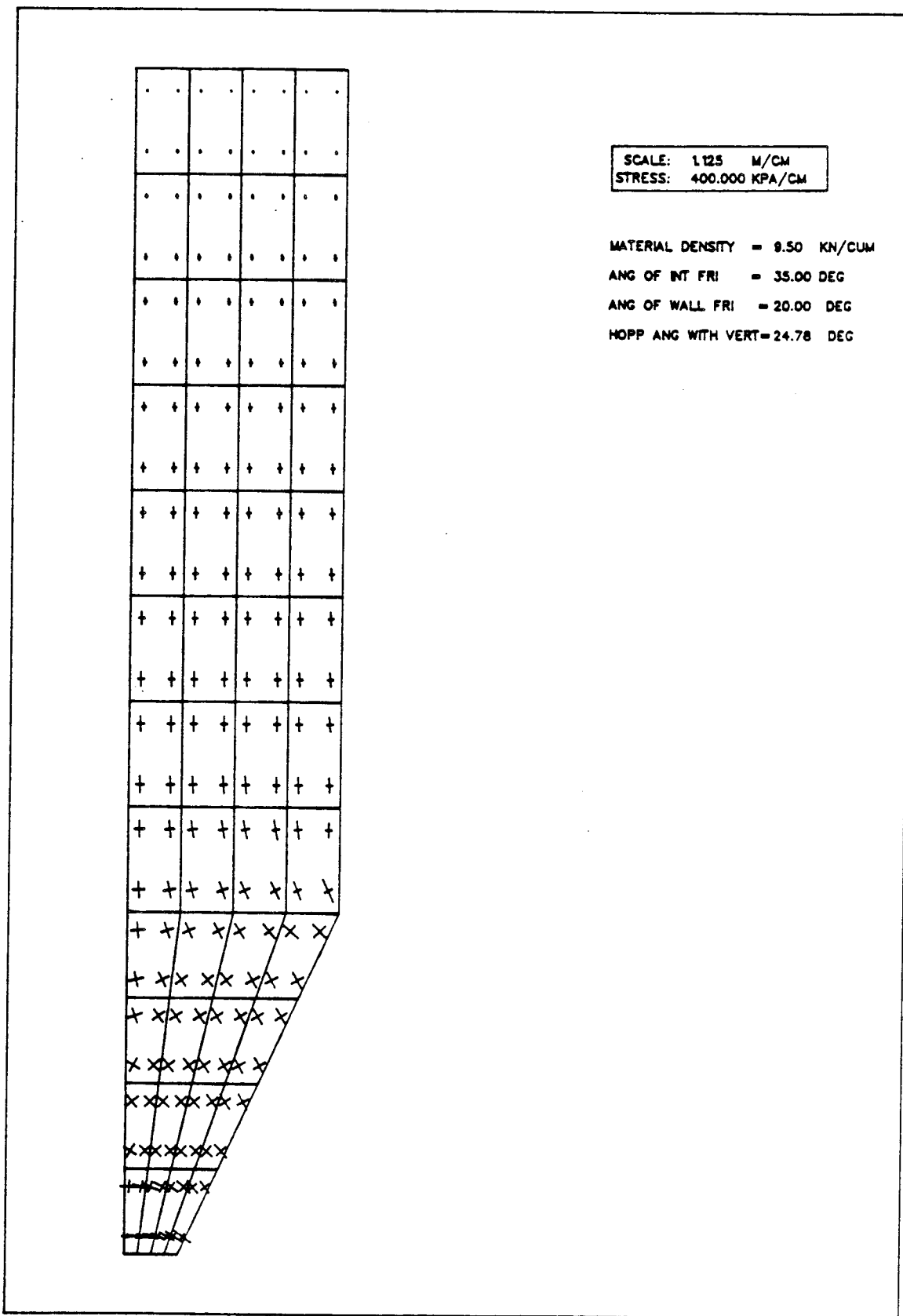


Fig. 5.5 Stress Field During Flow for $\theta' = 24.78^\circ$

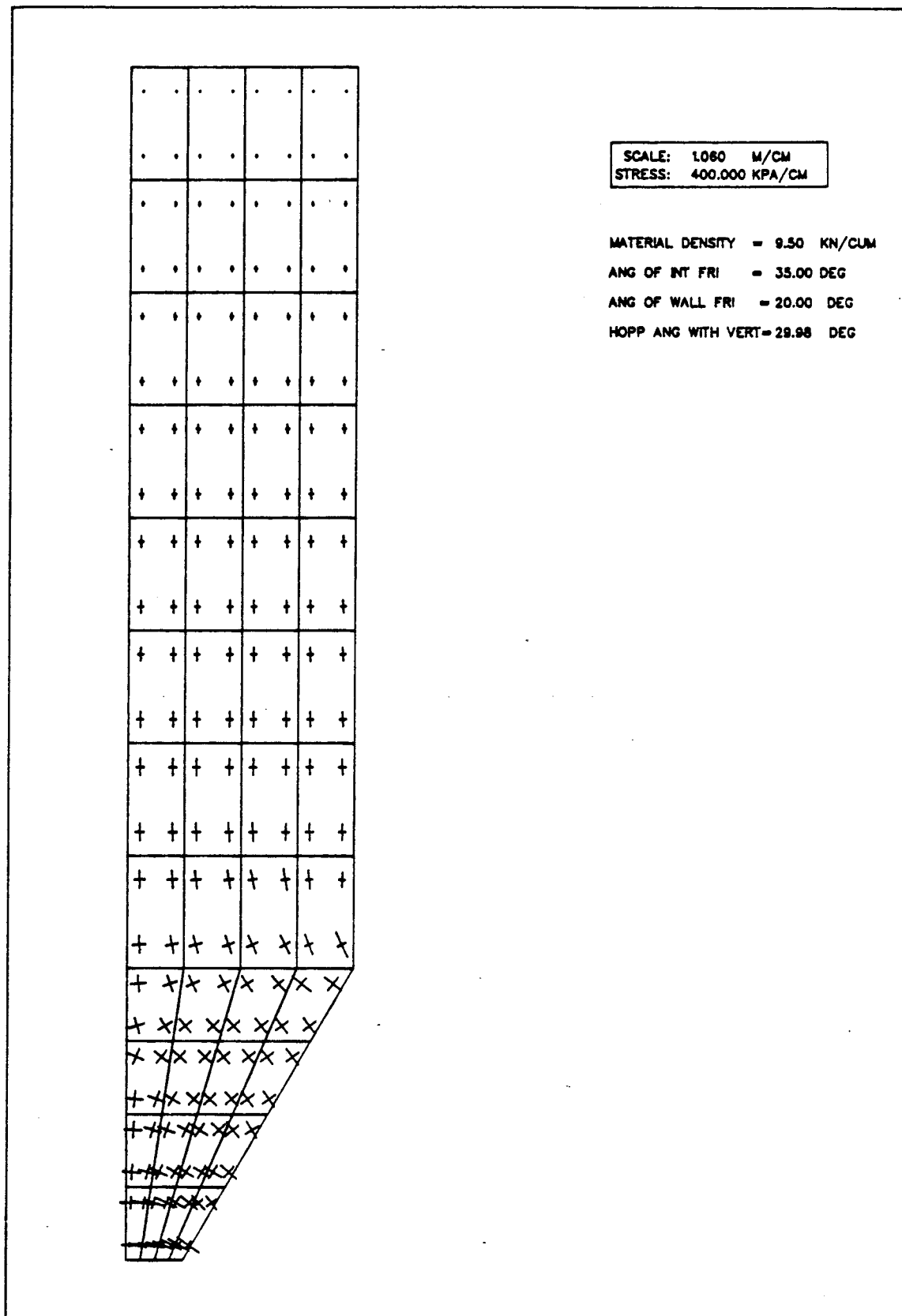


Fig. 5.6 Stress Field During Flow for $\theta' = 29.98^\circ$

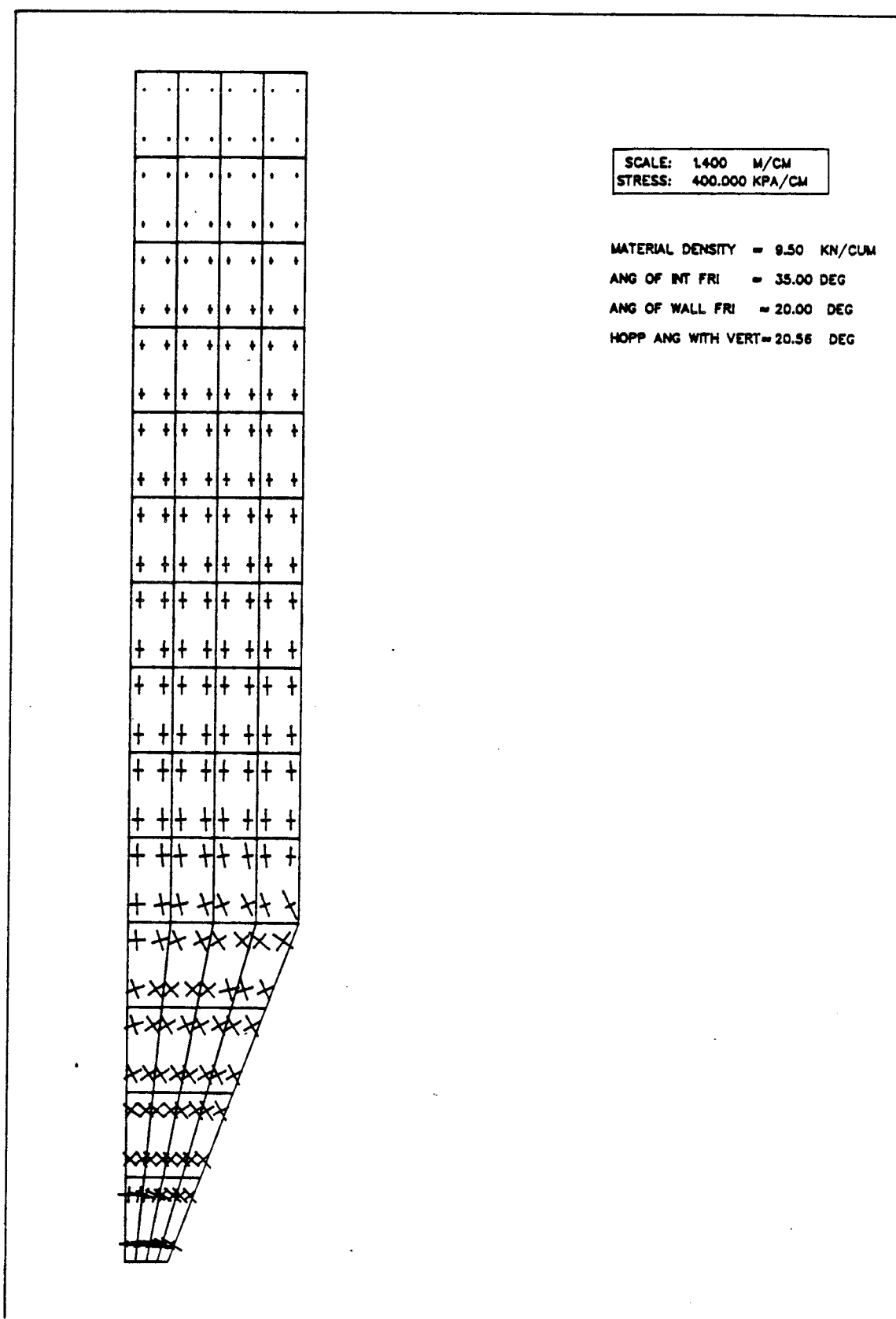


Fig. 5.7 Stress Field During Flow for $H/D = 2.5$

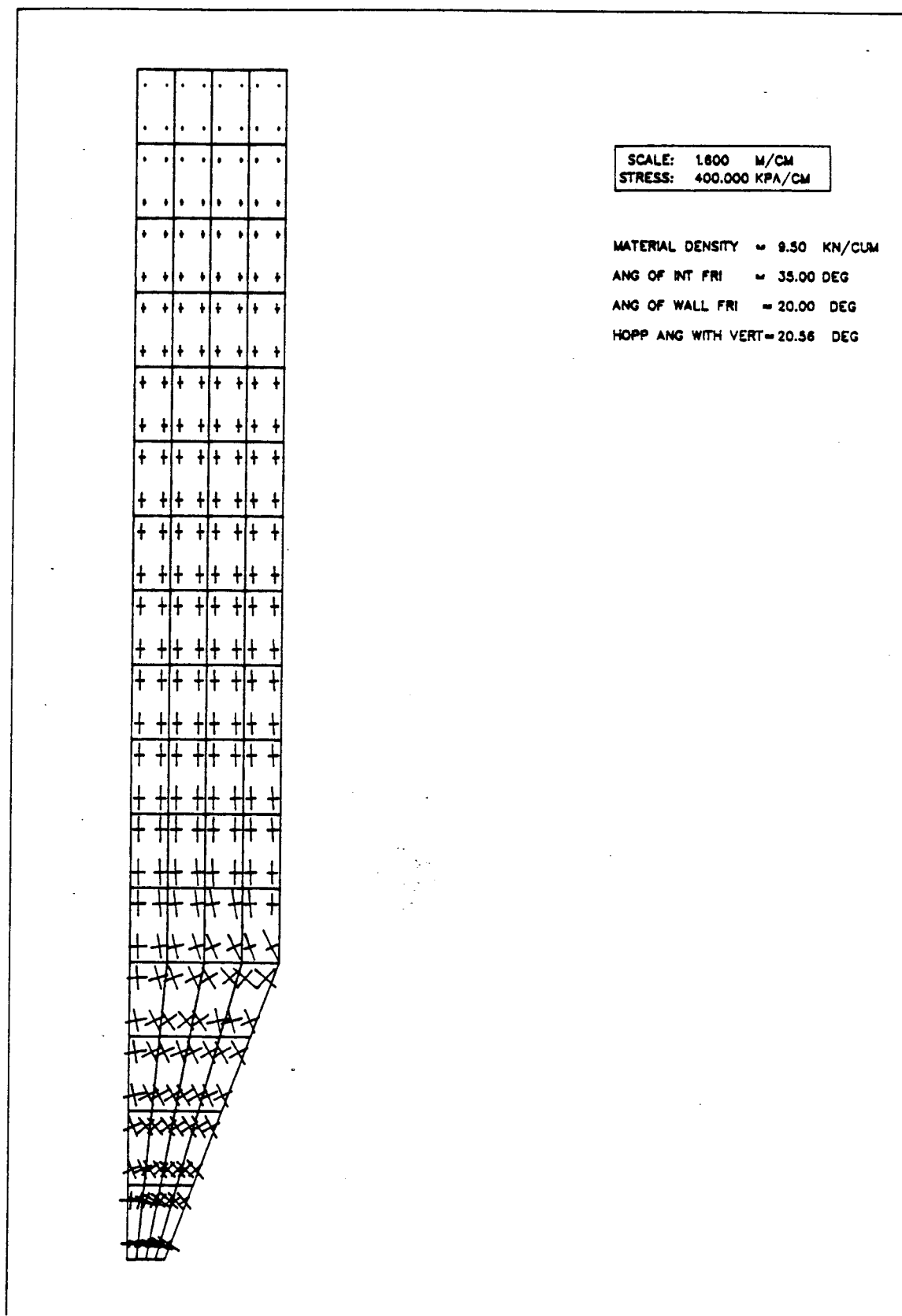


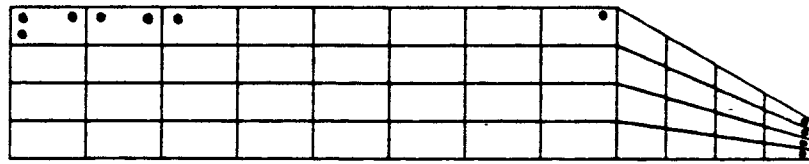
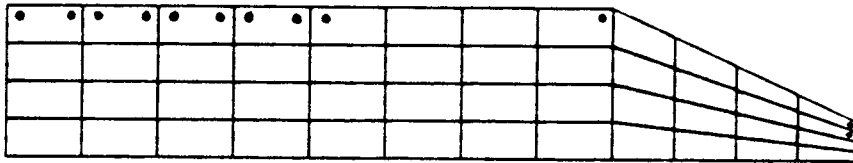
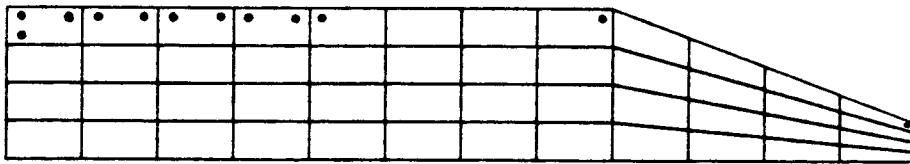
Fig. 5.8 Stress Field During Flow for $H/D = 3.0$

transition, while the finite element result shows that this radial stress field may extend only from 2 to 2.5 times the diameter of the outlet above the outlet level. Above this height the radial stress field does not exist.

Program FEPILS outputs yielding information at gaussian points. Fig. 5.9 shows the yielded zones of material for different hopper geometry. The yielded zone propagates downwards from the free surface along the silo wall to the transition with an increase in angle of wall friction and decrease in angle of internal friction of the material. A decrease in Poisson's ratio does not change this effect. These have been illustrated in Figs. 5.10 to 5.12.

5.3.3 Displacement/Velocity Field

The deformed mesh is illustrated in Fig. 5.13 to 5.15 for angles of wall frictions of 15° , 20° and 25° , respectively. The broken line shows the original mesh whereas the solid line indicates a deformed mesh. It is obvious that the Coulomb friction mechanism has considerable influence on the displacement/velocity field of the flowing mass of the solid. The resistance to the flow increases with increase in angle of wall friction. This is an effect of high shear stress near the wall and especially in the region above the outlet. However, the flow velocity is approximately constant in the cylindrical area of silo indicating that the material moves as a rigid body. Whereas in the hopper area the flow velocity near the centre line is

(c) $\theta' = 29.98$ (b) $\theta' = 24.78$ (a) $\theta' = 20.56$ Fig. 5.9 Yielded Zones when θ' is Varied

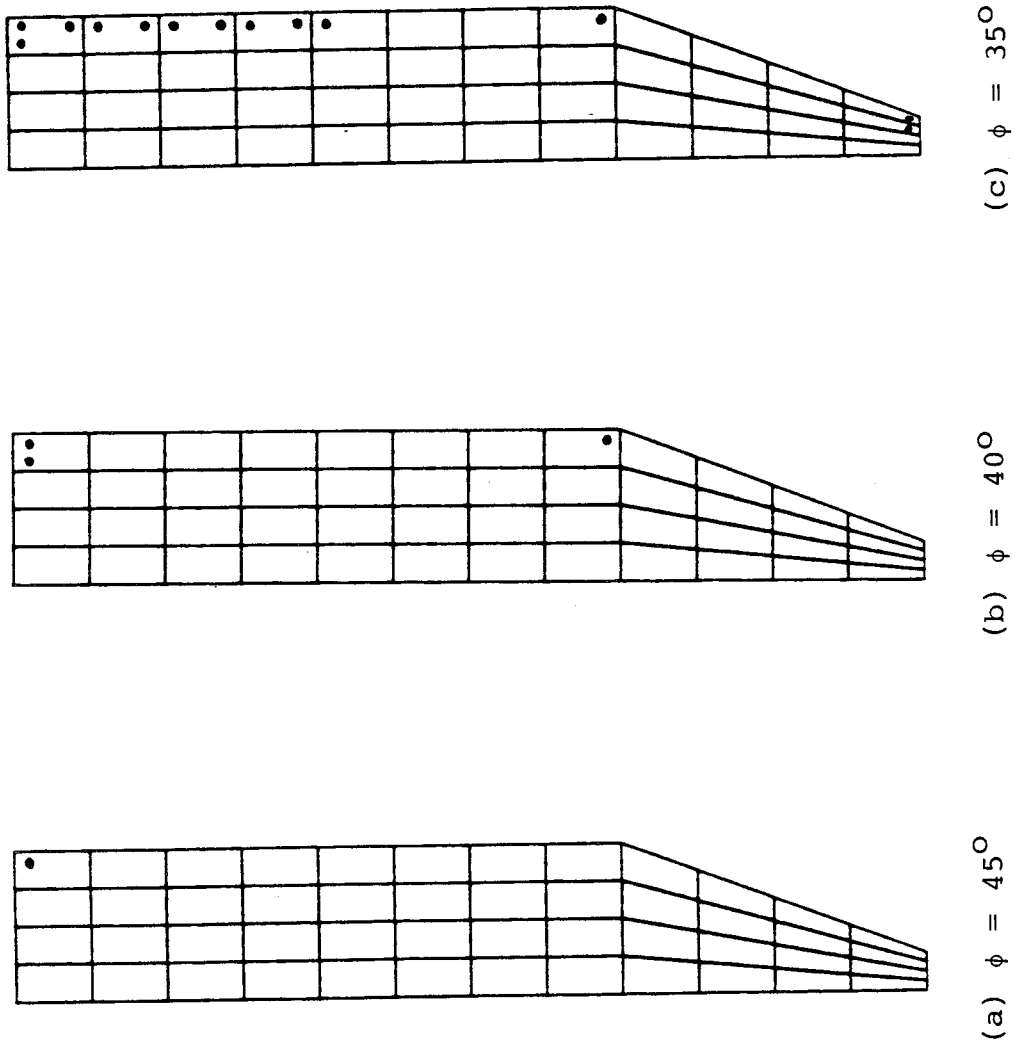
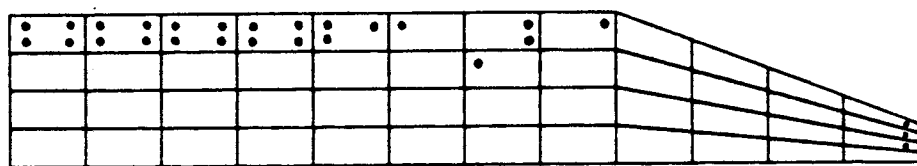
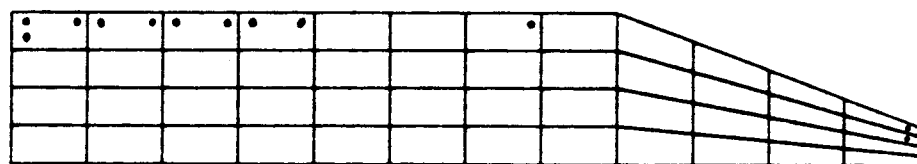
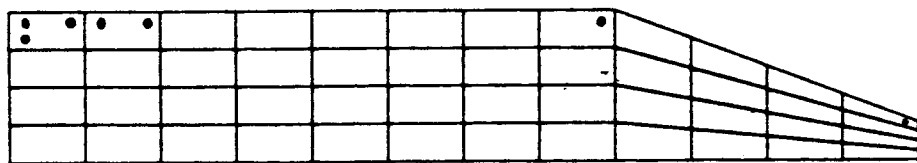
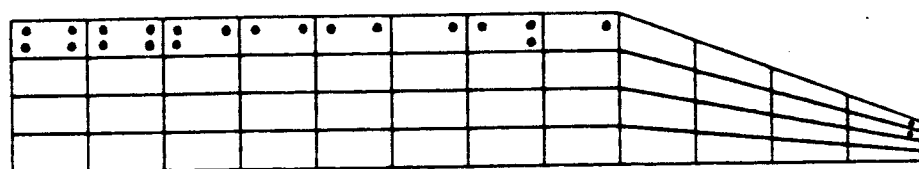
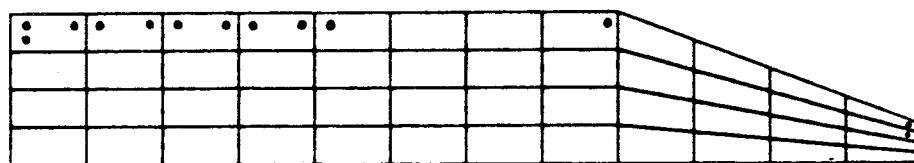
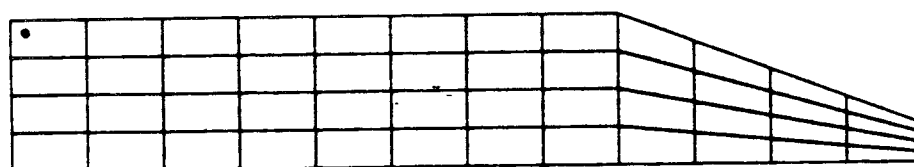


Fig. 5.10 Yielded Zones when ϕ is Varied

(c) $\phi' = 25^\circ$ (b) $\phi' = 20^\circ$ (a) $\phi' = 15^\circ$ Fig. 5.11 Yielded Zones when ϕ' is Varied

(c) $\nu = 0.25$ (b) $\nu = 0.30$ (a) $\nu = 0.35$ Fig. 5.12 Yielded Zones when ν is Varied

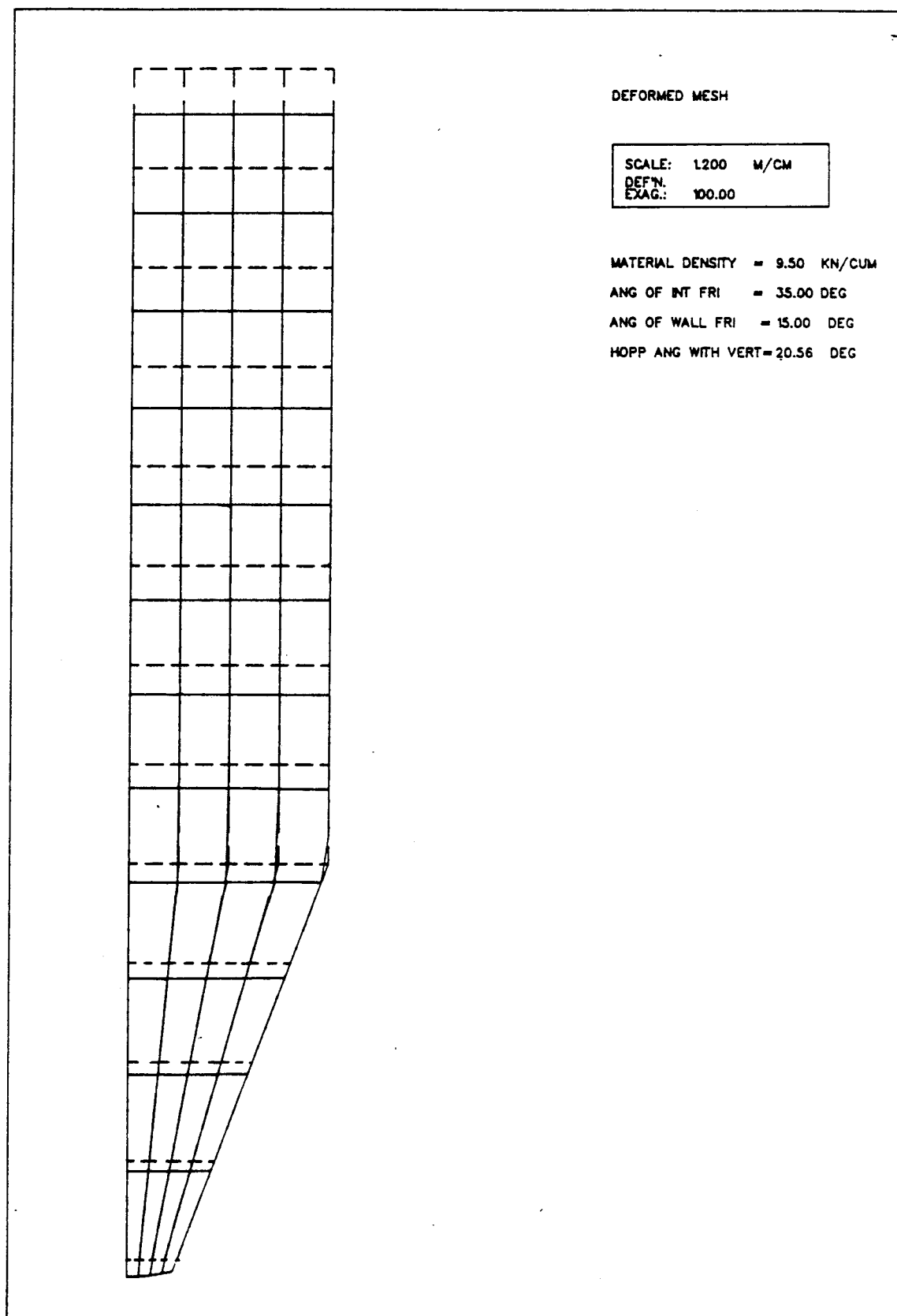


Fig. 5.13 Displacement/Velocity Field for $\phi' = 15^\circ$

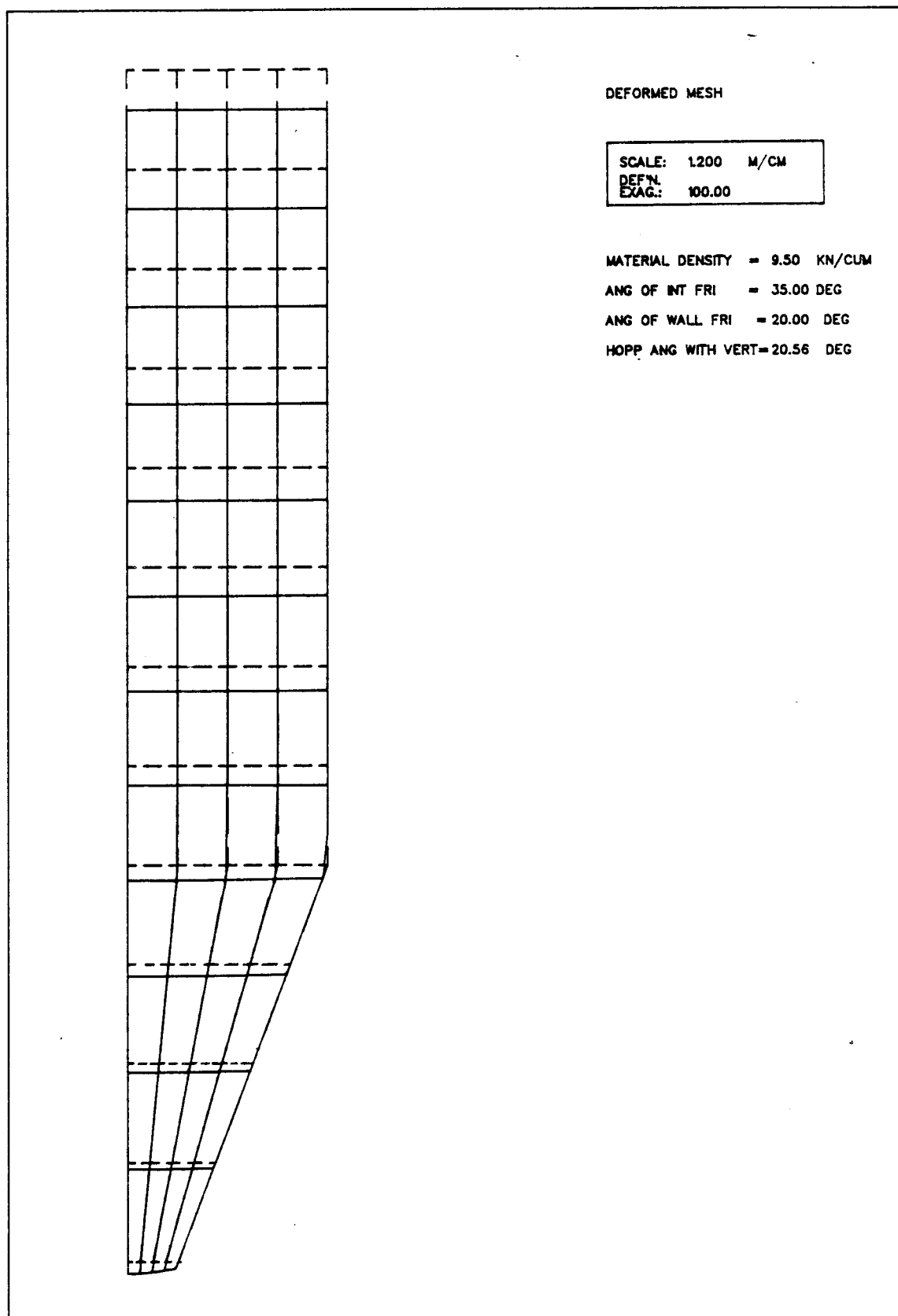


Fig. 5.14 Displacement/Velocity Field for $\phi' = 20^\circ$

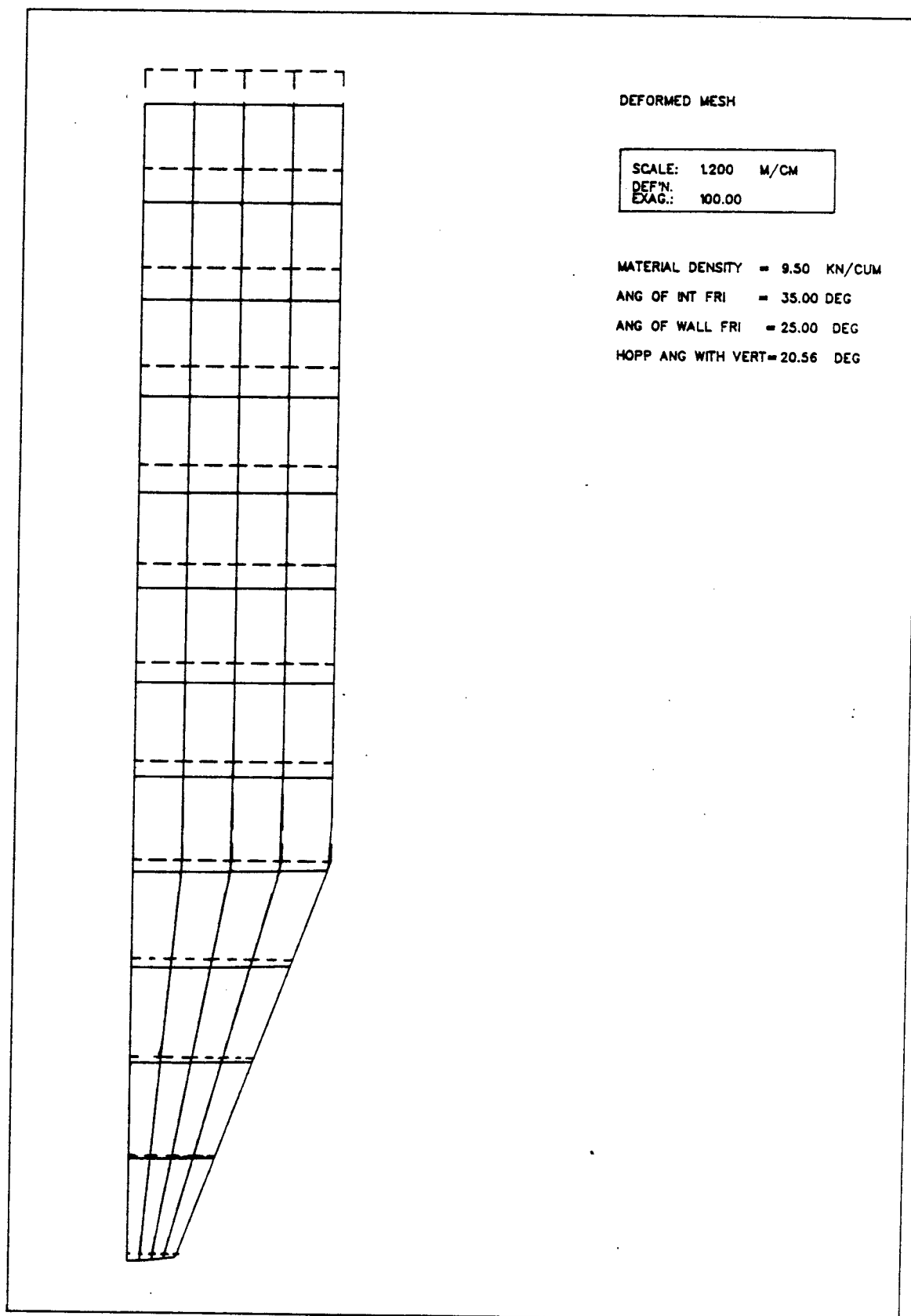


Fig. 5.15 Displacement/Velocity Field for $\phi' = 25^\circ$

considerably larger than those near the wall of the hopper.

5.3.4 Influence of Various Variables on Lateral Wall

Pressure

The finite element results for lateral wall pressures are presented in Figs. 5.16 to 5.20. The variables examined are the angle of internal friction, the angle of wall friction, the hopper slope, the cylindrical height to diameter ratio and Poisson's ratio. One variable is varied, while the others are kept constant. For example, to investigate the effect of varying the angle of internal friction ϕ , the angle of wall friction ϕ' , the density, γ , the hopper slope with vertical, θ' , the height to diameter ratio, modulus of elasticity and Poisson's ratio are kept constant.

Analysis of Fig. 5.16 reveals that variation of angle of internal friction does not have any significant effect on lateral wall pressure. This variable does not appear in any classical theory formulation for lateral wall pressure.

The effect of the angle of wall friction on the pressures at the wall is illustrated in Fig. 5.17. The diagram indicates an increase in wall pressure with decrease in angle of wall friction. This trend is also indicated by Janssen's and Reimbert's formulas. The difference between the pressure is greater at the transition and in the hopper area. This is obviously a direct result of the amount of load transmitted to the wall through friction. The

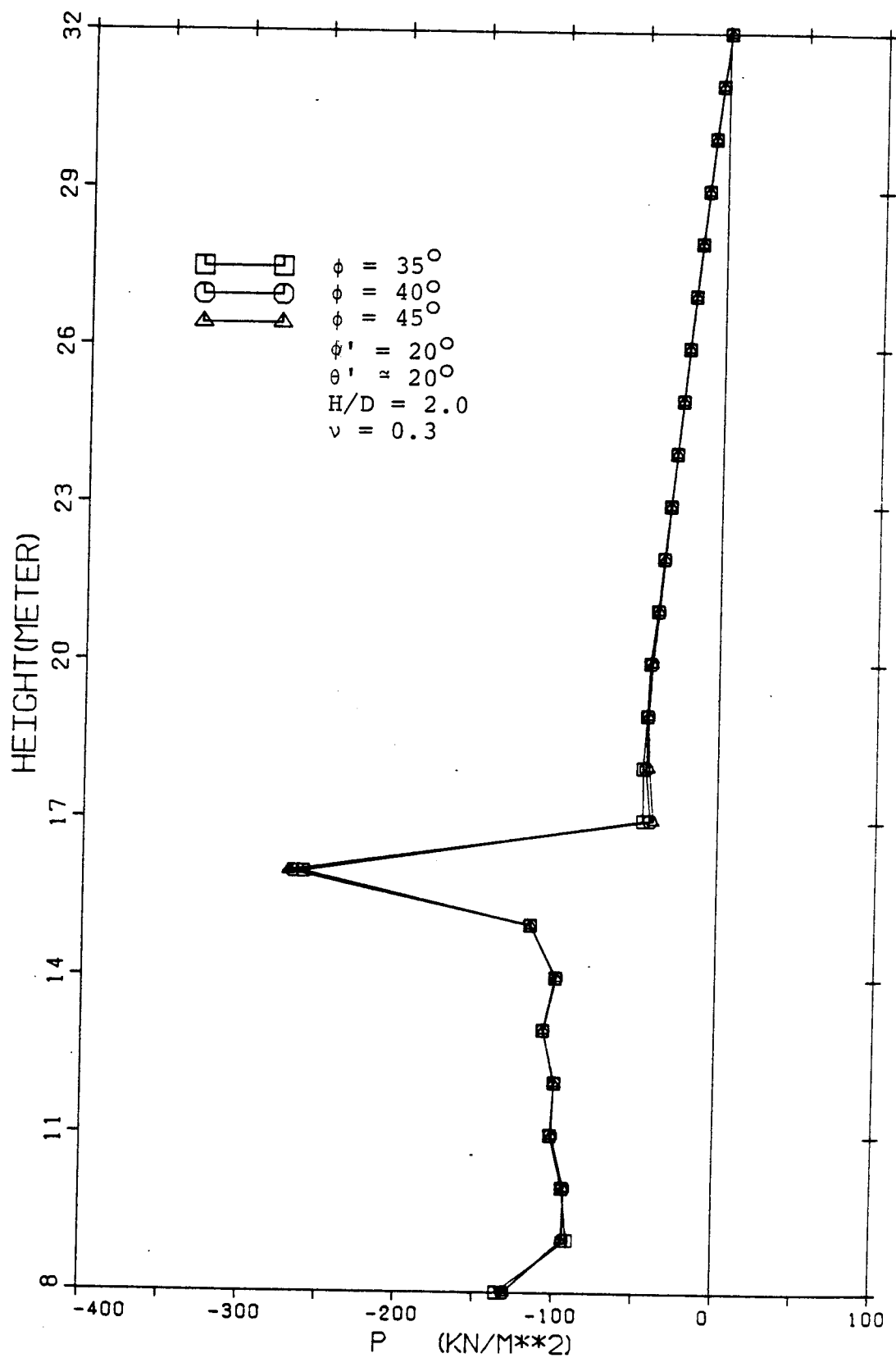


Fig. 5.16 Pressure Distribution when ϕ is Varied

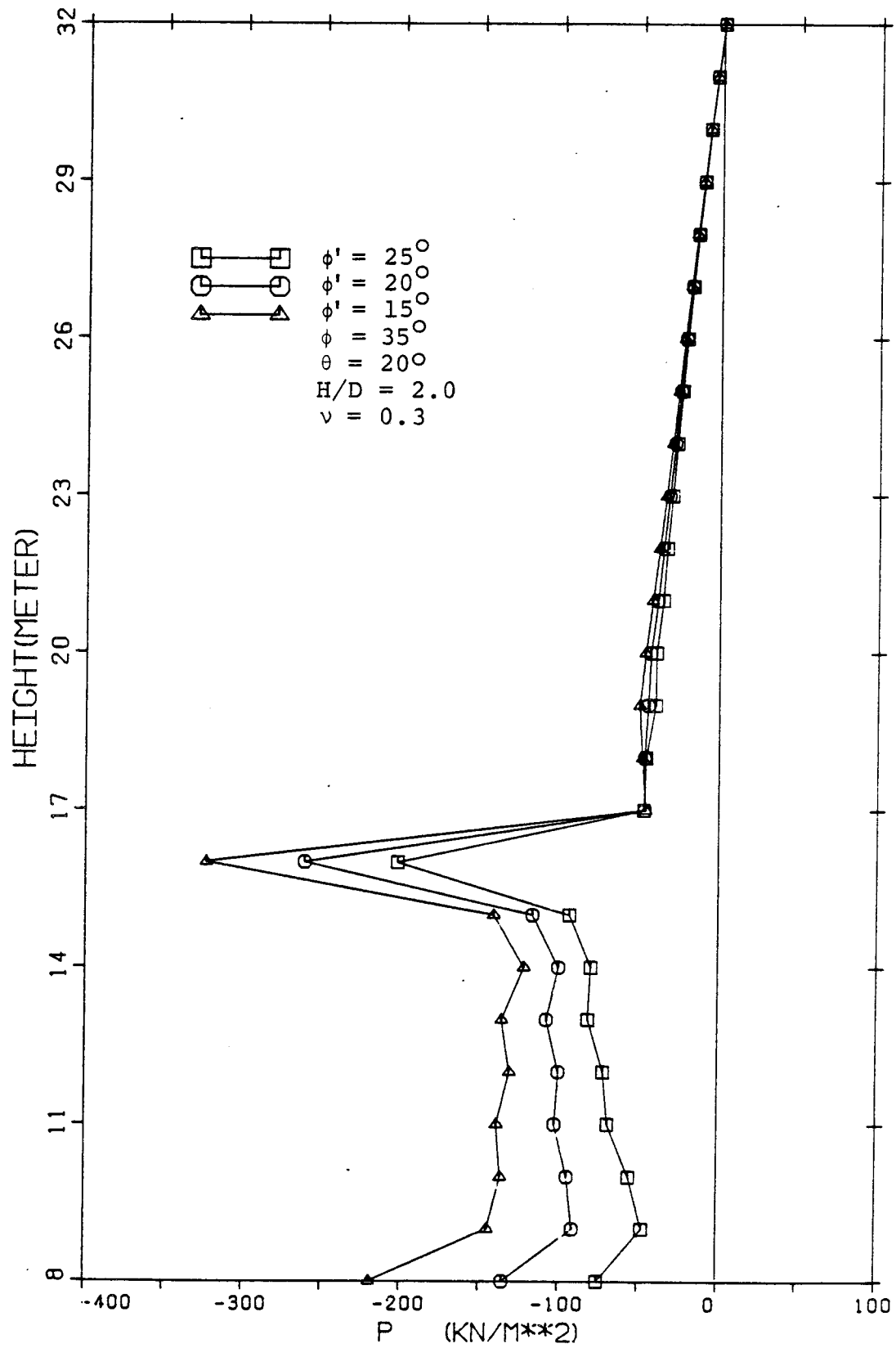


Fig. 5.17 Pressure Distribution when ϕ' is Varied

percentage of load carried by the silo wall increases with increase in angle of wall friction. If it is assumed that the ratio of horizontal pressure does not change, then the horizontal pressure is proportional to the vertical pressure at any point in the material, and hence the lateral wall pressure is inversely proportional to the angle of wall friction.

The influence of hopper slope on wall pressure is shown in Fig. 5.18. There is a slight increase in pressure in the cylindrical part of the silo. The peak pressure at transition changes greatly with increase in hopper slope. Also, the average pressure normal to the hopper wall and at the outlet increases with increase in hopper slope.

Fig. 5.19 illustrates the case when the hopper geometry is not changed and the vertical height of the cylinder is increased. A tremendous increase in peak pressure at the transition and normal to hopper wall is observed. The horizontal pressure on the cylindrical wall increases in similar fashion with depth of material. Jenike's formula (1969) for peak pressure at transition also gives an increase in pressure with depth of stored material, while his solution for radial stress field in the hopper does not account for the depth of material in the silo above transition. The finite element solution shows that pressure normal to the hopper wall also increases with an increase in depth of material above transition.

The last parametric variable investigated in this study

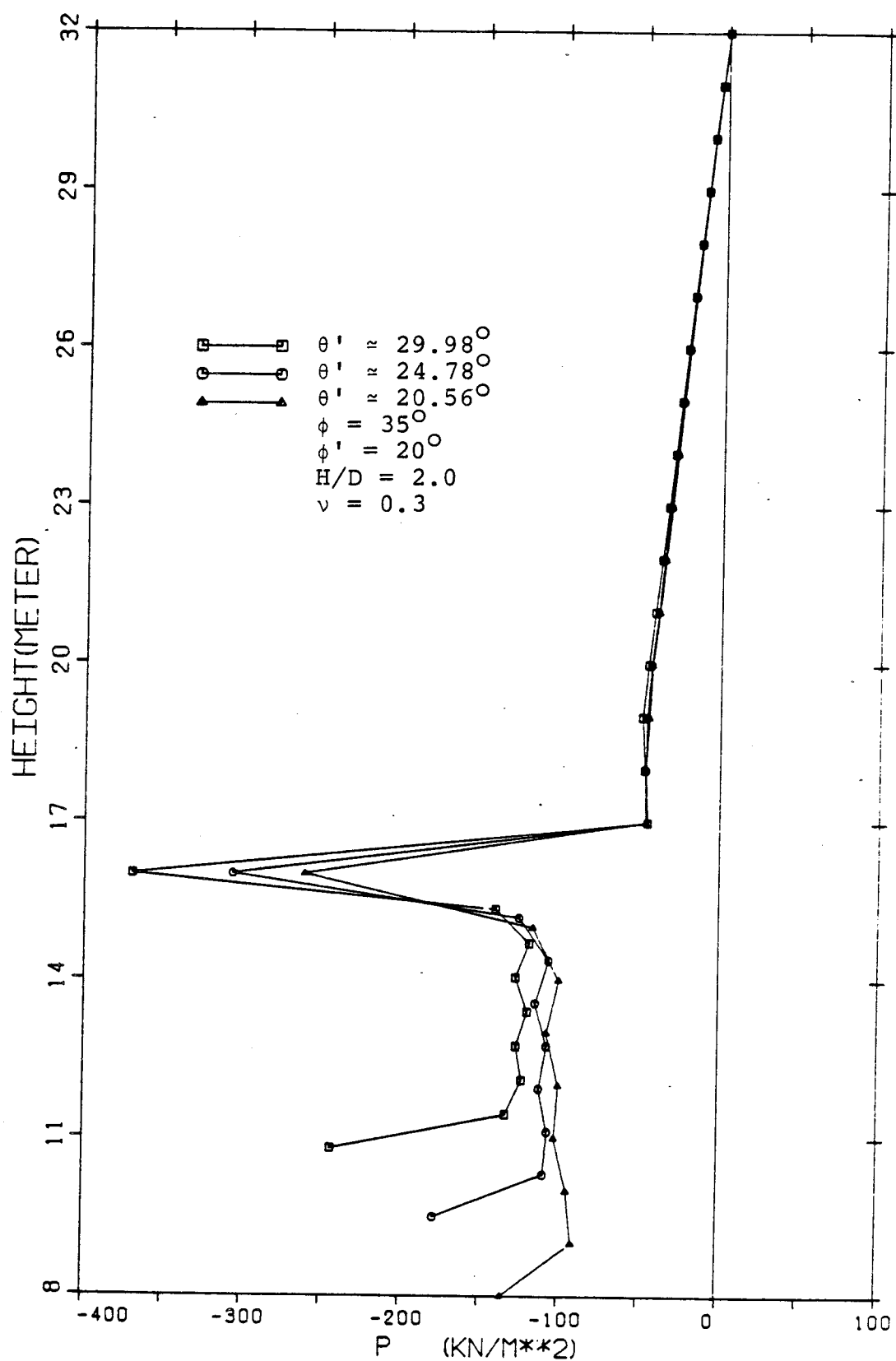


Fig. 5.18 Pressure Distribution when θ' is Varied

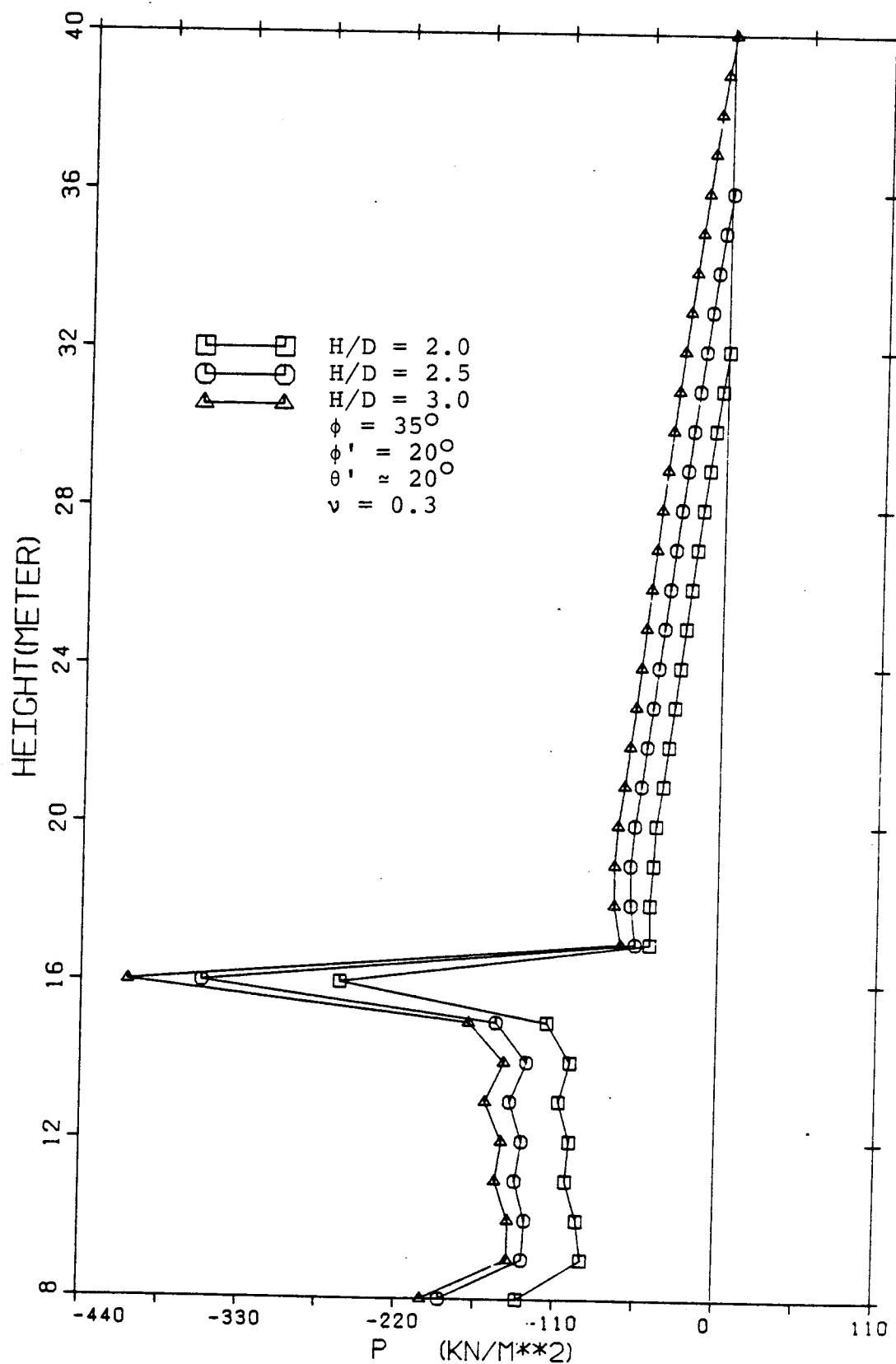


Fig. 5.19 Pressure Distribution when H/D is Varied

is Poisson's ratio, ν . Fig. 5.20 shows its influence on wall pressure. In the hopper portion the pressure increases with a decrease in Poisson's ratio. At transition and in the cylindrical part of the silo the pressure increases for $\nu = 0.3$ and for Poisson's ratio of 0.35 and 0.25 identical distribution is observed.

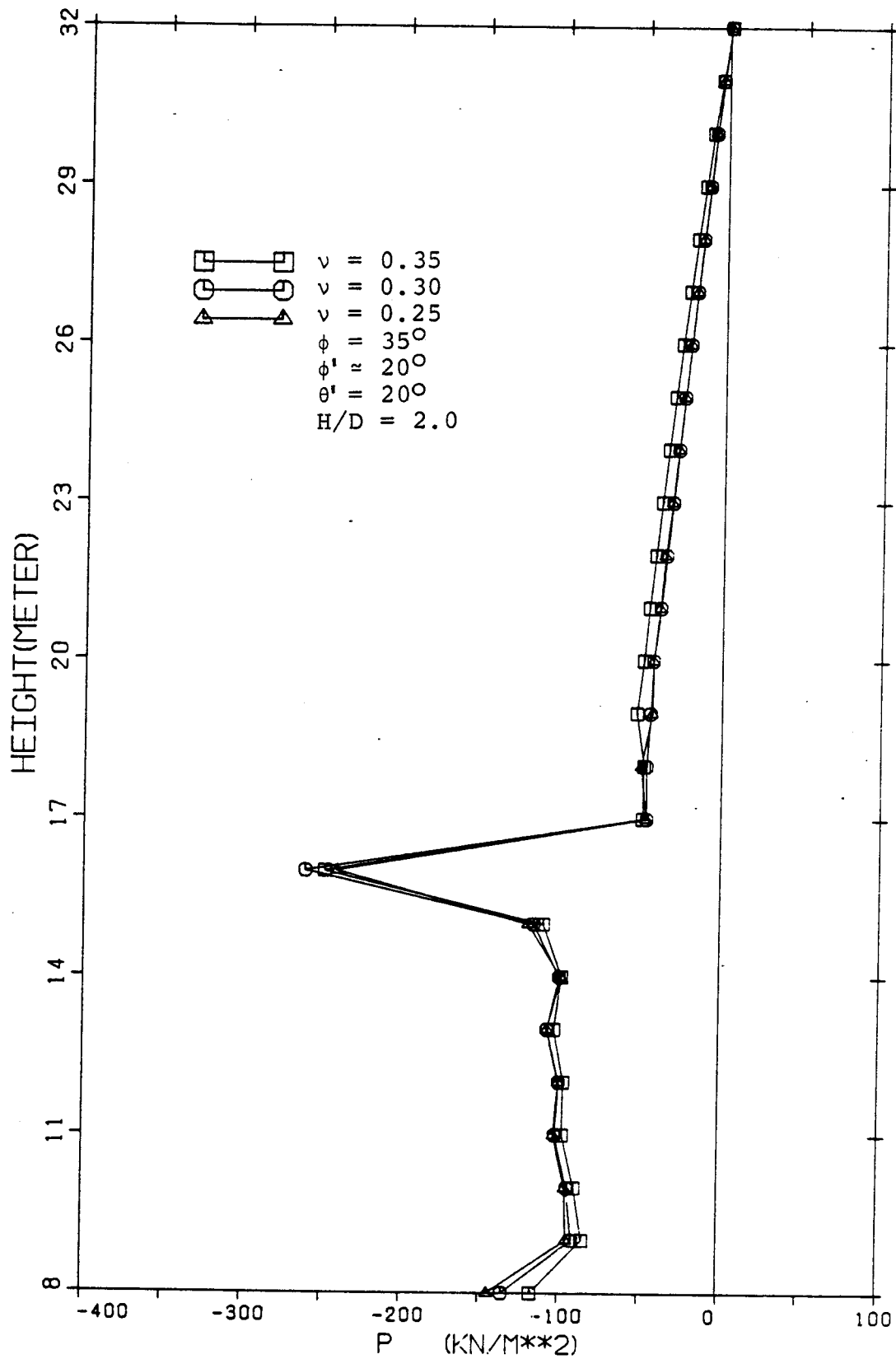


Fig. 5.20 Pressure Distribution when ν is Varied

CHAPTER 6 - SUMMARY AND RECOMMENDATIONS

An incremental finite element formulation has been developed to analyze displacement/velocity, stress and pressure fields in axisymmetric silos during discharging. A variational approach based on the principle of virtual work has been employed, where Coloumb friction terms are incorporated. The flowing solid material in a silo appears to behave in a viscoplastic manner (Eibl et al. 1984). Due to nonavailability of rate-dependent material law for coal, which is the primary direction of this study, an elastic-plastic material behaviour is proposed for this initial study.

An isoparametric finite element of the serindipity family is used to model the solid material in silos, and spring boundary elements are used to model the silo walls. The Gaussian integration technique and a Newton-Raphson iterative scheme are adopted in the program. Among three possible approaches proposed in Chapter 3 for contact problems incorporating Coloumb friction, an iterative approach has been chosen as a first step for the rigorous solution of the problem. The proposed friction model and constitutive law are incorporated in program FEPILS.

Two iterative levels are involved. The first iterative level is at the material level and the second is at the friction force level. The algorithm used for the material model is limited to strong materials with a lower bound on

the angle of internal friction of 35° . Although a crude initial stress option exists it must of necessity be limited to small values in order not to affect the final outcome. Thus improvement of that model is necessary. On the other hand, iterating over the friction forces implies reversal of the displacement increment and hence oscillations of both the normal pressure and the friction forces. In order to smooth out the oscillation of convergence, an under-relaxation factor has been introduced over the friction forces. This factor appears to be problem dependant, and hence judgement should be exercised to choose an efficient value.

The results of finite element analyses of axisymmetric silos during discharging are presented. They are compared with the solutions of classical theories. The lateral wall pressure in the cylindrical portion of silos shows good agreement with Janssen's solution. The peak pressure at transition is found to be 20 percent above Jenike's solution. A decreased tolerance in friction forces produces a better result. A tremendous variation in the pressure field in the hopper area is found as compared to Jenike's prediction. This variation may, in part, be due to the severe dilation characteristics of the Drucker-Prager yield surface, and in part due to the use of an elastic perfectly plastic algorithm. The results may be improved by using a more realistic yield surface which depends on all three invariants of the stress tensor and perhaps by implementing

a strain softening plastic algorithm.

A local pressure peak is found at the outlet. This may be due to the rigid displacement boundary conditions imposed on the model at the outlet. Eibel and Häusler (1984) used a zero force boundary condition at that location. In practice it is known that the outlet design is generally soft. However, it does have some stiffness. Therefore, future studies should attempt to clarify the existence of a peak relative to a given outlet stiffness.

The stress distribution shows good agreement with Jenike's predictions under both initial and flow conditions, an active field when the outlet is closed, and a passive field in the hopper when material discharges from the silo. Jenike proposed a radial stress field for hoppers but the finite element solution shows that this field may exist only up to a distance equal to 2 to 2.5 times the outlet diameter above the outlet.

A parametric study is carried out to predict the influence of pertinent variables on lateral wall pressure. It is found that variation of the angle of internal friction and Poisson's ratio have negligible effect on pressure field. The lateral wall pressure increases with a decrease in angle of wall friction. The peak pressure at transition and pressure in hopper area increases with increase in hopper slope with the vertical. An increase in height to diameter ratio causes an increase in peak pressure at transition and pressure on the hopper wall. The pressure

field in the cylindrical part have identical distributions with respect to depth of stored material.

The present method is an initial approach to modelling the material behavior in a mass flow silo. Further research in this area is necessary. The alternative approaches proposed in Section 3.2 may be investigated for better performance. An experimental study and formulation of a rate dependent constitutive law of material is necessary. A failure surface similar to Willam-Warnke surface, for solid materials subjected to triaxial compression may be developed for better representation of material response. A model or full scale test may be carried out to investigate the lateral wall pressure in order to compare with the finite element solution. A numerical study on the convergence criteria to handle ill conditioning of the material model is necessary. This condition occurs when the hydrostatic stress is small and deviatoric stress is very large as compared to the yield stress of the failure surface.

REFERENCES

1. ACI Committee 313, Recommended Practice for the Design and Construction of Concrete Bins, Silos and Bunkers for Storing Granular Materials. ACI Standards 313-77, American Concrete Institute, Detroit, 1977, 40 pp.
2. Airy, W., The Pressure of Grain, Minutes of Proceedings, Institute of Civil Engineers, London, Vol. 131, 1897, pp. 347-358.
3. Argyris, J.H., Faust, G., Szimat, J., Warnke, E.P., and Willam, C.J., Recent Developments in the Finite Element Analysis of Prestressed Concrete Reactor Vessels, Nuclear Engineering and Design, 28, 1974, pp. 42-75.
4. Almroth, B.O., Stren, P. and Brogan, F.A., Future Trends in Nonlinear Structural Analysis, Computers and Structures, Vol. 10, 1979, pp. 368-374.
5. Arnold, P.C. and Robert, A.W., A Useful Procedure for Predicting Stresses of the Walls of Mass Flow Bins, AISCE, 80th National Meeting, Boston, Paper No. 49B, 1975.
6. Bagster, D.F., A Note on Pressure Ratio in the Janssen Equation, Powder Technology, Vol. 4, 1970/71, pp. 235-237.
7. Bathe, K.J., Finite Element Procedures in Engineering Analysis, Prentice-Hall Inc., New Jersey, 1982.
8. Bergau, W., Measurements of Pressures of Filling Materials Against Walls, Proc. No. 17, Royal Swedish

- Geotechnical Institute, 1959, pp. 47-71.
9. Bernstein, M.S., Rastchot Konstruktsii s Odnostronnimi Sviazami, (Design of Structures with One Sided Connections), Gossfroyizdat, Moscow, 1947, p. 85.
 10. Bishara, A.G., Ayoub, S.F., and Mahdy, A.S., Static Pressures in Concrete Circular Silos Storing Granular Materials, ACI Journal, May-June, 1983, Title No. 80-21, pp. 56-62.
 11. Bishara, A.G., and Chandrangsu, Karoon, Nonlinear Finite Element Analysis of Farm Silos, Proceedings ASCE, Vol. 104, ST7, July, 1978, pp. 1045-1059.
 12. Bishara, A.G. and Mahmoud, M.M., Silage Constitutive Laws and Finite Element of Silage-Silo Interaction, Proceedings IASS, World Congress on Space Enclosures, Concordia University, Montreal, Canada, July, 1976, pp. 867-877.
 13. Blanchard, M.H., and Walker, D.M., Coal Flow - Pressures in Experimental Hoppers, Central Electricity Generating Board, South Western Region, Portishead, England, Aug. 1966.
 14. Blight, G.E., and Midgley, D., Pressure Measured in a 20M Diameter Coal Load-out Bin, International Conference on Design of Silos for Strength and Flow, Powder Advisory Centre, London, England, 1980.
 15. Bovey, H.T., Experiments on Grain Pressures in Deep Bins and the Strength of Wooden Bins, Engineering News, Vol. 52, 1904, pp. 32-34.

16. Bransby, P.L., Blair-Fish, P.M., and James, R.G., An Investigation of the Flow of Granular Materials, Powder Technology, Vol. 8, 1973, pp. 197-206.
17. Campos, L.T., Oden, J.T. and Kikuchi, N., A Numerical Analysis of a Class of Contact Problems with Friction in Elasto-Plastic, FENOMECH '81, Proceedings of the 2nd International Conference on Finite Element in Nonlinear Mechanics, Stuttgart, W. Germany, August, 1981.
18. Clague, K., and Wright, H., Pressures in Bunkers, ASME, Material Handling Division, Paper No. 73-MH-4, 1973.
19. Dabrowski, R., Shell Analysis of Intermediate Silo Bin, Journal of the American Concrete Institute, Vol. 62, No. 7, July, 1965, pp. 795-804.
20. Drucker, D.C. and Prager, W., Soil Mechanics and Plastic Analysis or Limit Design, Q. Appl. Math., Vol. 10, No. 2, July, 1952, pp. 157-165.
21. Eibl, J., and Häussler, U., Numerical Investigations on Discharging Silos, Journal of the Engineering Mechanics, ASCE, Vol. 110, No. 6, June, 1984, pp. 957-971.
22. El-Azazy, S.S., Finite Element Analysis of Bottom Unloading Farm Silos, Ph.D. Dissertation, The Ohio State University, Columbus, Ohio, 1982.
23. Elwi, A.A., and Murray, D.W., Nonlinear Analysis of Axisymmetric Reinforced Concrete Structures, Structural Engineering Report No. 87, Department of Civil Engineering, The University of Alberta, Edmonton,

- Alberta, Canada, May, 1980.
24. Elwi, A.A., and Murray, D.W., FEPARCS5 - A Finite Element Program of the Analysis of Axisymmetric Reinforced Concrete Structures - Users Manual, Structural Engineering Report No. 93, Department of Civil Engineering, The University of Alberta, Edmonton, Alberta, Canada, Nov. 1980.
 25. Elwi, A.E., and Murray, D.W., 'Substructure Analysis of Plane Frames', Structural Engineering Report No. 64, Department of Civil Engineering, University of Alberta, Edmonton, Alberta, June 1977.
 26. Fayed, M.E., and Otten, L., Handbook of Powder Science and Technology, Van Nostrand Reinhold Company, 1984.
 27. Fellipa, C.A., 'Procedures for Computer Analysis of Large Non-Linear Structural System', Large Engineering Systems, ed. A. Wexler, Pergamon Press, London, U.K., 1976, pp. 60-101.
 28. Fellipo, C.A., 'Finite Element Analysis of Three Dimensional Cable Structures, Computational Methods in Nonlinear Mechanics, The Texas Institute for Computational Mechanics, 1974, pp. 311-324.
 29. Handley, M.F., and Perry, M.G., Stresses in Granular Materials Flowing in Converging Hopper Sections, Presented at Symposium of Powder Flow and Storage, University of Bradford, England, Sept., 1967, Powder Technology, Vol. 2, No. 2, Mar., 1968.
 30. Janssen, H.A., Versuche Weber Getreidedruck in

- Silozellen, (Experiments about Pressure of Grain in Silos), Zeitschrift, Verein Deutscher Ingenieure, Vol. 39, Aug., 1985, pp. 1045-1049.
31. Jenike, A.W., Better Design for Bulk Handling, Chemical Engineering, Vol. 61, Dec., 1954, pp. 175-180.
 32. Jenike, A.W., and Shield, R.T., On the Plastic Flow of Coulombs Solids beyond Original Failure, Journal of Appl. Mech., Trans., ASME, Vol. 26, No. 4, Series E, 1959, pp. 599-602.
 33. Jenike, A.W., Gravity Flow of Bulk Solids, Bulletin 108, Utah Engineering Experimental Station, University of Utah, 1961.
 34. Jenike, A.W., Storage and Flow of Solids, Bulletin 123, Utah Engineering Experiment Station, University of Utah, 1964, (Revised 1976).
 35. Jenike, A.W., Steady Gravity Flow of Frictional-Cohesive Solids in Converging Channels, Journal of Applied Mechanics, Series E, Vol. 31, No. 1, 1964, pp. 5-11.
 36. Jenike, A.W., and Johanson, J.R., Bin Loads, Journal of the Structural Division, ASCE, Vol. 94, No. ST4, April, 1968, pp. 1011-1041.
 37. Jenike, A.W., and Johanson, J.R., On the Theory of Bin Loads, Journal of Engineering for Industry, Trans., ASME, Series B, Vol. 91, No. 2, May, 1969, pp. 339-344.
 38. Jenike, A.W., Johanson, J.R., and Carson, J.W., Bin Loads-Part 2: Concepts, Trans., ASME, Journal of Engineering for Industry, Vol. 95, No. 1, 1973, pp. 1-5.

39. Jenike, A.W., Johanson, J.R. and Carson, J.W., Bin Loads - Part 3: Mass Flow Bins, Trans. ASME, Journal of Engineering for industry, Vol. 95, No. 1, 1973, pp. 6-12.
40. Jenike, A.W., Johanson, J.R., and Carson, J.W., Bin Loads - Part 4: Funnel Flow Bins, Trans., ASME, Journal of Engineering for Industry, Vol. 95, No. 1, 1973, pp. 13-16.
41. Jofriet, J.C., Lelievre, B., and Fwa, T.F., Friction Model for Finite Element Analyses of Silos, Trans., ASAE, Vol. 20, No. 4, 1977, pp. 735-740 and 744.
42. Jofriet, J.C., and Czajkowski, J., A Parametric Study of Whole Plant Corn Silage Pressures and Loads in Tower Silos, Canadian Agricultural Engineering, Ottawa, Vol. 22, No. 1, June, 1980, pp. 1-7.
43. Jofriet, J.C., and Dickinson, R.R., Wall Pressure in Bottom Unloading Silos, ACI Journal, Jan-Feb., 1984, pp. 61-67.
44. Johanson, J.R., Stress and Velocity Fields in the Gravity Flow of Bulk Solids, Journal of Applied Mechanics, Series E, Vol. 86, Sept., 1964, pp. 499-506.
45. Johanson, J.R., Methods of Calculating Rate of Discharge from Hoppers and Bins, Trans., Am. Inst. Min. Metal. Eng., Vol. 232, March, 1965, pp. 69-80.
46. Ketchum, M.S., The Design of Walls, Bins, and Grain Elevators, McGraw-Hill Book Co. Inc., New York, 1909.
47. Kim, V.S., Davlenie Zerna i Sovershensrvovanie

- Konstruktsii Silosov Zernovikh Elevatorov, (Grain Pressure and Improvement of Construction of Silos and Grain Elevators), Khleboizdat, Moscow, 1959.
48. Kötter, F., Der Bodendruck Von Sand in Verticalem Cylindrischen Gefässen, Journal of Pure and Applied Math., Berlin, 1899, p. 189.
49. Kovtun, A.P., and Platonov, P.N., Davlinie Zerna na Strenki Silosov Elevator (The Pressure of Grain on Silos Walls), Mukomol 'no Elevatornaia Promyshlennost, Moscow, Vol. 25, No. 12, Dec. 1959, pp. 22-24.
50. Lade, P.V., Elasto-Plastic Stress-Strain Theory for Cohesionless Soil with Curved Yield Surface, International Journal of Solids and Structures, Vol. 13, 1977, pp. 1019-1035.
51. Luin, J.B., Analytical Evaluation of Pressures of Granular Materials on Silo Walls, Powder Technology, Vol. 4, 1969-70, pp. 280-285.
52. Motzkus, U., Belastung von Siloböden und Auslauftrichtern durch körnige Stutgart, Dissertation, Technical University of Braunschweig, Germany, 1974.
53. Nanninga, D., Gibt die Übliche Berechnungsart der Drücke auf die Wände und den Boden Von Silobauten Sichere Ergebnisse?, De Ingenieur, Vol. 44, Nov. 1956.
54. Nielsen, J. and Kristiansen, N., Related Measurements of Pressure Conditions in Full-Scale Barley Silo and in Model Silo, International Conference on Design of Silo for Strength and Flow, Powder Advisory Centre, London,

England, 1980.

55. Ohde, J., Silo-Aufgaben, Hütte Des Ingenieurs Taschenbuch, Vol. 3, W. Ernst & Sohn, Berlin, W. Germany, 1950, pp. 921-922.
56. Pian, T.H.H., Variational Principles for Incremental Finite Element Methods, Journal of Franklin Institute, Vol. 302, No. 5 and 6, Nov/Dec., 1976.
57. Pieper, K., Mittelman, G., and Wenzel, F., Messungen des Horizontalen Getreidedruckes in einer GSM hohen Silozelle, Beton-und-Strahlbetonbau, Vol. 11, Nov., 1964, pp. 241-246.
58. Pieper, K. and Wenzel, F., Druckverhältnisse in Silozellen, W. Ernst & Sohn, Berlin, 1964.
59. Ravenet, J., Flow of Cohesive Powder Products, Second International Conference on Design of Silos for Strength and Flow, Powder Advisory Centre, London, England, Nov., 1983.
60. Reimbert, M., Suppression dans les Silos lors de la Vidange, Travanx, Vol. 38, Nov., 1954, pp. 780-784.
61. Reimbert, M., The Design of Silos, Concrete and Construction Engineering, Vol. 50, No. 9, April, 1955, pp. 170-172.
62. Reimbert, M. and Reimbert, A., Silos - Theory and Practice, Clausthal, Germany, Trans. Tech. Publications, 1976.
63. Roberts, I., Determination of the Vertical and Lateral Pressures of Granular Substances, Proceedings, Royal

- Society, London, Vol. 36, 1884, pp. 225-240.
64. Sadler, J.E., More Research Needed in Coal Silo Technology, Coal Mining and Proceedings, May, 1976, pp. 70-72.
 65. Sadler, J.E., Silo Problems, International Conference on Design of Silos for Strength and Flow, University of Lancaster, Powder Advisory Centre, London, England, Sept., 1980.
 66. Shumsky, D.W., Elevatorno-Skiadskoye Chozyaystvo, Part 2, Zagozdiagat, Moscow, 1941, p. 115.
 67. Simmonds, S.H. and Smith, A.B.B., Lateral Coal Pressures in a Mass Flow Silo, Structural Engineering Report No. 113, Department of Civil Engineering, The University of Alberta, Edmonton, Alberta, Canada, Nov., 1983.
 68. Smoltczyk, H.W., Druckberechnung in Einem Smotrichter, Beton-und Stahlbe-tonbau, Vol. 48, Aug. 1953, pp. 192-194.
 69. Theimer, O.F., Failures of Reinforced Concrete Silos, Journal of Engineering for Industry, Trans., ASME, Series B, No. 2, Vol. 91, May, 1969, pp. 460-477.
 70. Toltz, M., Discussion on Grain Pressures in Deep Bins, Transactions, CSCE, Vol. 17, 1903, p. 641.
 71. Turitzin, A.M., Dynamic Pressure of Granular Material in Deep Bins, Journal of the Structural Division, ASCE, Vol. 89, No. ST2, April, 1963, pp. 49-73.
 72. Walker, D.M., An Approximate Theory for Pressures and Arching in Hoppers, Chemical Engineering Science, Vol.

- 21, 1966, pp. 975-997.
73. Walters, J.K., Theoretical Analysis of Stresses in Silos with Vertical Walls, Chemical Engineering Science, Vol. 28, No. 1, Jan., 1973, pp. 13-21.
74. Walters, J.K., Theoretical Analysis of Stresses in Axially Symmetric Hoppers and Bunkers, Chemical Engineering Science, Vol. 28, No. 3, March 1973, pp. 779-789.
75. Willam, K.J. and Warnke, E.P., Constitutive Model for Triaxial Behavior of Concrete, IABSE Seminar on Concrete Structures Subjected to Triaxial Stresses, ISMES, Bergamo, Italy, IABSE Proceedings, Vol. 19, 1975.
76. Williams, J.G., The Rate of Discharge of Coarse Granular Materials from Conical Hoppers, School of Powder Technology, University of Bradford, 1974.
77. Zienkiewicz, O.C., The Finite Element Method in Engineering Science, McGraw Hill, 1971.
78. Zienkiewicz, O.C., Valliappan, S., and King, J.P., Elasto-Plastic Solutions of Engineering Problems, Initial Stress Finite Element Approach, Int. J. Numer. Methods Engg., Vol. 1, 1969, pp. 75-100.
79. Zienkiewicz, O.C., and Nayak, G.C., Elasto-Plastic Stress Analysis, A Generalization for Various Constitutive Relations Including Strain Softening, Int. J. Numer. Methods Eng., Vol. 5, 1972, pp. 113-135.

APPENDIX A - PROGRAM STRUCTURE (FEPILS)

A.1 Introduction

Program FEPILS is a finite element Fortran Code for analysis of material behavior flowing through axisymmetric silos. The program assumes small displacements/velocities, negligible rotations and infinitesimal strains. It is originally designed for elastic-perfectly plastic type of materials, but it can also handle linear problems.

This Appendix deals with the general description of the program, the solution techniques and the flow of operations.

A.2 General Description

Program FEPILS is based on the finite element program FEPARCS5 (Elwi and Murray, 1980). The program handles combinations of linear, quadratic and cubic isoparametric elements.

The elastic-plastic constitutive relation presented in Chapter 4 is implemented in program FEPILS as the material model.

The program is basically designed for analysis of problems under gravity loads only. However it can handle other types of loads, such as hydrostatic pressures, concentrated nodal loads and normal and tangential surface pressures. These loads can be combined using the users's specified load factors. Dead loads can be a combination of gravity loads, hydrostatic pressures, and concentrated nodal

loads. A separate load vector for live concentrated loads is provided. Normal and tangential surface pressures are handled in two separate load vectors.

The input to the program is composed of control parameters, material properties, nodal geometry, spring boundary conditions, solid element information, material to silo wall contact surface information, concentrated nodal loads, normal and tangential surface pressure nodal intensity distributions and hydrostatic pressure nodal intensity distribution.

The output is composed of nodal displacements/velocities in the global coordinates, friction forces, normal forces or reactions, normal and tangential displacements/velocities of nodes lying on friction surfaces, and local coordinate stress components for solid elements.

Numerical integration is used for the evaluation of the different element relations as well as the loads, whenever necessary. A number of Gaussian integration rules can be chosen by the user, ranging from one point rule for linear four node elements to a three by seven two dimensional rule for higher order elements.

The program can use a tangential stiffness approach or the initial load method (see Elwi and Murray, 1980). A skyline in-core equation solver package (see Elwi, 1977 and Wilson and Bathe, 1975) is employed for equation solving.

An iterative method for friction forces is employed

using Coloumb's friction law as described in Chapter 3.

Element shape functions and derivatives evaluated at the integration points, stresses and strains at integration points and material properties are stored on sequential files.

A.3 Solution Techniques

A.3.1 Numerical Method for Load and Friction Forces

A finite element friction model formulation for the analysis of material behavior flowing through an axisymmetric silos is presented in Chapter 3. This is a displacement/velocity model. Therefore, it satisfies kinematic compatibility everywhere and it approximately satisfies equilibrium only on a global level. The incremental variation formulation of Section 3.2 leads to the following set of equations.

$$[k]\{\Delta r\} = \{\Delta R\} - \{\Delta Q\} \quad (A.1)$$

where $[k]$ is the structure stiffness matrix, $\langle \Delta \rangle$ is the increment of nodal displacement velocities, $\langle \Delta R \rangle$ is the increment of prescribed loads and $\langle \Delta Q \rangle$ is the unbalanced load at the end of the previous load step. Eq. A.1 together with the condition 3.4b make up a nonsingular system of equations which can be solved for the increment of displacement velocity $\langle \Delta r \rangle$.

$\langle \Delta R \rangle$ is a predetermined magnitude of load vector. As

described in Section 3.3.1 the friction forces are not known in advance. Therefore, the problem is initially solved without incorporating friction effects. After completing the first iteration of the problem, the increment of displacements/velocities at nodes are known. Using nodal displacements/velocities at the friction surface the friction force at nodes can be determined. These forces are multiplied by an under-relaxation factor and added to the corresponding nodal values in load vector $\langle \Delta R \rangle$. The second and successive iterations for friction is carried out using newly formed load vectors until convergence, as described in Section 3.3.1.

For nonlinear and elastic-plastic material response the Eq. A.1 is solved by incremental piecewise linearization. The increment of displacements/velocities obtained upon solving Eq. A.1, yields an increment of strain. The stress increment is obtained using constitutive matrix $[c]$ and strain increment $\langle \Delta \epsilon \rangle$. The difference between the applied loads and equilibrating loads, equivalent to the stress state which satisfies the constitutive law is called the unbalanced load. The state of stress which satisfies both kinematic compatibility and equilibrium can be arrived at by eliminating the unbalanced load through an iterative scheme.

The iterative schemes employed in this study are the tangential stiffness method (Argyris, et al., 1974), sometimes known as the Newton-Raphson method (Zienkiewicz, 1971) and the initial load method (Argyris, et al., 1974),

sometimes known as modified Newton-Raphson method (Zienkeiwicz, 1971).

In the tangential stiffness method, the stiffness matrix may be evaluated at the beginning of each load increment based on the current material properties. The initial load method retains the initial stiffness matrix until the material converges. This method needs a larger number of iterations to satisfy equilibrium. The main disadvantage of the tangential stiffness method is that it may lose its positive definite character or become ill conditioned when strain softening behavior is exhibited. An improved convergence may be obtained for both methods as follows.

- (a) introducing an over-relaxation factor to improve convergence of the initial load method
- (b) using an under-relaxation factor and numerical damping to enlarge the convergence domain of the tangential stiffness method (Almroth, Stren and Brogan, 1979 and Fellipa, 1974 and 1976).
- (c) re-evaluating the stiffness matrix after every few iterations in an initial load method. i.e. combination of the two iteration schemes.

All the above methods of improvement have been implemented in program FEPILS.

The Eucleadian norm method has been adopted to test the convergence of displacements/velocities, loads and friction forces of the iterative schemes. They can be described as

follows

$$\frac{||\Delta r^i||}{||r||} < \lambda_r \quad (A.2a)$$

$$\frac{||\Delta Q^i||}{||R||} < \lambda_R \quad (A.2b)$$

$$\frac{||\Delta F_T^i||}{||F_T||} < \lambda_R \quad (A.2c)$$

where λ_r and λ_R are the user specified tolerances on the displacements/velocities and loads (and friction forces) respectively, Δr^i is the increment of displacement/velocity vector obtained in i th iteration, r is the current displacement vector, ΔQ^i is the unbalanced load at the end of the i th iteration, R is the total load vector, ΔF_T^i is the increment of friction force vector at the end of i th iteration and F_T is the total sum of friction force vector. The symbol $|| \quad ||$ denotes the Euclidean norm.

A.3.2 Incremental Method for Plastic Model

This section deals with the numerical technique adopted for incorporating the elastic-plastic constitutive model presented in Chapter 4. The strain increment is obtained from the displacement/velocity increment solution of Eq. A.1 as

$$\{\Delta \epsilon\} = [B] \{\Delta r\} \quad (A.3)$$

The strain increment thus obtained may be relatively large to cause drift of the solution, particularly when the resulting stress point, which does not satisfy the constitutive relation, falls outside the yield surface. This problem has been overcome by splitting the strain increment into an equal number of smaller subincrements as

$$\langle \Delta \epsilon_s \rangle = \langle \Delta \epsilon \rangle / NI \quad (A.4)$$

where NI is the number of subincrements. In this manner, the stress point is changed gradually allowing close simulation of the behavior and hence convergence to the right answer. Let the stress components $\langle \sigma \rangle_n$ at the end of nth iteration be known. A set of elastic trial stresses are obtained as

$$\{\sigma^i\}_{n+1}^e = \{\sigma\}_n + [c]^e \{\Delta \epsilon_s^i\}_{n+1} \quad (A.5)$$

in which $\langle \Delta \epsilon_s^i \rangle_{n+1}$ denotes the ith strain subincrement at the end of (n+1)th iteration, and the second term on the right hand side of Eq. A.5 denotes elastic subincrement $\{\Delta \sigma^i\}_{n+1}^e$. These stresses are then tested with respect to the yield condition. If the trial stresses do not violate the yield condition, the material behavior is elastic. If the yield condition is violated, the element has reached a plastic state. Let the stress state at the end of (i-1)th strain subincrement be elastic

$$f(\{\sigma^{i-1}\}_{n+1}) = f_i < 0 \quad (A.6)$$

Let the next strain subincrement with stress $\{\sigma^i\}_{n+1}$ lead the stress path to point B, penetrating yield surface, such that

$$f(\{\sigma^i\}_{n+1}) = f_1 > 0 \quad (A.7)$$

violates yield condition. This indicates a transition from elastic to plastic states occurs during i th strain subincrement and $(n+1)$ th iteration. In this case the stress increment is subdivided into an elastic portion, A_c , and a plastic portion after the yield surface. The stress at the point where stress path penetrates yield surface is given by

$$\{\sigma^i\}_{n+1} = \{\sigma\}_{n+1} + x\{\Delta\sigma^i\}_{n+1}^e \quad (A.8)$$

where $x\{\Delta\sigma^i\}_{n+1}^e$ is the portion of the stress increment at which the plastic behavior is encountered, i.e. $f(\{\sigma^i\}_{n+1}) = 0$. The simplest approximation of the scaling factor, x , is obtained by a linear interpolation in f (Zienkiewicz et al. 1969) i.e.

$$x = x_1 = - \frac{f_0}{f_1 - f_0} \quad (A.9)$$

The nonlinearity of function f may yield

$$f(\{\sigma\}_n + x_1 \{\Delta\sigma^i\}_{n+1}^e) = f_s \neq 0 \quad (A.10)$$

A better estimate for x is given by Nayak and Zienkiewica (1972) by

$$x = x_1 - \frac{f_2}{\langle \partial f / \partial \sigma \rangle \{\Delta\sigma^i\}_{n+1}^e} \quad (A.11)$$

once the elastic portion of the strain subincrement $x\{\Delta\epsilon_s\}$ and the plastic portion of the strain subincrement $(1-x)\{\Delta\epsilon_s\}$ have been determined the final stresses at the end of i th subincrement and $(n+1)$ th iteration is

$$\{\sigma^i\}_{n+1} = \{\sigma\}_n + x[c]^e \{\Delta\epsilon_s^i\} - (1-x)[c]^p \{\Delta\epsilon_s^i\} \quad (A.12)$$

in which the second and third terms denote elastic stress subincrement $\{\Delta\sigma^i\}_{n+1}^e$ and plastic stress subincrement $\{\Delta\sigma^i\}_{n+1}^p$ respectively. Fig. A.1 represents the flow chart of this incremental solution technique.

A.4 Flow Chart for Program FEPILS

Program FEPILS is divided into two main execution stages, namely the problem preparation stage and the solution stage. The former is performed to check the data, whereas the latter is performed for solution of the actual problem. A dry run option in the problem preparation stage allows a check on the data. The number of subincrement,

iterative scheme, tolerance on convergence, relaxation factor, load factors and the number of iterations before reevaluation of the stiffness matrix are specified by the user. Numerical problems such as an ill conditioned stiffness matrix, oscillatory convergence and exceeding the maximum number of iterates stops the program automatically and prints the current state of stresses, displacements/velocities, friction forces, and reactions for the user's consideration.

Fig. A.2 and A.3 show the flow operations of the two stages of program.

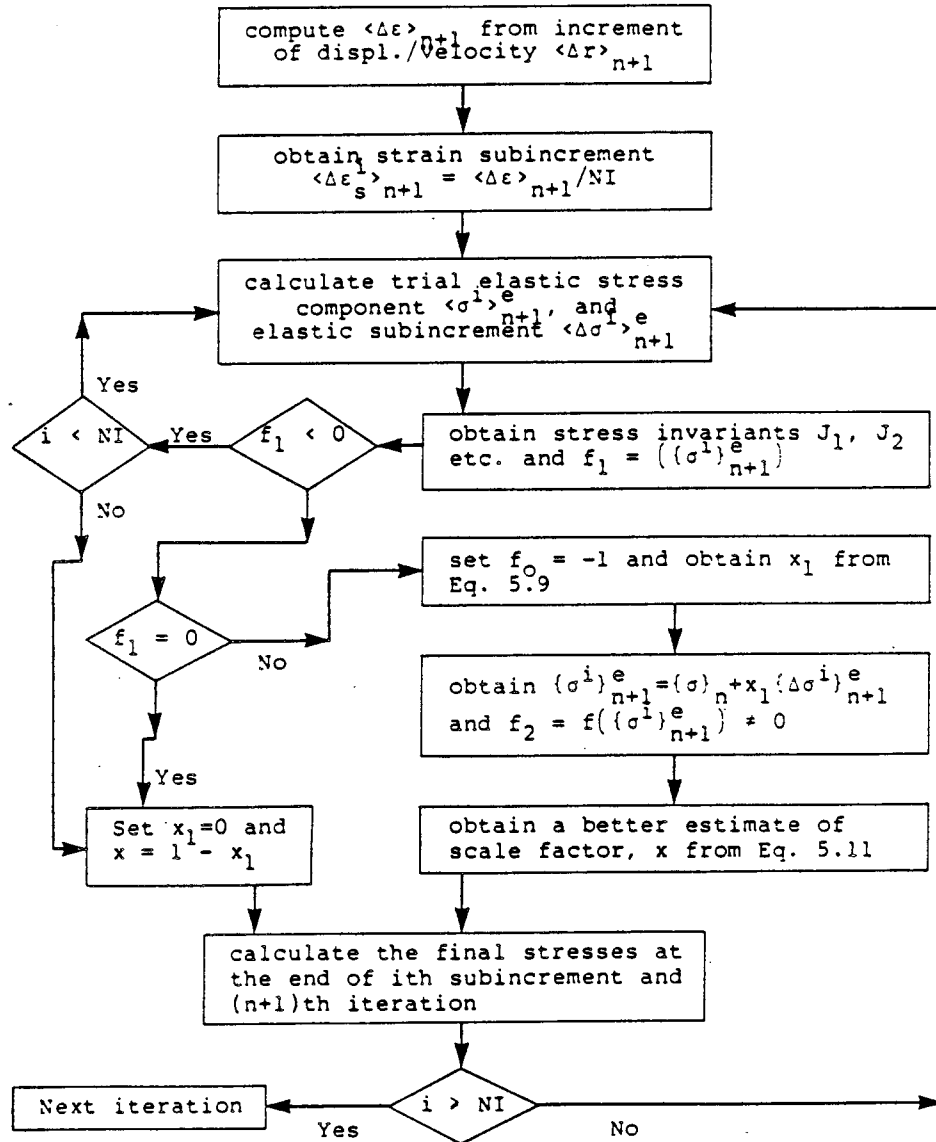


Fig. A.1 Flowchart for Elastic-Plastic Constitutive Law

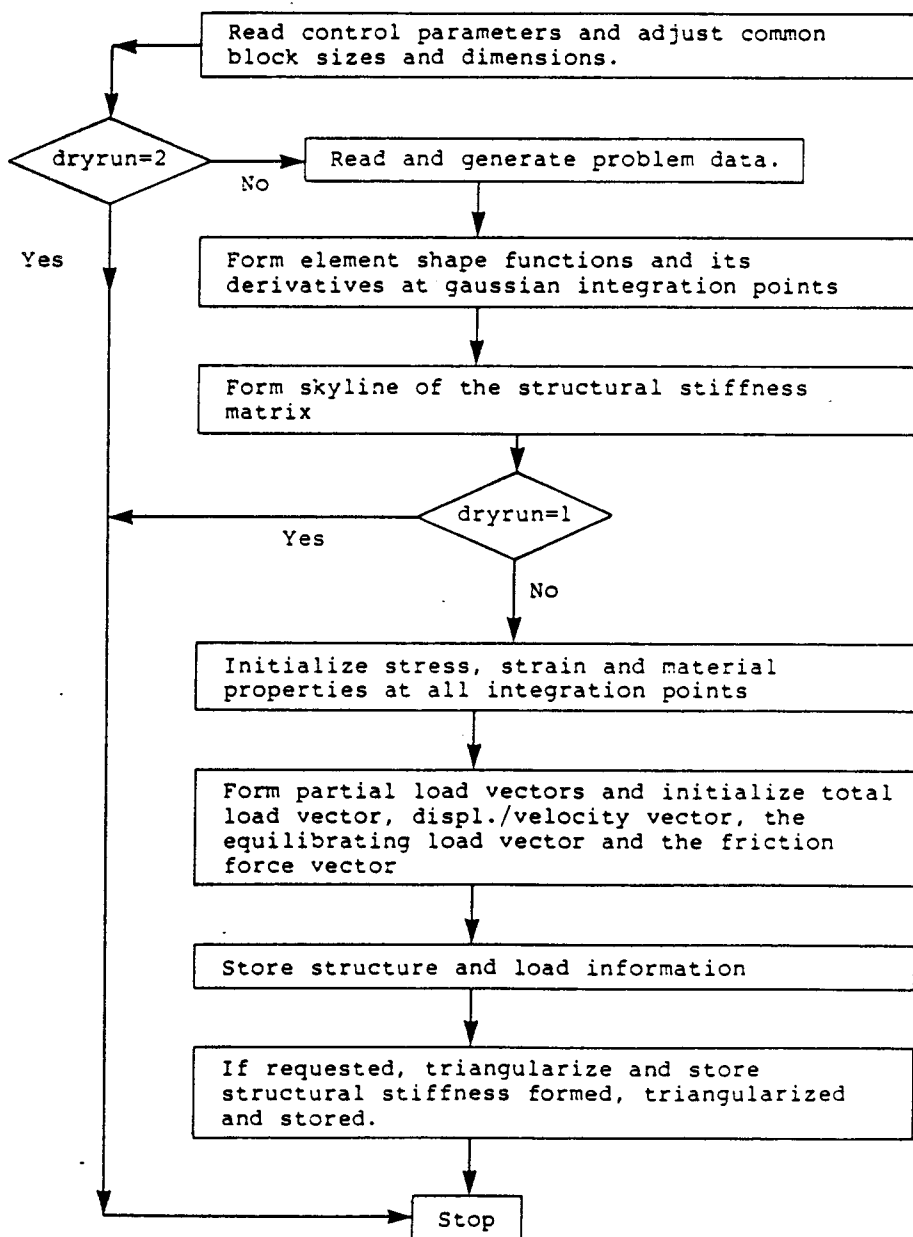


Fig. A.2 Flowchart of Problem Preparation Stage

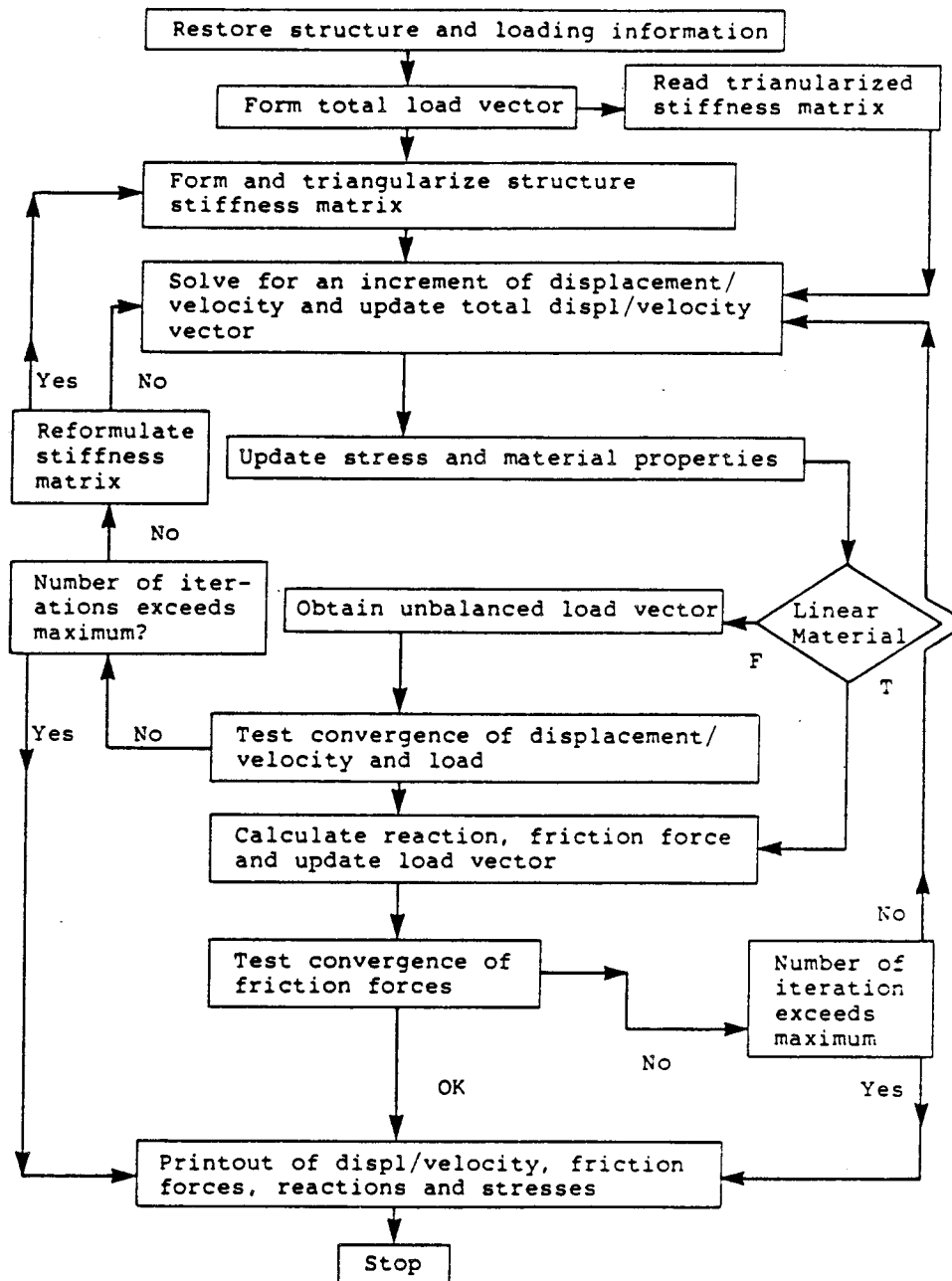


Fig. A.3 Flowchart of Solution Stage